

**Radiochemical Studies Related to the
Development of New Production Routes of
some Diagnostic and Therapeutic
Radionuclides**

INAUGURAL-DISSERTATION

zur
Erlangung des Doktorgrades
der Mathematisch-Naturwissenschaftlichen Fakultät
der Universität zu Köln

vorgelegt von
Ingo Spahn
aus Köln

Druckerei der Forschungszentrum Jülich GmbH
2006

Berichtersteller: Prof. Dr. Dr. h.c. S.M. Qaim
Prof. Dr. H.H. Coenen

Tag der mündlichen Prüfung: 13.02.2007

Die vorliegende Arbeit wurde in der Zeit von März 2003 bis Dezember 2006 am Institut für Nuklearchemie (INC) der Forschungszentrum Jülich GmbH unter der Anleitung von Herrn Prof. Dr. Dr. h.c. S. M. Qaim durchgeführt. Teile der experimentellen Arbeiten wurden am Institute of Experimental Physics der Universität von Debrecen und dem Institute of Nuclear Research der Ungarischen Akademie der Wissenschaften (ATOMKI) in Debrecen, Ungarn, sowie am iThemba Laboratory of Accelerator Based Sciences in Kapstadt, Südafrika, durchgeführt.

Abstract

Nuclear reaction cross section measurements were done in connection with the development of new production routes of the therapeutic and diagnostic radionuclides ^{32}P , ^{71}As , ^{72}As , ^{73}As , ^{74}As , ^{82}Sr , ^{90}Y , ^{153}Sm and ^{169}Yb . Investigations on the production of n.c.a. ^{73}Se using novel targetry were also performed.

Integral cross sections were measured for the $^{\text{nat}}\text{S}(n,p)^{32}\text{P}$, $^{\text{nat}}\text{Zr}(n,p)^{90}\text{Y}$ and $^{\text{nat}}\text{Eu}(n,p)^{153}\text{Sm}$ reactions using a 14 MeV d(Be) neutron field. The neutron spectrum was characterised using multiple foil activation and the code SULSA. Existing cross section data were validated within 10 - 15 %, thereby substantiating earlier evaluated and recommended excitation functions of the investigated reactions. It is inferred that for production of radionuclides via the (n,p) reaction, a fast neutron spectral source (e.g. spallation or fusion) would be better suited than a fission reactor.

Proton and α -particle induced reactions were investigated in the high-mass area for the production of ^{153}Sm and ^{169}Yb via alternative routes. Measurements were done for the first time on the $^{\text{nat}}\text{Nd}(\alpha,n)^{153}\text{Sm}$ process over the energy range of 10 to 26.5 MeV and the possible production yield of ^{153}Sm amounts to 2 GBq. The excitation function of the $^{169}\text{Tm}(p,n)^{169}\text{Yb}$ reaction was determined over the energy range from threshold to 45 MeV and compared with the results of nuclear model calculation based on the ALICE-IPPE code. A good agreement was found. The calculated possible production yields are lower than those via the conventional (n, γ) production route, but the produced ^{153}Sm and ^{169}Yb are in no-carrier-added form.

Cross sections were also measured with regard to the production of ^{71}As , ^{72}As , ^{73}As and ^{74}As via the $^{\text{nat}}\text{Ge}(p,xn)$ processes and the results were compared with those from the ALICE-IPPE calculations. Possible yields were calculated together with potential impurities. The various processes contributing to the formation of ^{71}As in the irradiation of $^{\text{nat}}\text{Ge}$ were analysed by performing some additional measurements on enriched ^{72}Ge .

For the standardisation and validation of data for the production of ^{82}Sr via the $^{\text{nat}}\text{Rb}(p,xn)$ process, cross section measurements on the formation of the long-lived impurity ^{85}Sr were done over the energy range of 25 to 45 MeV, a range where a gap still existed. Integral yields were calculated, allowing for an evaluation of the best production conditions of ^{82}Sr .

Preliminary studies on the production of n.c.a. ^{73}Se via the $^{75}\text{As}(p,xn)$ reaction using AIAs as a novel target material were also carried out. Thick target yields were determined and first tests on the radiochemical separation of n.c.a. radioselenium from the target were performed.

Kurzzusammenfassung

Es wurden Reaktionswirkungsquerschnitte gemessen, die für die Entwicklung neuer Produktionswege der therapeutischen und diagnostischen Radionuklide ^{32}P , ^{71}As , ^{72}As , ^{73}As , ^{74}As , ^{82}Sr , ^{90}Y , ^{153}Sm und ^{169}Yb von Interesse sind. Zur Produktion von n.c.a. ^{73}Se wurden Versuche mit einem neuen Target-Material durchgeführt.

Die integralen Wirkungsquerschnitte der $^{\text{nat}}\text{S}(n,p)^{32}\text{P}$ -, $^{\text{nat}}\text{Zr}(n,p)^{90}\text{Y}$ - und $^{\text{nat}}\text{Eu}(n,p)^{153}\text{Sm}$ -Reaktionen in einem 14 MeV d(Be)-Neutronenfeld wurden gemessen. Das Neutronenspektrum wurde mit Hilfe der „multiple-foil-activation“ - Technik und dem Computerprogramm SULSA charakterisiert. Bereits existierende Wirkungsquerschnitte konnten innerhalb einer Unsicherheit von 10 – 15 % validiert werden, wodurch die für diese Prozesse empfohlenen Anregungsfunktionen bestätigt werden konnten. Aufgrund der gemessenen Daten wurde gefolgert, dass zur Produktion von ^{32}P , ^{90}Y und ^{153}Sm über die (n,p)-Reaktion eine intensitätsreiche Quelle schneller, spektraler Neutronen (z.B. Spallation oder Fusion) besser geeignet wäre.

Im Bereich höherer Massen wurden protonen- und α -teilcheninduzierte Reaktionen als alternative Produktionswege von ^{153}Sm und ^{169}Yb untersucht. Der $^{\text{nat}}\text{Nd}(\alpha,n)^{153}\text{Sm}$ -Prozess im Energiebereich von 10 bis 26.5 MeV wurde in dieser Arbeit erstmalig untersucht. Die mögliche Produktionsausbeute beläuft sich auf ca. 2 GBq an ^{153}Sm . Die Anregungsfunktion der $^{169}\text{Tm}(p,n)^{169}\text{Yb}$ -Reaktion konnte im Bereich von der Reaktionsschwelle bis zu 45 MeV ermittelt und in guter Übereinstimmung mit den Ergebnissen des ALICI-IPPE-Rechenkodes verglichen werden. Die mögliche Produktionsausbeute ist geringer als bei der konventionellen Produktion über die (n, γ)-Reaktion am Reaktor, jedoch liegt das produzierte ^{169}Yb in trägerfreier Form vor.

Weitere Reaktionswirkungsquerschnitte wurden bezüglich der Produktion von ^{71}As , ^{72}As , ^{73}As und ^{74}As über die $^{\text{nat}}\text{Ge}(p,xn)$ -Reaktionen gemessen, und die Ergebnisse wurden mit denen der ALICE-IPPE-Berechnungen verglichen. Die möglichen Ausbeuten und potentiellen Verunreinigungen der Reaktionen wurden berechnet. Zur genaueren Bestimmung der individuellen Reaktionskanäle des $^{\text{nat}}\text{Ge}(p,xn)^{71}\text{As}$ -Prozesses wurden erste Experimente mit angereichertem ^{72}Ge durchgeführt.

Zur Standardisierung und Validierung der ^{82}Sr -Produktionsdaten über die $^{\text{nat}}\text{Rb}(p,xn)$ -Reaktion wurden die Wirkungsquerschnitte zur Bildung des langlebigeren Nebenproduktes ^{85}Sr im bisher noch lückenhaften Energiebereich von 25 bis 45 MeV gemessen. Die integralen Ausbeuten wurden berechnet und die besten Produktionsbedingungen ermittelt.

Vorbereitende Versuche zur Produktion von n.c.a. ^{73}Se über die $^{75}\text{As}(p,3n)$ -Reaktion wurden unter Verwendung von AIAs als neuem Target-Material durchgeführt. Es wurden Produktionsausbeuten bestimmt und erste Tests zur radiochemischen Trennung des n.c.a. Radioselens durchgeführt.

1	Introduction	1
1.1	Structure of the atomic nucleus	1
1.2	Nuclear reactions	2
1.2.1	Reaction mechanisms	2
1.2.2	Energetics of nuclear reactions	7
1.2.3	Nuclear reaction cross section	7
1.3	Neutron sources for irradiations	9
1.3.1	The ${}^9\text{Be}(d,n){}^{10}\text{B}$ neutron source at the Forschungszentrum Jülich	11
1.3.2	Determination of neutron flux	12
1.4	Irradiations with charged particles	13
1.4.1	Energy degradation of charged particles in matter	13
1.4.2	Determination of particle flux	15
1.5	Measurement of radioactivity	15
1.5.1	Determination of the absolute radioactivity	16
1.6	Differential and integral yield	16
1.7	Integral tests of differential data	17
1.8	Radiochemical separation	21
1.8.1	Separation of lanthanides	21
1.8.2	Separation of Se from As	22
1.9	Radionuclides in medicine	23
1.9.1	Radiotherapy	23
1.9.1.1	<i>External radiation therapy</i>	23
1.9.1.2	<i>Internal radiotherapy</i>	24
1.9.2	Radionuclides in medical diagnosis	25
1.9.3	Nuclear data for medical application	27
1.10	Properties of the investigated nuclides	29
2	Aims of this work	33

3	Experimental	35
3.1	General	35
3.2	Target preparation	36
3.2.1	Preparation of thin targets via sedimentation	36
3.2.2	Preparation of targets for the production of ^{73}Se	38
3.2.3	Preparation of targets for neutron irradiations	38
3.3	Irradiation experiments	39
3.3.1	Irradiations with d(Be)-breakup neutrons	39
3.3.1.1	<i>Characterisation of the neutron spectrum</i>	40
3.3.1.2	<i>Determination of the neutron flux density</i>	41
3.3.2	Irradiations with charged particles	45
3.3.2.1	<i>Irradiation facilities</i>	45
3.3.2.2	<i>Determination of charged particle flux</i>	48
3.3.3	Irradiation experiments	51
3.4	Radiochemical separation	53
3.4.1	Radiochemical separation of n.c.a. $^{73,75}\text{Se}$	53
3.4.2	Radiochemical separation of ^{153}Sm	55
3.5	Determination of radioactivity	57
3.5.1	γ -ray spectrometry	57
3.5.2	β^- -counting	60
3.6	Determination of nuclear reaction cross sections and their uncertainties	63
3.6.1	Determination of the absolute activity	63
3.6.2	Calculation of nuclear cross sections	64
3.6.3	Calculation of differential and integral yield	65
3.6.4	Uncertainties of the results	65
3.6.4.1	<i>Uncertainties of mass determination</i>	65
3.6.4.2	<i>Uncertainties in particle energies</i>	66
3.6.4.3	<i>Uncertainties in the determination of radioactivity</i>	66
3.6.4.4	<i>Overall uncertainty of the results</i>	67
4	Nuclear model calculations	68

5	Results and discussion	70
5.1	Integral tests of differential data	70
5.1.1	Measurement of integral cross sections	70
5.1.2	Comparison of integral and integrated data	72
5.2	New production routes of the therapeutic radionuclides ^{32}P, ^{90}Y, ^{153}Sm and ^{169}Yb	73
5.2.1	Possibility of production of ^{32}P , ^{90}Y and ^{153}Sm with fast d(Be) neutrons	73
5.2.2	Production of ^{153}Sm and ^{169}Yb using charged particle induced reactions	75
5.3	Cross sections for the formation of the radionuclides ^{71}As, ^{72}As, ^{73}As and ^{74}As	84
5.3.1	Cross section measurements using $^{\text{nat}}\text{Ge}$ as target	84
5.3.2	Investigation on the production possibilities of ^{71}As , ^{72}As , ^{73}As and ^{74}As	91
5.3.3	Cross section measurements using enriched ^{72}Ge as target	94
5.4	Standardisation and validation of data for the production of ^{82}Sr via the $^{\text{nat}}\text{Rb}(p,xn)$ process	97
5.5	Preliminary tests on the production of n.c.a. ^{73}Se via the $^{75}\text{As}(p,3n)^{73}\text{Se}$ reaction using novel targetry	102
6	Summary	106
7	Appendix	109
7.1	Standard sources for calibration	109
7.2	Target materials and chemical compounds	110
8	References	111

1. Introduction

1.1 Structure of the atomic nucleus

So far, the experimental results on the structure and behaviour of atomic nuclei cannot be combined in a single theory. Therefore different theoretical models have been developed to describe the various aspects. One of the first theories is the **liquid-drop model**, which was introduced by Niels Bohr in 1940 [Weizsäcker, 1935]. It compares the nucleus with a drop of liquid, whose molecules are connected through the van der Waals forces. This way several nuclear properties, like the near constant density within the atomic core or the near constant binding energy of each nucleon, can be described. In 1949 the **nuclear shell model** was introduced [Mayer, 1949, Haxel et al., 1950], which presumes a weak interaction of independent nucleons. Analogous to the idea of electron shells the nuclear shell model presumes that the nucleons are arranged in shells. This way the model is able to describe the phenomenon of the “magic numbers”, which refers to the circumstance that nuclei with specific proton or neutron numbers are especially stable or show many stable nuclides. Nuclei having 2, 8, 20, 50, 82 or 126 protons or neutrons are presumed to have complete shells, responsible for the increased stability of such nuclei. In the case of magic number 126, the closed shell with 126 protons, has as yet not been shown. Although these models are very useful to describe many nuclear properties, they become quite inadequate for dealing with high excitation energies. Considering scattering processes and nuclear reactions up to 100 MeV, where a projectile generally interacts with all nucleons within the core, the **optical model** is a useful theoretical approach [Bethe, 1940, Fernbach et al., 1949]. The basis of this model is the assumption that an atomic nucleus shows certain penetrability for an incident particle on one hand and some kind of interaction with the core’s nucleons on the other, thus showing similar properties as they are known for the interaction of light and matter in optical science. In order to describe the identified energy levels of nuclei and the phenomenon of longer-lived isomeric states, a further model had to be developed. The **Fermi gas model** [cf. Musiol, 1988] regards the nucleons as freely moving particles within the nucleus, comparable to gas molecules of an ideal gas. The nucleons in their ground state are considered to be in a potential minimum, they cannot escape. The solution of the Schrödinger equation of such a particle ensemble leads to discrete nuclear levels, which show increasing density with increasing

excitation energy, resulting in an energy continuum. If a transition from an excited state towards a lower energy level is not allowed, the respective nuclide becomes a metastable long-lived or even isomeric state, e.g. ^{89m}Y ($T_{1/2} = 16.0 \text{ s}$) or ^{186m}Re ($T_{1/2} = 2 \cdot 10^5 \text{ a}$).

1.2 Nuclear reactions

1.2.1 Reaction mechanisms

When two nuclei approach each other, there are various possibilities to interact with each other, depending on the kinetic energy of the accelerated nucleus. Those interactions can be divided into scattering processes and nuclear reactions. Generally, the interacting nuclei are classified as the target nucleus and the projectile. If the kinetic energy of the projectile is too low to penetrate the target nucleus, it will be scattered elastically or inelastically, thus transferring excitation energy to the target nucleus in the latter case.

If the energy of the interacting nuclei is high enough, a nuclear reaction may occur resulting in a change of the atomic number and/or mass number of the target nucleus. Nuclear reactions are generally expressed in the following term:



where A is the target nucleus, B the product nucleus, x the projectile and y the ejectile.

Depending on the energy of the projectile, an intermediate **compound nucleus** can be formed [Bohr, 1936, Weisskopf et al., 1940]. With projectile energies of up to 25 MeV this type of reaction is favoured. According to the compound model the incoming projectile disperses its energy equally to the nucleons of the target. This intermediate compound nucleus adopts a highly excited state with a typical life-time of about 10^{-15} s and has various possibilities, viz. reaction channels, to achieve a stable state through the emission ("evaporation") of nucleons and γ -rays. Due to the statistical distribution of the excitation energy the emission takes place symmetrically around 90° of the projectile course [cf. Lieser, 1991]. Besides this statistically determined particle evaporation, there is the possibility of resonance reactions. This

phenomenon is unique for compound nucleus reactions and is observable as distinctive resonances in the excitation function of a nuclear reaction. This effect occurs, when the kinetic energy of a captured particle leads to a discrete excitation state of the compound nucleus. This resonance structure is investigated well for (n,γ) processes, whose cross sections are very well known. In Figure 1-1 an example is shown for cross section resonances of the $^{152}\text{Sm}(n,\gamma)^{153}\text{Sm}$ reaction taken from [Kopecky, 1997].

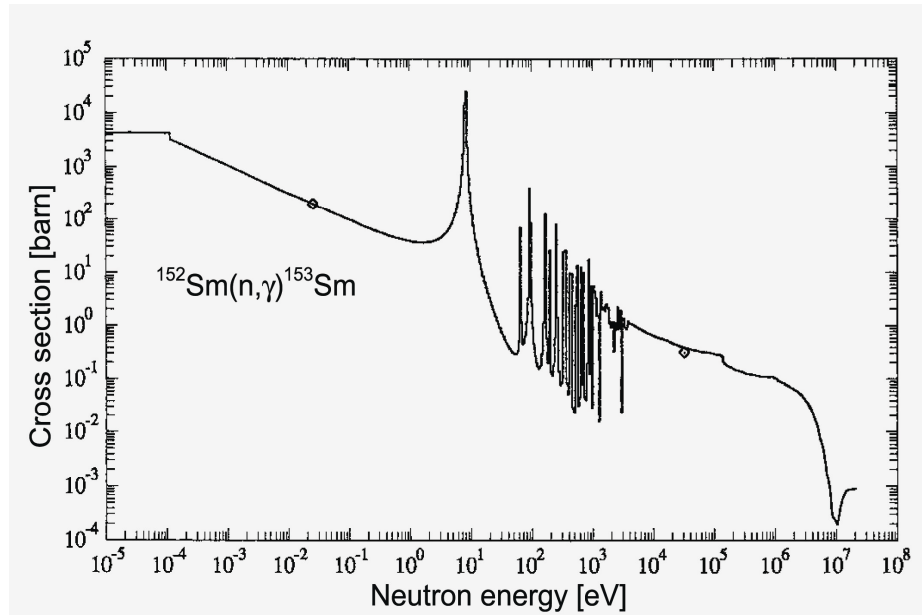


Fig. 1-1 Excitation function of the $^{152}\text{Sm}(n,\gamma)^{153}\text{Sm}$ reaction as a function of the neutron energy. Cross section resonances occur between 5 eV and 5 keV [Kopecky, 1997].

Generally, the resonance areas lie within the neutron energy range of 1 eV to 10 keV. Above this margin the resonance peaks begin to interfere so that no discrete peaks can be identified. Thus for higher energies the compound nucleus cannot be described through discrete energy levels anymore but through a multitude of levels interfering with each other, which can be treated statistically.

Beginning with projectile energies of about 10 MeV, **precompound reactions** occur. Above energies of 30 MeV these processes play a significant role in the nuclear reaction. Due to the higher energy delivered into the target nucleus, nucleon emission occurs before the excitation energy is distributed equally to all nucleons within the target. This effect leads to an average life-time of the precompound state

of about 10^{-18} s and a slightly forward oriented emission of nucleons. Precompound reactions can be described using the Exciton model [Griffin, 1966] that is based on the Fermi-gas model. The nucleus is regarded as Fermi-gas with single-particle ground states, which are occupied up to the Fermi-energy ϵ_F . Due to the projectile energy, particles of the Fermi-gas are excited, resulting in pairs of particles (p) and holes (h) in the scheme of energy levels (Fig. 1-2), which are called excitons. After their formation, either an emission of nucleons may occur, or new exciton pairs may be formed, due to the remaining weak interaction.

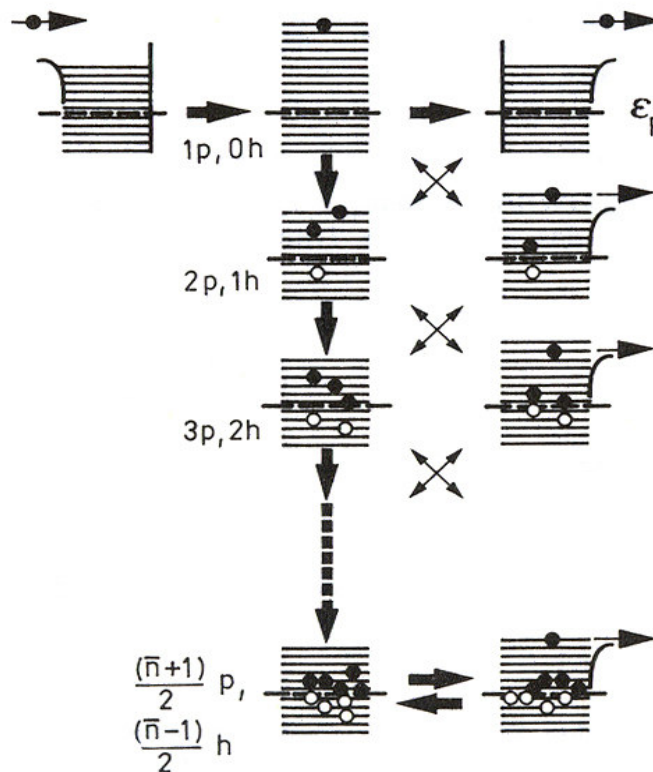


Fig. 1-2 Example of a nuclear reaction according to the exciton model [cf. Musiol et al., 1988].

In this chain of transmissions, emission of nucleons is possible at each stage, resulting in various possible reaction channels before an equilibrium state is reached. For higher projectile energies **direct processes** can be observed, which are preferential with light target nuclei and take place within 10^{-23} to 10^{-21} s. In this case the kinetic energy of the projectile is mainly transmitted to the nucleons directly involved in the collision. These are emitted before their excitation energy can be distributed to the other target nucleons and no intermediate nucleus is formed. Due

to this effect the emitted particles show a distinctive forward orientation. Associated with direct processes are so-called “knock-out” reactions and transfer reactions. In a “knock-out” reaction, like the ${}^7\text{Li}(n,t){}^4\text{He}$ process, a preformed cluster is detached from the target. A transfer reaction describes the transition of one or several nucleons from the projectile to the target or the other way around. In Figure 1-3, a scheme of the nuclear reactions is shown in form of a time line.

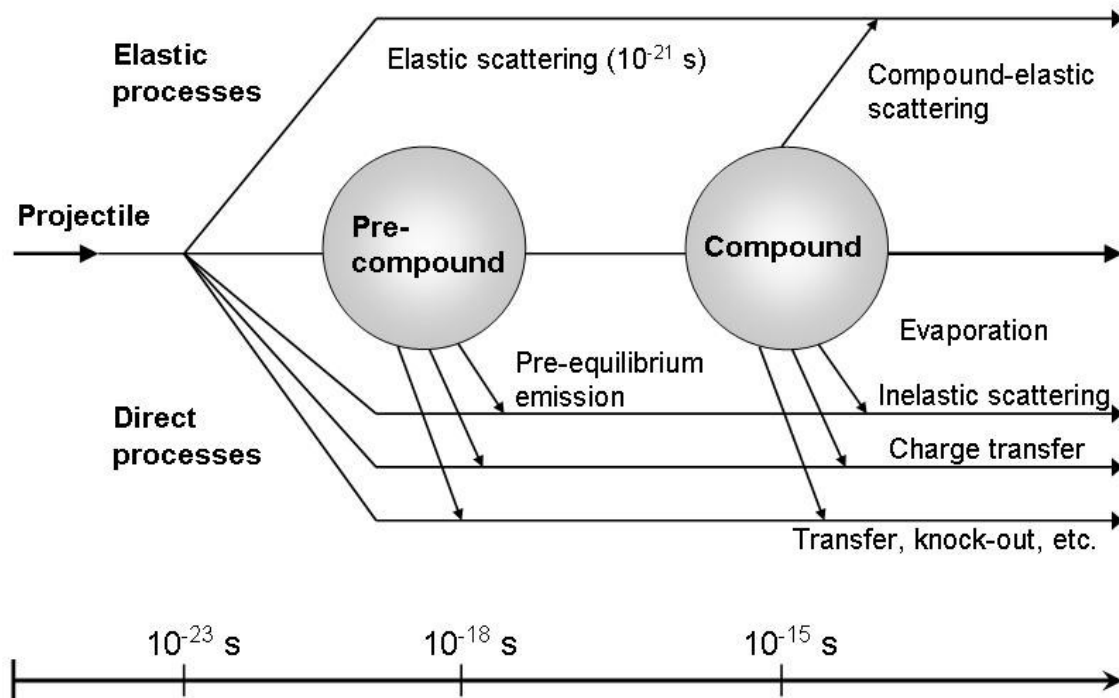


Fig. 1-3 Chronology of different nuclear reactions [adapted from Gadioli, 1992].

In the case that the kinetic energy of a projectile is very high, the spallation process can be observed. Caused by elastic and inelastic collisions with the target nucleons, an intra-nuclear cascade occurs, resulting in the evaporation of nucleons and complex particle clusters. In this direct process, no metastable compound nucleus can be formed, like in the nuclear fission process. The **nuclear fission** is either the result of spontaneous fission or is caused by the excitation through an incoming projectile. In both cases a highly excited compound nucleus is formed that fissions into two high energetic fragments, which de-excite through the emission of 2 - 3 prompt neutrons and γ -rays, before eventually entering the radioactive decay chain. The resulting fission products generally are nuclei with masses between 70 and 160

u. The nuclear **spallation** is a direct process with energies too high for the formation of any compound nuclei. Nuclear spallation is an endoenergetic process triggered by a high-energy projectile, like protons of 800 MeV or more. On first contact of the projectile with the target nucleus the intra-nuclear cascade takes place. The kinetic energy is transferred to individual nucleons, which may lead to the emission of these energetic particles, who may initiate further spallation processes in their course (*“inter-nucleus cascade”*). Following the initial cascade the energy spreads evenly throughout the nucleus, leading to further nucleon emission and finally resulting in the evaporation of nucleons from the excited nucleus according to the statistical model. Due to the greater excitation of the evaporated nucleons, the neutron energy spectrum of the spallation process includes a large part of high energetic neutrons [cf. Bauer, 2001]. Figure 1-4 shows a comparison of a fission neutron spectrum and the spectrum resulting from spallation of tungsten nuclei through 800 MeV protons.

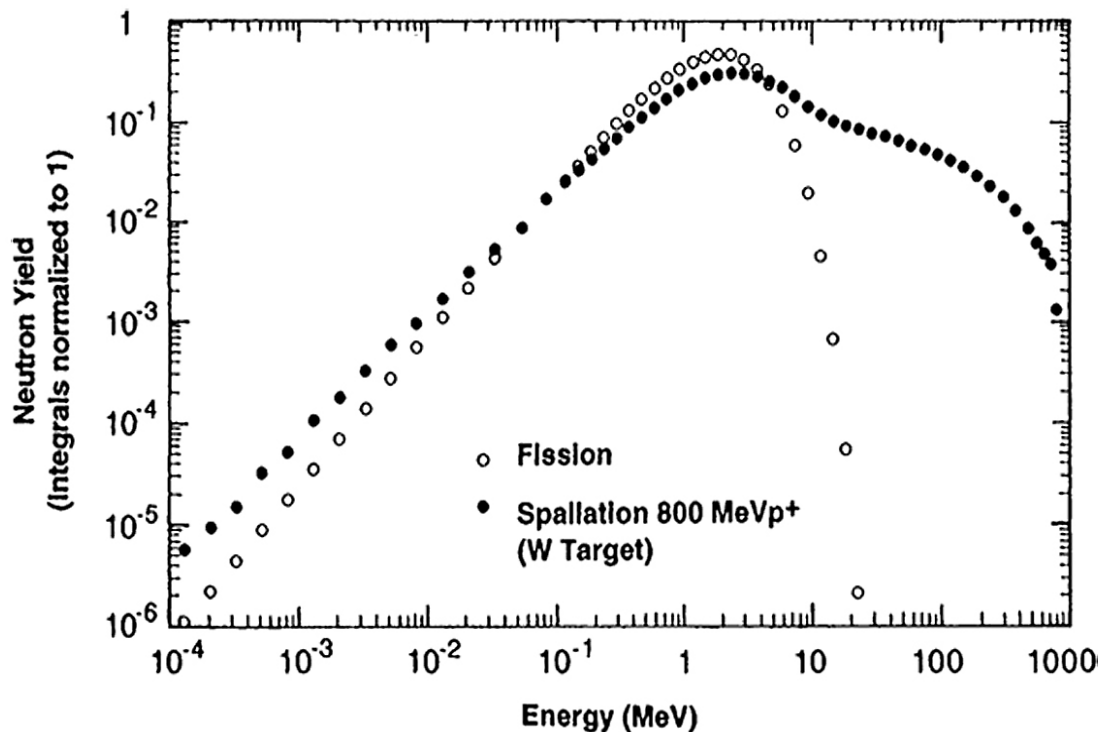


Fig. 1-4 Energy distribution of fission neutrons in comparison with spallation neutrons, obtained from the $W(p,spall)$ process with 800 MeV protons [Bauer, 2001].

1.2.2 Energetics of nuclear reactions

For the calculation of the energetics of a simple binuclear reaction, one has to consider the conservation of momentum, analogous to a macroscopic system, as well as the conservation equation of mass and energy introduced by Einstein. The Einstein equation states that the product of mass and energy is constant ($E = m \cdot c^2$). On the basis of this correlation, it is possible to calculate the energy difference ΔE , which appears during a nuclear reaction, using the masses of the reacting particles before and after the reaction.

$$\Delta E = ((m_B + m_Y) - (m_A + m_X)) \cdot c^2 \quad (2)$$

The variable m_i means the mass of the corresponding particle (see Eq. 1).

The term ΔE is also known as Q-value and can be regarded as analogue to the reaction enthalpy known for macroscopic systems. A nuclear reaction is exoenergetic when ΔE is positive. In case of an endoenergetic process, where ΔE is negative, the necessary energy has to be delivered through the kinetic energy of the projectile. Due to the conservation of momentum, the latter is, however, partially transferred to the target nucleus, thus reducing the energy available for the excitation. Resulting from the laws of the conservation of momentum this minimum threshold energy E_{thr} , that is necessary to induce the nuclear reaction, can be calculated as

$$E_{\text{thr}} = -\Delta E \cdot \left(1 + \frac{M_X}{M_A} \right) \quad (3)$$

If both target and projectile are charged particles, the threshold energy is increased by the Coulomb energy E_C , that is necessary to overcome the potential barrier. However, nuclear reactions induced by projectiles of lower energy are possible due to the so called tunnelling effect.

1.2.3 Nuclear reaction cross section

The nuclear reaction cross section (σ) represents the probability with which a projectile and a target nucleus interact according to a specific reaction channel. Nuclear cross section values are generally given in barn (b), with $1 \text{ b} = 10^{-28} \text{ m}^2$. This dimension of an area is deduced from the macroscopic picture of a projectile aimed at a target, according to which the probability of hitting the target is proportional to its

area. In reality this picture proved to be quite inaccurate, since nuclear interaction and Coulomb force strongly affect this probability, leading to deviations of several orders of magnitude in specific cases. Due to these effects, the nuclear cross section is not only dependent on the specific nuclear process under consideration, but also varies as a function of the projectile energy.

This relation of cross section and energy is known as the **excitation function**. In the case of neutron induced reactions no Coulomb barrier has to be surmounted, leading to high cross section value in the low energy range, which decreases linearly with increasing velocity, viz energy, until entering the resonance range (see 1.2.1). For charged particle induced reactions, where the projectiles need additional kinetic energy to overcome the potential barrier, the shape of the excitation function normally shows an increasing trend, reaching a maximum and then an asymptotic decline with the increasing energy.

The activation equation

The formation of a nuclide via the irradiation of a target material having the particle number N_x and the isotopic abundance H is proportional to the flux density Φ of the projectiles.

$$\frac{dN}{dt} = \sigma \cdot \Phi \cdot H \cdot N_x \quad (4)$$

If the newly formed nuclei (N_B) are unstable, both their formation and their decay have to be considered.

$$\frac{dN}{dt} = \sigma \cdot \Phi \cdot H \cdot N_x - \lambda \cdot N_Y \quad (5)$$

λ : decay constant

The decay of the produced nuclei, represented in the last term, is identical with the radioactivity A_Y of the nuclide, which can be measured experimentally. The solution of this differential equation leads to the **activation equation**:

$$A_Y = N_Y(t) \cdot \lambda = \sigma \cdot \Phi \cdot H \cdot N_x \cdot (1 - e^{-\lambda t}) \quad (6)$$

Here it should be kept in mind that the cross section σ is not a constant but is dependent on the projectile energy. This implies that equation 6 is only valid for projectiles of constant energy, leading to the prerequisite of a thin target, i.e. excluding significant projectile energy absorption in the target (see 1.4.1).

1.3 Neutron sources for irradiations

Since the discovery of the neutron through James Chadwick in 1932, this particle is of utmost importance in energy generation as well as for the production of radionuclides for nuclear medicine [Stöcklin et al., 1995]. Due to these reasons, many types of neutron sources have been developed.

For scientific use, especially the generation of mono-energetic neutrons is of high interest. For this purpose primarily nuclear reactions of the type $A(x,n)B$ are available. To implement such a reaction either projectiles produced via a particle accelerator can be used, or the decay products emitted from heavy radioactive nuclei. The latter method has the advantage of being a relatively cheap technique, which can be handled easily but has the drawback of producing only a low neutron flux of about 10^4 particles per second and GBq of the radioactive source. Furthermore most of such neutrons are not strictly mono-energetic, except for those generated with a photon neutron source. The lifetime of the latter source is, however, rather short. In Table 1-1 gives examples of neutron sources using the decay of heavy nuclei.

The accelerator based neutron generators are more expensive and technically much more demanding than the radionuclidic sources. However, they enable much larger neutron yields, due to their high projectile current. Furthermore they can produce not only mono-energetic or quasi monoenergetic neutrons, but can also, to some degree, affect the kinetic energy of the generated neutrons, depending on the nuclear reaction utilised.

Table 1-1. Examples of neutron sources utilising the decay of heavy atoms [Knoll, 1983]

Neutron source	Nuclear reaction	Half-life	Neutron yield (neutrons per second and GBq)
$^{210}\text{Po}/\text{Be}$	(α, n)	138.4 d	$6.8 \cdot 10^4$
$^{210}\text{Pb}/\text{Be}$	(α, n)	22.3 a	$6.2 \cdot 10^4$
$^{228}\text{Th}/\text{Be}$	(α, n)	1.9 a	$5.4 \cdot 10^5$
$^{239}\text{Pu}/\text{Be}$	(α, n)	$2.4 \cdot 10^{10}$ a	$3.8 \cdot 10^4$
$^{241}\text{Am}/\text{Be}$	(α, n)	432.6 a	$5.9 \cdot 10^4$
$^{124}\text{Sb}/\text{Be}$	(γ, n)	60.2 d	0.3 bis $1.4 \cdot 10^6$

In Table 1-2 a list of possible nuclear reactions is given, that can be employed to generate quasi-monoenergetic neutrons up to about 20 MeV, which in fact have a certain energy distribution, but have a distribution maximum, which is distinctive enough for nuclear data measurements. The neutron generation via the $^2\text{H}(d, n)^3\text{He}$ reaction can be done up to 12 MeV and the flux achieved is about $3 \cdot 10^7$ neutrons per second and square centimetre [Qaim et al., 1984].

Table 1-2. Examples of nuclear reactions used for the generation of quasi-monoenergetic neutrons at an accelerator [Uttley, 1983]

Nuclear reaction	Q-value [MeV]	Neutron energy at maximum [MeV]	Target material	Energy width [keV]
$^7\text{Li}(p, n)^7\text{Be}$	- 1.64	0.2 – 1	Li	50
$^3\text{H}(p, n)^3\text{He}$	- 0.76	0.7 – 3	TiT T ₂ -Gas	100 100
$^2\text{H}(d, n)^3\text{He}$	+ 3.27	3 – 8 8 – 12	TiD D ₂ -Gas	500 120
$^3\text{H}(d, n)^4\text{He}$	+ 17.59	14 – 20	TiT T ₂ -Gas	500 120

The low flux quasi-monoenergetic neutron sources are generally suitable for fundamental nuclear studies. For other applications, like isotope production, higher neutron fluxes are demanded. This can be achieved via fission, breakup or spallation processes. Another way of producing neutrons is the photonuclear process. The most important neutron source to date is the nuclear reactor, which can generate neutron fields of about 10^{14} to 10^{15} particles per second and square centimetre. However, the fission reactor produces neutrons with an energy distribution up to 20 MeV, with only about 10 % of the neutrons having kinetic energies larger than 4 MeV. The maximum intensity is at about 1 MeV, which is beneficial for (n,γ) reactions but leads to very low cross sections in case of nuclear reactions with higher thresholds. Another way of obtaining high neutron fluxes up to 10^{18} n/s are photonuclear processes induced at an electron accelerator [Knoll, 1983]. This technique uses a linear electron accelerator to provide fast electrons with energies of 30 MeV or more, which are directed onto a heavy-element target, e.g. lead. The resulting Bremsstrahlung leads to photonuclear (γ,xn) reactions providing neutrons of about 0.1 to 1 MeV energy. The most potent source for fast neutrons is the spallation of heavy nuclei using high-energy protons. The kinetic energy of the neutrons is dependent on the target material and proton energy. The neutron flux is dependent on the proton beam current, with possible values of 10^{17} particles per second.

1.3.1 The ${}^9\text{Be}(d,n){}^{10}\text{B}$ neutron source at the Forschungszentrum Jülich

The principle of the d(Be) neutron source is based on the break-up reaction of 14 MeV deuterons on the light beryllium nuclei, due to inelastic collisions (Fig. 1-4).

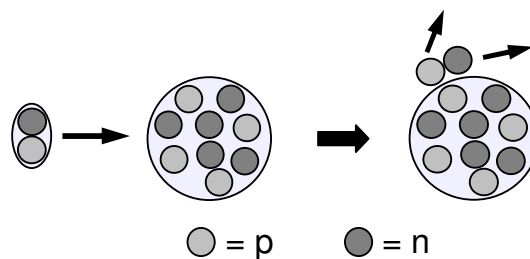


Fig. 1-4 Scheme of deuteron break-up on a beryllium nucleus.

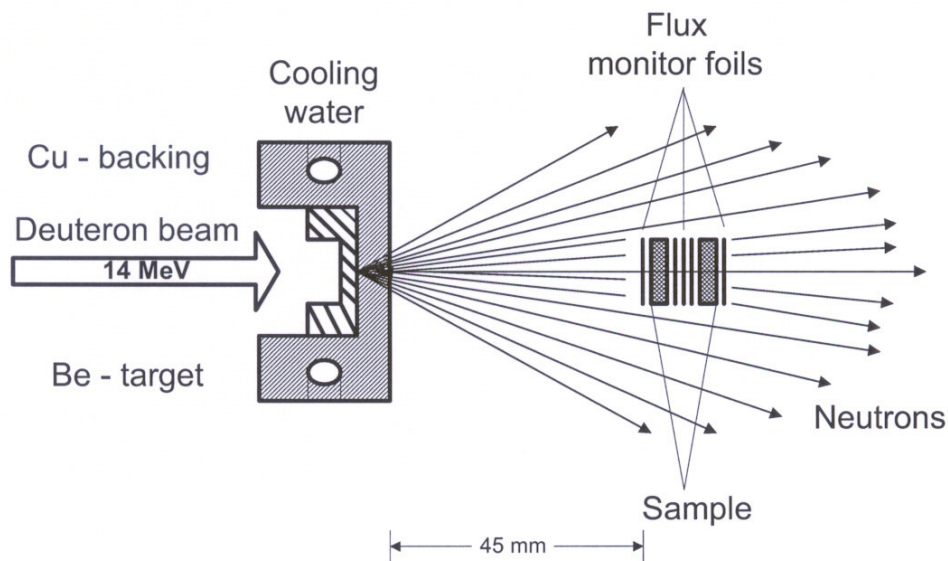


Fig. 1-5 Scheme of the $d(\text{Be})$ neutron source at the compact cyclotron CV 28.

Figure 1-5 shows the sketch of a $d(\text{Be})$ source as it is installed at the CV 28 in Jülich. Placed in the centre is a metallic Be disk of 1.9 mm thickness and 19.7 mm diameter. The Be disk has a chemical purity of 98 % and is embedded into a 2 mm thick water cooled copper holder. The collimated deuteron beam hits the metal directly, producing a cone shaped neutron field, as discussed for direct processes above. The sample is placed in a movable target holder, thus enabling an adjustment of the neutron flux in the target by changing the distance to the source. The characteristics of the $d(\text{Be})$ target and the neutron field are described in more detail in the references [Qaim, 1987] and [Olah et al., 1998]. A detailed analysis of the neutron spectrum was also done in this work and is described in section 3.3.1.1. It should be kept in mind that the nuclear cross sections determined with this technique are values which are averaged over the neutron spectrum of the specific neutron source. Nevertheless, the $d(\text{Be})$ break-up neutron source enables valuable conclusions on nuclear data.

1.3.2 Determination of neutron flux

An analysis of the neutron flux density within a target sample is essential for nuclear data measurement. In this work the flux was determined via the use of monitor foils which were positioned in front and at the back of each irradiated sample. A mean of

the two values was taken to average the flux density in the target. This is important, since the neutron flux density decreases rapidly with the increasing distance from the source. As monitor reactions nuclear, processes were used, which possess well known cross sections of adequate magnitude in the applied energy range. On the basis of the known cross section and the measurable activity, which was produced during the bombardment, the particle flux could be calculated. Details of the determination of the neutron flux, performed in this work, are given in the experimental section 3.3.3.

1.4 Irradiations with charged particles

Irradiations with charged particles are of considerable interest in nuclear chemistry and physics. Modern particle accelerators are able to produce beam currents of more than 10^{15} particles per second. An important feature of cyclotrons and linear accelerators used to produce the charged particles is the ability to provide adjustable projectile energies. Medium sized cyclotrons like the CV 28 in Jülich provide proton energies up to 20 MeV, but large accelerator arrays like the LHC of CERN, which is under construction in Switzerland, can produce particle energies of up to 7 TeV.

1.4.1 Energy degradation of charged particles in matter

When in section 1.3.1 the dependence of the neutron flux density on the distance to the target had to be considered, in the case of charged particle irradiations the degradation of energy in matter is significant. As a consequence of scattering, ionisation and excitation processes, charged particles lose kinetic energy up to a complete stop, whenever they travel through matter. After the first classical calculations of this energy degradation by Bohr, Bethe and Bloch introduced a mathematical model considering quantum mechanical aspects as well [Bethe, 1930, Livingston, 1937, Bloch, 1933]. This Bethe-Bloch formalism is given in equation 7.

$$-\frac{dE}{dx} = \frac{Z^2 \cdot e^4 \cdot n_e}{m \cdot c^2 \cdot \beta^2 \cdot \epsilon_0^2} \cdot \left[\ln \left(\frac{2 \cdot m \cdot c^2 \cdot \beta^2}{I \cdot (1 - \beta^2)} \right) - 2 \cdot \beta^2 \right] \quad (7)$$

Z = nuclear charge number

e = elementary charge

m = electron mass

c = speed of light

E = projectile energy

β = ratio of projectile speed and c

n_e = electron density

I = mean ionisation potential of target

x = distance

Equation 7 is based primarily on the interaction of a charged projectile with the electron shells within the target material. This calculation was modified by Williamson et al. [Williamson et al., 1966], taking into account that inner-shell electrons do not participate in the interaction and that recombination processes result in a reduction of the mean charge of the projectile. The energy degradation has to be specifically taken into account when performing irradiations with charged particles, due to its significant influence on the experimental results. On the other hand, the degradation effect holds the possibility to cover a large energy range with a single irradiation experiment, as it is done in the **stacked-foil technique** [Weinreich et al., 1974]. The combination of thin target samples with monitor and absorber foils enables the adjustment of different projectile energies in the individual samples, thus simultaneous activation of a number of targets is possible for cross section measurements. Essential for this technique is the deliberate calculation of the energy degradation to determine the precise projectile energy in each sample. In the scope of this work, this has been done using the computer code STACK 2.3, which is based on the formalism of Bethe [1930] and the tables of Williamson et al. [1966]. In Figure 1-6 a schematic view of a stack of foils used for irradiation can be seen. In order to perform precise cross section measurements, it is essential that target samples and monitor foils are very thin, so that the projectile energy can be considered as constant within the samples.

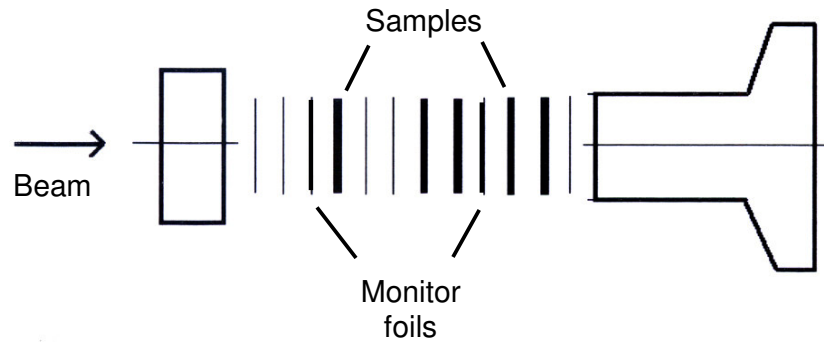


Fig. 1-6 Irradiation of thin samples via the stacked-foil technique.

1.4.2 Determination of particle flux

For the determination of the particle flux in irradiations with charged particles, two different methods can be used. Due to the charge of the projectiles it is possible to determine their number by measuring the electric current in the target. The precision of this method is only limited by the technical setup available at irradiation facilities, but may lead to bigger uncertainties when dealing with very low currents. The second method of flux determination uses monitor foils, as is described in section 1.3.2.

1.5 Measurement of radioactivity

For the determination of radioactivity different techniques can be applied, depending on the type of radiation that shall be detected. Of major importance is the γ -ray spectrometry, because a multitude of radionuclides can be investigated easily and non-destructively with this technique. The detection of γ - and X-rays is done mostly using semi-conductor detectors, which allow a fast analysis of photon emission over a large energy range. The detection of corpuscular radiation is technically more demanding, due to the low permeation of these particles. Here, often liquid scintillation counters or gas flow proportional counters are utilised, since the emitted particles may not be able to enter the counting volume of the otherwise more advantageous semi-conductor detectors. A disadvantage of techniques like the gas flow proportional counting is the inability to simultaneously analyse the energy of a detected β -particle. Thus the β emitting radionuclide has to be identified via additional absorption measurements.

1.5.1 Determination of the absolute radioactivity

For deducing the absolute radioactivity from the number of counted impulses several factors have to be considered. The detector **efficiency** (ϵ) represents the probability with which an emitted particle or photon is detected in the counter. The efficiency includes the physical aspects within the counting volume of the detector as well as the geometrical aspect indicating the probability that the emitted radiation reaches the detector. The efficiency is a function of the sample distance and its radiation energy, and can be determined using radioactive standards, which are listed in the appendix. In addition, the use of standard sources allows the determination of the **dead time** (T_D). This is the period after an impulse, needed by the detector electronics to register a new impulse. An additional correction that has to be made is the **coincidence effect** (f_c). This effect is caused through the simultaneous detection of two γ -impulses, either from two decay processes of different nuclei in a sample (“pulse pile-up”) or due to a cascade decay of one nucleus (“true coincidence”). In both cases the two impulses are summed up as one.

Equation 8 shows the calculation of the absolute radioactivity considering the factors explained above.

$$A = \frac{P}{\epsilon \cdot f_c \cdot T_D \cdot I} \quad (8)$$

P : number of counted impulses

I : intensity

The **intensity** is a constant describing the emission probability of a particle or γ -ray according to a specific decay process.

1.6 Differential and integral yield

Whereas the deliberate fabrication and use of thin irradiation targets for nuclear data measurements allow considering the projectile energy and flux as almost constant, this cannot be done in the case of thick target irradiation for the purpose of isotope production. The **differential yield** describes the production yield in a thin target, where the energy degradation can be described as an infinitesimal interval ΔE . It can

be calculated using the activation equation (Eq. 6). In order to calculate the possible production yield in a thick target, the latter is considered to be a sum of thin targets. This way the yield is calculated by integrating the relevant differential yields over the energy range covered in the thick target, leading to the **integral yield** (Y_I) in an irradiation (Eq. 11).

$$Y_I = \Phi \cdot H \cdot m \cdot (1 - e^{-\lambda \cdot t}) \cdot \int_{E_1}^{E_2} \left(\frac{dE}{d\rho x} \right)^{-1} \cdot \sigma(E) dE \quad (11)$$

ρ = density of material x = distance travelled in target;
 E_1 = incident energy E_2 = exit energy
 m = mass of target

The term $(dE/d\rho x)^{-1}$ is called the stopping power or the differential range of the projectile in the target, and can be obtained from tables and online data files [cf. Berger et al., 2005].

This way the yield of a thick target can be calculated by dividing the excitation function of the reaction into small energy intervals. Using the average cross section in the interval the activity can be calculated for that segment of the excitation function, and the integral yield can be obtained by summing up all intervals. Commonly, the integral yield of a nuclear reaction is given in units of (Bq/ μ A·h) or (MBq/ μ A·h). It is a very important parameter for the evaluation of radionuclide production processes [Qaim, 2003]. It should be noted, that the calculated integral yield of a nuclear reaction is, generally, higher than the experimentally determined thick target yield, due to scattering based beam losses in a target and due to changes of the target density caused by radiation damage and heating up of the material [cf. Qaim, 1989].

1.7 Integral tests of differential data

Differential nuclear data measurements are not only important for the validation of nuclear models, but are of great significance for radionuclide production, particularly when done for medical application [Qaim, 2001a, Qaim, 2001b, Qaim, 2001c]. As described in section 1.9, integral data can be deduced from differential data

measurements, thus making the integral test an important tool for the validation of nuclear cross section measurements.

An important part of this work is the validation of excitation functions of (n,p) reactions related to the production of therapeutic radionuclides in different mass regions, viz. ^{32}P , ^{89}Sr , ^{90}Y and ^{153}Sm , via integral cross section measurements. The spectrum averaged cross sections ($\langle\sigma\rangle$), determined with the d(Be) neutron source (see 1.3.1), could be used to check the differential data for the formation of the radionuclides under investigation. The spectrum averaged cross section is given by [Ibn Majah et al., 2001]:

$$\langle\sigma\rangle = \frac{\int_{E_1}^{E_2} \sigma(E) \cdot \Phi(E) dE}{\int_{E_1}^{E_2} \Phi(E) dE} \quad (12)$$

The nuclear processes under investigation in this work are the $^{32}\text{S}(n,p)^{32}\text{P}$, $^{89}\text{Y}(n,p)^{89}\text{Sr}$, $^{90}\text{Zr}(n,p)^{90}\text{Y}$ and $^{153}\text{Eu}(n,p)^{153}\text{Sm}$ reactions. The aim was to compare the experimental cross section data with evaluations available in the literature to develop the best fitted excitation function for each nuclear reaction. This data validation has been requested by the IAEA [Sublet et al., 2004] and is considered to be an integral part of the data base standardisation for production of therapeutic radionuclides via (n,p) reactions at present day fission reactors as well as at future fusion or spallation neutron sources. Figures 1-7 to 1-10 show the cross sections of the (n,p) reactions under consideration as a function of neutron energy as well as theoretical curves based on nuclear model calculations. All the data shown were taken from the EXFOR data file [2003]. After a careful scrutiny, the data points encircled are suggested to be ignored. The results of nuclear model calculations are also shown. For each reaction the recommended curve is described (for more details cf. [Al-Abyad et al., 2006]). This curve was used to calculate the spectrum averaged cross section needed in integral tests.

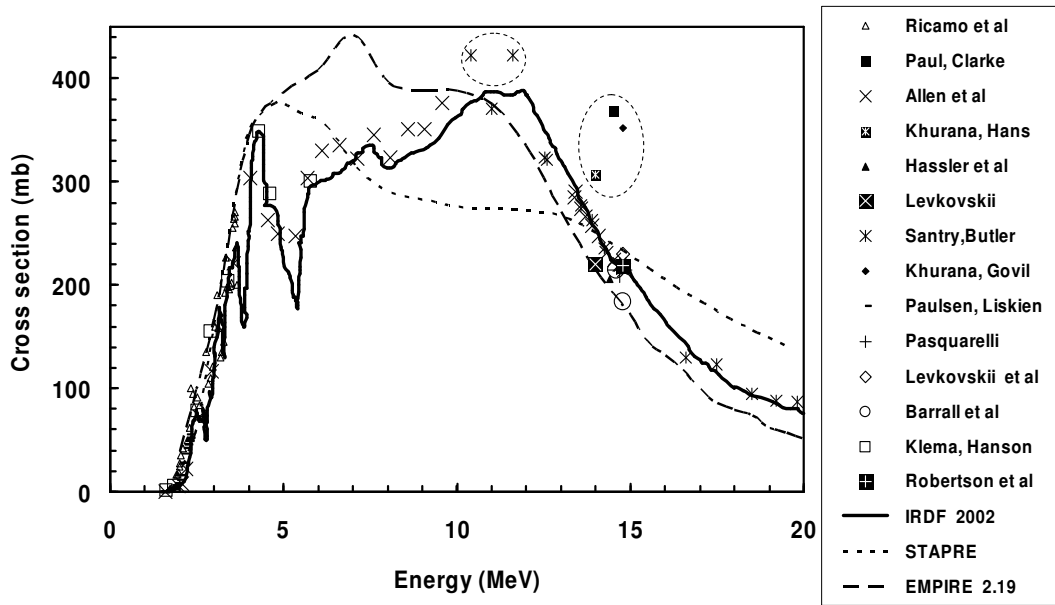


Fig. 1-7 Excitation function of the $^{32}\text{S}(n,p)^{32}\text{P}$ reaction [cf. EXFOR, 2003]. The discrepant data are encircled and should be neglected. The nuclear model calculations (STAPRE and EMPIRE 2.19) cannot sufficiently reproduce the experimental data. The curve from [IRDF 2002] is recommended.

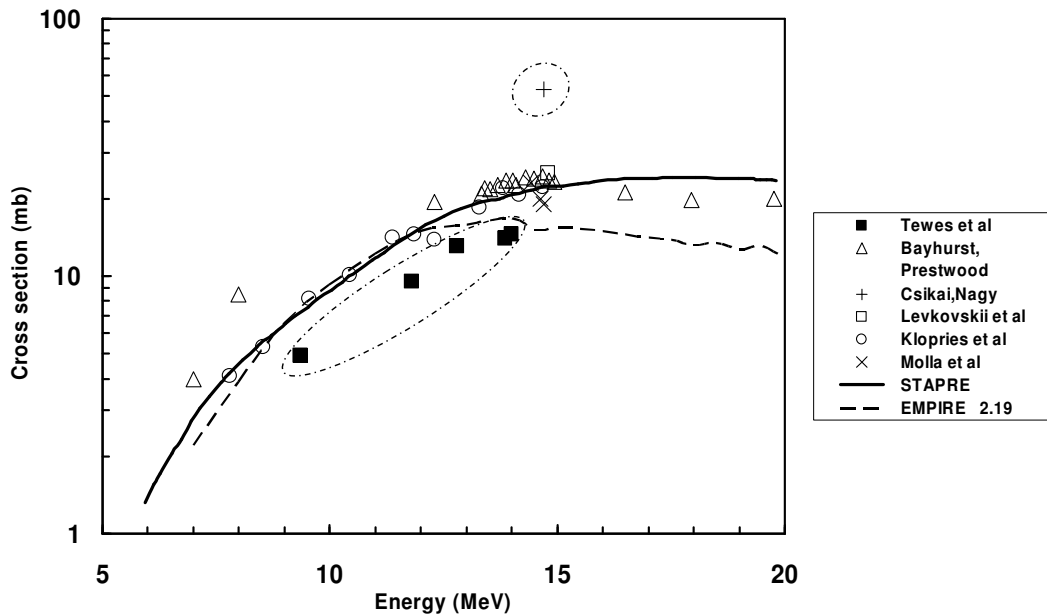


Fig. 1-8 Excitation function of the $^{89}\text{Y}(n,p)^{89}\text{Sr}$ reaction [cf. EXFOR, 2003]. The discrepant data are encircled and should be neglected. The nuclear model calculation is able to describe the data well up to a neutron energy of 20 MeV. The STAPRE curve is recommended.

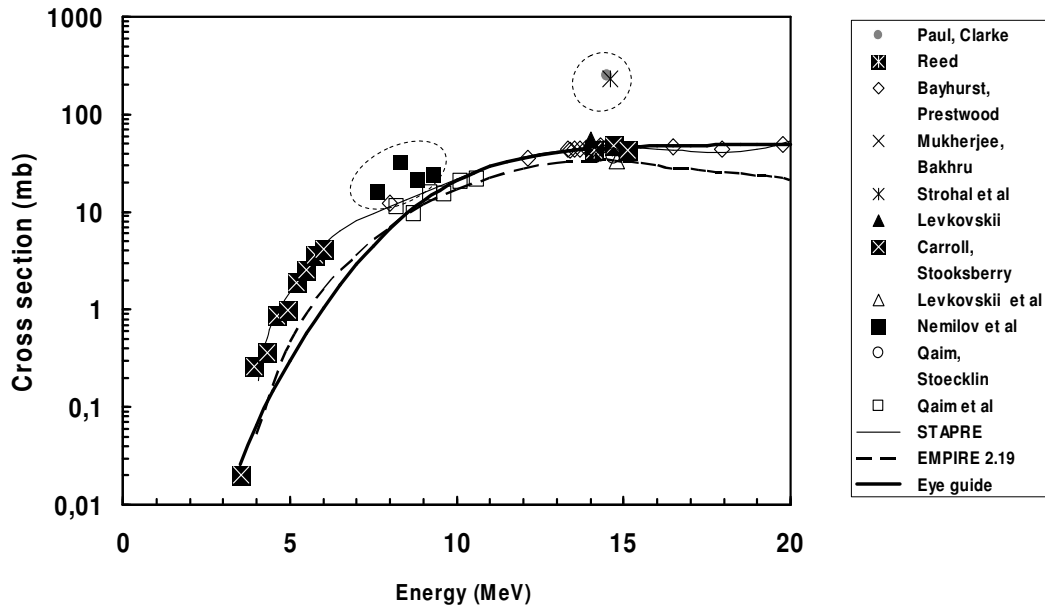


Fig. 1-9 Excitation function of the $^{90}\text{Zr}(n,p)^{90g}\text{Y}$ reaction [cf. EXFOR, 2003]. The discrepant data are encircled and should be neglected. The data of Carroll and Stooksberry [cf. EXFOR, 2003] were shown to be shifted towards lower energies. Therefore an eye guide curve is drawn, concentrating on the newer data from Jülich, and this curve is recommended.

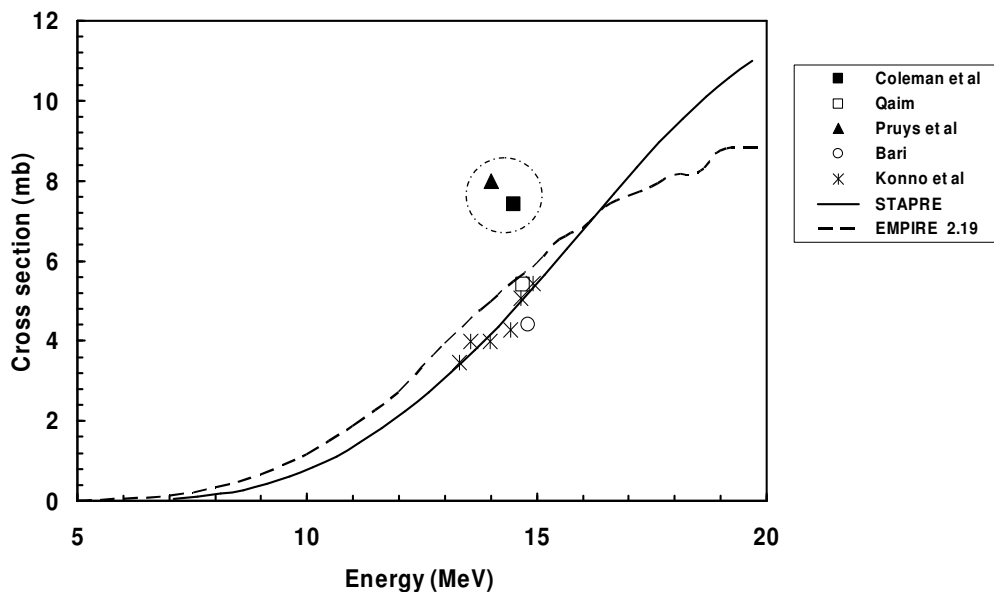


Fig. 1-10 Excitation function of the $^{153}\text{Eu}(n,p)^{153}\text{Sm}$ reaction [cf. EXFOR, 2003]. The discrepant data are encircled and should be neglected. The results of the nuclear model calculation (STAPRE) are recommended.

1.8 Radiochemical separation

The radiochemical processing of irradiated materials is demanded not only for applications of radionuclides in several fields of science, but may be necessary for nuclear data measurements as well. The reasons may be high matrix activity, which masks the radiation of a radionuclide of interest, or the need to remove bulk material from the original target in order to detect soft, or corpuscular radiation (see 1.5). Commonly employed methods are chromatographic techniques, like ion-exchange chromatography or thermo-chromatography, where the separation is achieved by introducing a mobile and a stationary phase. Depending on the different chemical properties (volatility, solubility, complex stability, etc) the separation may be developed. Other important radiochemical methods are solvent extraction and co-precipitation. Within the scope of this work solvent extraction and different chromatographic techniques have been applied.

1.8.1 Separation of lanthanides

Due to their nuclear and chemical properties, several radionuclides of the elements of the lanthanide group are of high interest for nuclear medical applications (cf. 1.9). The chemical separation of the lanthanides from each other, however, is very difficult. This is due to the fact that the 14 elements of the lanthanide group differ only in the occupation of the fourth electron shell (the f-shell). The difference in the ionic radius of the lightest lanthanide Ce, and the heaviest Lu, is only about 0.15 Å, leading to the possibility of isomorphic tenability, and thus to very similar chemical properties.

Over the years, miscellaneous techniques for the separation of lanthanides have been developed, the first of which were the fractionated crystallisation and precipitation [cf. Wieberg, 1995]. These techniques are of mere historical interest today, since they require hundreds of separation cycles and provide only low yields of the pure element. After the introduction of solvent extraction for separation in 1952, which enabled the first extraction of kilogram amounts of pure rare earth elements, the separation of these elements is nowadays done via **ion-exchange chromatography** [cf. Wieberg, 1995]. The reaction scheme beneath (Eq. 9) shows the chemical equilibrium, which is obtained between the lanthanide ion Ln^{3+} and the exchange resin HR [cf. Amphlett, 1964].



The affinity of Ln^{3+} ions towards the exchange resin grows stronger with the increasing ionic radius, thus leading to a faster migration of the lighter lanthanides through the column. This technique proved to be very effective in combination with complex ion chromatography, whose reaction scheme is shown in Equation 10.



The tendency to complexation increases with the decreasing ionic radius, which results in a better solubility of the lighter lanthanides in a solution of a complexing agent (HA) (e.g. α -hydroxy isobutyric acid (AHIB); or di(2-ethylhexyl)orthophosphoric acid (HDEHP)), thus supporting the effect of the ion-exchange.

1.8.2 Separation of Se from As

The quantitative separation of ^{73}Se from an arsenic target is one aim of this work. Since this radiochemical procedure is meant to be applied for the production of several MBq of ^{73}Se for application in PET, the separation technique has to be fast without causing high radiation exposure to the executing employee.

As a radiochemical method, which complies with those demands, the thermochromatography can be utilised. This technique makes use of the different volatility of the compounds to be separated. The spatial separation of the substances is achieved with a carrier gas, which can either be chemically inert or a reagent in the separation. The latter is used for the radiochemical separation of Se and As. Both compounds are oxidised in an O_2 gas stream and volatilised. Since the generated As_2O_3 reacts at lower temperatures than the SeO_2 , a separation is possible. Other systems include temperature gradients, separating inserted compounds through their different condensation temperatures and/or their transport properties.

1.9 Radionuclides in medicine

One of the most important applications of radioactivity is in life sciences, especially in medicine. Today both cyclotron and reactor produced radionuclides find wide applications in diagnosis as well as in palliation therapy and treatment of miscellaneous types of cancer [Qaim and Coenen, 2005].

In the beginning radioactivity was used as a powerful tool for measurements within enclosed systems, since radioactive tracers show not only high sensitivity but they also do not disturb the system under investigation. The first biological experiments applying ^{212}Pb labelled tracers were done by George de Hevesy in 1920 [Hevesy, 1923], followed by metabolic studies of Bi in rabbits [Christiansen et al., 1924]. Based on the availability of further radionuclides provided by small neutron sources and cyclotrons, nuclear methods quickly found their way into medicine [cf. Stöcklin et al., 1995].

1.9.1 Radiotherapy

The therapeutic effect of a radionuclide is based on the destruction of tissue, caused by the ionising radiation generated by radioactive decay. This way, cancerous tumours can be treated, as well as palliative treatment in joints and bones can be conducted. Radiotherapy can be divided into two major categories, namely **external** and **internal radiotherapy**, which are defined through the way of dose application.

1.9.1.1 External radiation therapy

In external radiotherapy the ionising radiation used for treatment originates from an external source. This source can either be a hard β^- , γ - or X-ray emitting nuclide. Examples are ^{60}Co , ^{90}Sr (^{90}Y) and ^{192}Ir . A neutron source or a charged particle accelerator can also be used. Whereas the γ -ray and neutron sources are more suitable for treating tumours deeper in the body, the use of charged particles for therapy has some major advantages. Unlike the interactions of photons with matter, which are of mere stochastic nature, charged particles act directly ionising and possess defined penetration ranges. Due to the **Bragg-Peak effect** the energy deposition occurs mainly at the end point of the charged particle range. In Figure 1-11 a comparison of the behaviour of different radiation types, used for external tumour therapy, can be seen.

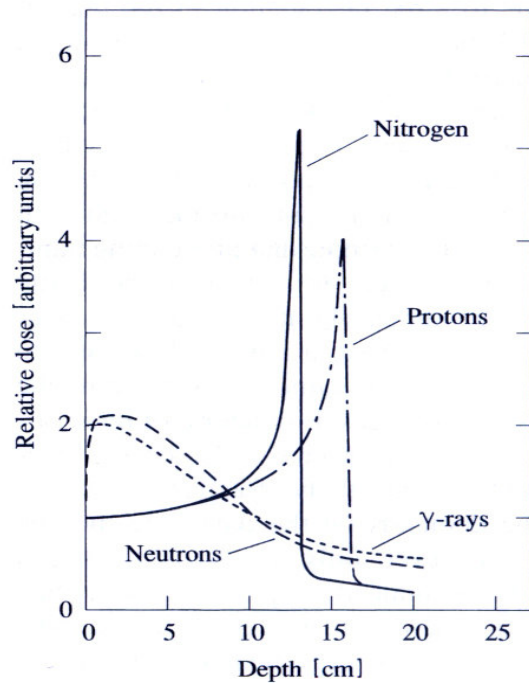


Fig. 1-11 Depth dose distribution of protons, nitrogen ions, neutrons and γ -rays [cf. Qaim, 2001a] in tissue. Whereas the penetration depth is energy dependent, the width of the Bragg-peak is affected by the nature of the projectile.

The neutral particles show an exponential curve progression, due to the statistical nature of their interaction with the tissue, whereas charged particles display the characteristic Bragg-Peak, whose width and intensity increases with the increasing projectile mass. The penetration depth can be influenced through the particle energy. This way it is possible to deliver the mean part of the energy dose into a tumour region, thus preventing unaffected tissue from larger damage.

1.9.1.2 Internal radiotherapy

In internal radiotherapy the source of radiation is brought into a patient's body, preferably into the tumour itself. This can either be achieved by physical means, like it is done in brachytherapy, or by biochemical means, known as endoradiotherapy.

In the **brachytherapy** (*closed source*) the radiation source, e.g. a radioactive seed, needle or colloid, is mechanically injected into the body part that is to be treated. Brachytherapy is a conventional method in cancer therapy as well as in palliation therapy [Hilaris, et al. 1975], and enables the application of high energy doses in a localised region of the body. A disadvantage of this technique, however, is that sensitive organs (e.g. heart, brain, etc.) cannot be treated this way, due to the danger of inserting an object into them. Additionally, brachytherapy demands the utilisation of high energy β - or X-ray emitting nuclides [Hilaris, et al. 1975, Bremer, 1981],

resulting in a larger area of effect, thus endangering healthy tissue within its range as well.

Endoradiotherapy (“*open source*”) is based on the metabolic transport of radioactively labelled tumour binding pharmaceuticals into pathogenic tissue [Schicha et al., 1997]. This kind of therapy became available through the development of such selective pharmaceuticals and is of increasing significance in cancer therapy. The great advantage of the endoradiotherapy is the high selectivity, with which pathogenic tissue can be irradiated. The use of suitable radionuclides enables the targeting of small areas down to the dimension of a cell nucleus [Qaim, 2001b]. Some examples of therapeutic radionuclides and the range of their corresponding radiation are given in Table 1-3. The limits of this technique are the availability of an appropriate pharmaceutical vehicle, showing *in vivo* stability and providing the transport of the applied radionuclide into a tumour.

Table 1-3 Some important therapeutic radionuclides and their corresponding nuclear data [Qaim et al., 2005]

Nuclide	T _{1/2}	Range in tissue*	Nuclide	T _{1/2}	Range in tissue*
³² P	14.3 d	7.5 mm	¹⁵³ Sm	1.9 d	3.8 mm
⁶⁴ Cu	12.7 h	2.6 mm	¹⁶⁹ Yb	32.0 d	15 µm
⁶⁷ Cu	2.6 d	2.6 mm	¹⁷⁷ Lu	6.7 d	0.16 mm
⁸⁹ Sr	50.5 d	6.0 mm	¹⁸⁶ Re	3.8 d	3.9 mm
⁹⁰ Y	2.7 d	8.8 mm	¹⁸⁸ Re	17.0 h	8.7 mm
¹³¹ I	8.0 d	2.0 mm	¹⁹² Ir	73.8 d	2.4 mm

* Calculated with *ESTAR* [Berger et al., 2005] for A-150 Tissue-equivalent Plastic

1.9.2 Radionuclides in medical diagnosis

Radionuclides find manifold application in emission tomography for medical diagnosis [Stöcklin et al., 1995, Schicha et al., 1997, Qaim, 2001c]. Other non-invasive imaging techniques, like computed tomography (CT) or magnetic resonance tomography (MRT), in general give information about tissue structure. The emission tomography shows special advantage in visualising (patho)physiological and metabolic processes, by radioactive labelling of appropriate biochemical compounds. Thus the application of radioactive nuclides enables improved ways of diagnosis in

oncology and in the study of generative diseases like Parkinson's and Alzheimer's disease. This type of tomography is applied either in form of Single Photon Emission Computed Tomography (SPECT), or as Positron Emission Tomography (PET). Important demands on both photon and positron emitting radionuclides employed in this technique are high specific activity, low energy of the emitted radiation and short half-lives. This way the exposure dose to the patient is kept low and, on the other hand, high-resolution images can be achieved. Table 1-4 shows a list of radionuclides important for PET.

Table 1-4 Important radionuclides and their respective nuclear data for PET [Stöcklin et al., 1995, Qaim, 2001c, Firestone, 1996]

Radionuclide	$T_{1/2}$	Mode of decay (%)	Particle energy (keV)	Production route
<i>PET</i>				
^{11}C	20.3 min	β^+ (99.8) EC (0.2)	961	$^{14}\text{N}(p,\alpha)$
^{15}O	122.24 s	β^+ + EC (100)	1732	$^{14}\text{N}(d,n)$
^{18}F	109.6 min	β^+ (97) EC (3)	632	$^{18}\text{O}(p,n)$, $^{20}\text{Ne}(d,\alpha)$
^{68}Ga	68 min	β^+ (90) EC (10)	1899	$^{68}\text{Ge}/^{68}\text{Ga}$ (generator)
^{82}Rb	1.27 min	β^+ + EC (100)	3300	$^{82}\text{Sr}/^{82}\text{Rb}$ (generator)

Although the PET technique generally provides higher sensitivity and quantification, the SPECT is more popular due to lower cost, better availability of the demanded radionuclides. The most important radionuclides for SPECT are $^{99\text{m}}\text{Tc}$ ($T_{1/2} = 6.0$ h), ^{123}I ($T_{1/2} = 13.3$ h) and ^{201}Tl ($T_{1/2} = 3.06$ d). In some cases, like $^{99\text{m}}\text{Tc}$, generator kits are established, which allow a very easy diagnostic application.

1.9.3 Nuclear data for medical application

Nuclear cross section data and decay data are important for applications in many areas of nuclear medicine. The choice of a radioisotope for medical application demands an accurate knowledge of radioactive decay data. In addition, the reaction cross section data are needed for the optimisation of established production routes and the development of new routes [Qaim., 1982, Qaim, 2001a].

With the increasing significance of emission tomography there is great interest in radioisotopes with suitable radiation. Nuclear data on half-lives, energies of emitted radiation and branching decays are necessary in order to develop new radionuclides for application in PET or SPECT, and to estimate internal radiation dose to the patient. As regards therapeutic radioisotopes, high specific activity and thus high radiation dose is deliberately desired, resulting in the demand of optimised production procedures. In Figure 1-12 some of the important types of relevant data are given. For the purpose of radionuclide production, not only the excitation function of the medical radionuclide under investigation is of interest, but the cross section data of other possible side products as well. This way the optimum energy range for production can be identified [Qaim, 2001a]. The atomic and nuclear processes involved in external radiation therapy are well understood; nevertheless, nuclear data are of interest in this field as well. Concerning neutron therapy, the investigation of reaction cross section data gives information on the generation of secondary neutrons and γ -rays, and thus is important for the calculation of radiation dose and transport; the latter is interesting also for shielding considerations. A study of the formation of activation products in the course of radiation therapy, especially when achieved via the emission of charged particles, is of interest for estimation of heat deposit in the tissue.

The preparation of nuclear data for data files and libraries is the basis for proper medical use and allows the choice of a radionuclide for application. For production of radionuclides nuclear reaction data are needed. (Example: IAEA-TECDOC-1211)

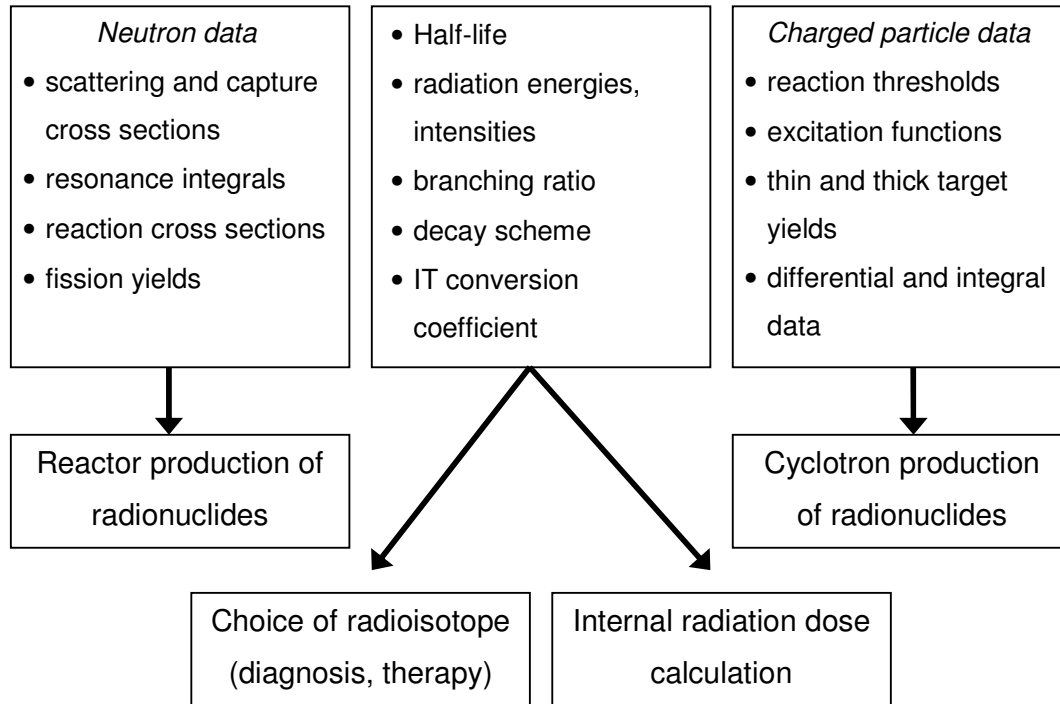


Fig. 1-12 Nuclear data relevant for medical applications [Qaim, 2001a].

1.10 Properties of the investigated nuclides

The radionuclides to be studied in this work are of considerable interest in diagnostic and therapeutic nuclear medicine. In Table 1-5 an overview of the investigated nuclides together with their decay data and the conventional production route is given.

³²P

Natural phosphorus as a monoisotopic element (³¹P) is an important constituent in the biosphere. It is a prevalent element in nature and, in living organisms in particular. It plays a significant role concerning blood, muscle and nerve tissue and is an important component of bones. Radiophosphorus was first used in medicine as orthophosphate for the treatment of myeloproliferative disease [cf. Harman et al., 1976]. Later the radioisotope was employed for palliative treatment of bone metastases and is used today in the form of colloids for the treatment of some cystic intracranial tumours [Taasan et al., 1985].

Table 1-5 Radionuclides under investigation in this work together with their corresponding mean β -energy and their conventional production route

Radionuclide	Half-life	Mode of decay (%)	E_{β} (keV)	Production route(s)
³² P	14.26 d	β^- (100)	1711	³¹ P(n, γ); ³² S(n,p)
⁷¹ As	65.28 h	β^+ (32); EC (68)	816	^{nat} Ge(p,xn) ⁷¹ As
⁷² As	26.01 h	β^+ (77); EC (23)	2500	⁷² Se / ⁷² As - generator
⁷³ As	80.30 d	EC (100)	---	---
⁷⁴ As	17.77 d	β^- (32.1); β^+ (30.9) EC (37.0)	1353; 944	^{nat} Ge(p,xn) ⁷⁴ As
⁷³ Se	7.15 h	β^+ (65); EC (35)	1290	⁷⁵ As(p,3n)
⁸² Sr	25.55 d	EC (100)	---	^{nat} Mo(p,spall); ⁸⁵ Rb(p,4n)
^{90g} Y	64.10 h	β^- (100)	2280	⁹⁰ Sr / ⁹⁰ Y - generator
¹⁵³ Sm	46.27 h	β^- (100)	705	¹⁵² Sm(n, γ)
¹⁶⁹ Yb	32.03 d	EC (100)	---	¹⁶⁸ Yb(n, γ)

The radionuclide ^{32}P is, nowadays, increasingly replaced by its isotope ^{33}P which, due to its longer half-life and considerable lower β -ray energy, is more suitable for therapeutic application.

^{71}As , ^{72}As , ^{73}As and ^{74}As

Elemental arsenic consists exclusively of ^{75}As . The element finds application in the form of many metal alloys and agents for pest control. Arsenic is, furthermore, essential for organisms, as it is involved in different metabolic processes, and non-radioactive arsenic compounds are of interest as anticancer agents. Due to the high toxicity of arsenic in its three-valent form, studies concerning behaviour and distribution of arsenic compounds are also important for ecological systems [cf. Ortiz Escobar, 2006, Basile et al., 1981].

For tracer studies in those two areas the radionuclides ^{76}As ($T_{1/2} = 26.4$ h) and ^{74}As ($T_{1/2} = 17.77$ d) have been suggested [Basile et al., 1981], although the former is rather short-lived. In addition several other radioisotopes of arsenic are very promising with regard to applications in different fields of pharmacology, diagnostics, and cancer treatment [cf. Wang, 2001, Evans et al., 2004, Jennewein et al., 2005]. Especially ^{72}As is a very promising radionuclide for Positron Emission Tomography (PET), as it is an intense β^+ emitter with a suitable half-life and positron energy. Furthermore the radionuclide ^{73}As appears to be more suitable for environmental studies than ^{74}As . Firstly, its half-life is longer and secondly, the emitted radiation is rather soft, thus causing less radiation hazard. The production methods of the four radionuclides of arsenic discussed here have not been fully worked out. Only a few test experiments have been described [Basile et al., 1981, Jennewein et al., 2005].

^{73}Se

The element selenium has six natural isotopes, namely ^{74}Se (0.89 %), ^{76}Se (9.36 %), ^{77}Se (7.63 %), ^{78}Se (23.78 %), ^{80}Se (49.61 %) and ^{82}Se (8.73 %). Selenium finds application in technology, due to its unique conducting properties. In physiology the element is known to be essential. On one hand, deficiency symptoms appear in case of its insufficient presence, and on the other, selenium and its compounds are highly toxic in doses larger than tracer concentrations. Organometallic compounds labelled with radioselenium have found several applications in medicine, i.e. receptor studies

PET using radioselenated adenosine receptor ligands [Blum et al., 2004]. The radionuclide ^{73}Se is a useful substitute for sulphur in PET diagnostics and may replace the more established isotope ^{75}Se ($T_{1/2} = 120$ d), due to its significantly shorter half-life of 7.1 h [cf. Plenevaux, 1990]. As shown in earlier studies on the synthesis of radioselenoethers [Blum et al., 2001] this nuclide may be a promising label for *in vivo* PET studies. It is generally produced via the $^{75}\text{As}(p,3n)$ process [Mushtaq et al., 1988].

^{82}Sr , ^{85}Sr

Strontium shows four stable isotopes in nature, viz. ^{84}Sr (0.56 %), ^{86}Sr (9.86 %), ^{87}Sr (7.00 %) and ^{88}Sr (82.58 %). The element finds its major application as luminescent material in colour screens. In physiology strontium behaves generally like its homologue calcium and is neither essential nor toxic for the human body. The $^{82}\text{Sr}/^{82}\text{Rb}$ radionuclide generator is used very commonly in positron emission tomography (PET). The radionuclide ^{82}Sr ($T_{1/2} = 25.5$ d) decays purely by EC to the short-lived ^{82}Rb ($T_{1/2} = 1.3$ min, $I_{\beta^+} = 95$ %, EC = 5 %; $E_{\beta^+} = 3.1$ MeV, $E_{\gamma} = 776.5$ keV, $I_{\gamma} = 13.4$ %) which finds application in cardiac blood flow studies. The parent ^{82}Sr is either produced via the spallation of Mo or via the (p,xn) reaction on $^{\text{nat}}\text{Rb}$. Occasionally the (p,4n) reaction on enriched ^{85}Rb is also used.

The importance of the radionuclide ^{85}Sr ($T_{1/2} = 64.9$ d) lies in its role as a by-product in the production of the diagnostic ^{82}Sr via the (p,xn) reaction. The production rate of ^{85}Sr is significant for the evaluation of the $^{\text{nat}}\text{Rb}(p,xn)^{82}\text{Sr}$ process for medical application.

^{90}gY

Yttrium is a monoisotopic element (^{89}Y). Due to the low neutron capture cross section, the element is of considerable significance in reactor technology. Additionally it is utilised as a luminescent material. Yttrium is not essential for the human body and is known to be toxic. In nuclear medicine ^{90}gY is used occasionally in palliation therapy of bone metastases [Kutzner et al., 1982]. The most important application of the radionuclide is in the form of ^{90}Y -glass microspheres (Thera Spheres), which are used in the treatment of liver and bone tumours [Herba et al., 1988, Shapiro et al., 1989]. It is generally obtained via the $^{90}\text{Sr}/^{90}\text{Y}$ generator system, the parent nuclide ^{90}Sr being available in large quantities as a fission product.

¹⁵³Sm

Samarium belongs to the group of lanthanides. It appears in the form of four stable nuclides, viz. (¹⁴⁴Sm (3.07 %), ¹⁵⁰Sm (7.38 %), ¹⁵²Sm (26.75 %) and ¹⁵⁴Sm (22.75 %), and three primordial isotopes, namely ¹⁴⁷Sm ($T_{1/2} = 1 \cdot 10^{11}$ a), ¹⁴⁸Sm ($T_{1/2} = 7 \cdot 10^{15}$ a) and ¹⁴⁹Sm ($T_{1/2} = 2 \cdot 10^{15}$ a). It finds application in luminescent materials and metal alloys. The radionuclide ¹⁵³Sm is produced via the (n,γ) reaction with relatively low specific radioactivity. In nuclear medicine, it is employed mainly as EDTMP chelate for the treatment of bone metastases, substituting ^{90g}Y and ³²P [cf. Stöcklin et al., 1995, Hoefnagel, 1991], mainly due to its more advantageous decay properties.

¹⁶⁹Yb

The lanthanide ytterbium consists of 7 stable isotopes, namely ¹⁶⁸Yb (0.13 %), ¹⁷⁰Yb (3.05 %), ¹⁷¹Yb (14.3 %), ¹⁷²Yb (21.9 %), ¹⁷³Yb (16.12 %), ¹⁷⁴Yb (31.8 %), ¹⁷⁶Yb (12.7 %). It is applied in the processing of metal alloys. The radionuclide ¹⁶⁹Yb is almost a pure Auger electron and X-ray emitter and has been gaining interest in brachytherapy as a potential substitute for ¹²⁵I and ¹⁹²Ir (Mason et al., 1992; Fan et al., 2001). Since it is a relatively high-energy X-ray emitter, ¹⁶⁹Yb has also found application in medical diagnostics, especially in cisternography as ¹⁶⁹Yb-DTPA (diethylene-triamine pentaacetic acid) complex (DeLand et al., 1971). To date ¹⁶⁹Yb is generally produced at a nuclear reactor via the (n,γ) process on highly enriched ¹⁶⁸Yb.

2 Aims of this work

The work to be performed during this study should have five major directions:

- (i) integral cross section measurements of a few nuclear reactions using a d(Be) neutron field,
- (ii) studies on new production routes of therapeutic radionuclides using neutrons and charged particle induced reactions,
- (iii) measurement of excitation functions of $^{nat}\text{Ge}(p,xn)^{71,72,73,74}\text{As}$ reactions up to 100 MeV,
- (iv) standardisation of the $^{nat}\text{Rb}(p,xn)^{82,85}\text{Sr}$ reaction data with reference to the production of ^{82}Sr , and
- (v) preliminary investigations on the production of ^{73}Se via the $^{75}\text{As}(p,3n)$ reaction using novel targetry.

The major aim of the integral cross section measurements should be to investigate the formation of the therapeutic radionuclides ^{32}P , ^{90}Y and ^{153}Sm via (n,p) reactions in a 14 MeV d(Be) neutron field. A comparison of the measured data with the integrated data obtained from the known excitation function and the neutron spectral distribution should then allow a validation of the excitation function.

Regarding new routes for production of some therapeutic radionuclides, both neutron and charged particle induced reactions should be investigated. The radionuclide ^{32}P is conventionally produced via the (n,p) process on ^{32}S . Since the (n,p) reaction cross section with fission neutrons is not very high, the application of a harder neutron spectrum, like the d(Be) breakup neutron spectrum, may be an interesting alternative to the conventional production route. Similarly the possibility of production of ^{153}Sm via the $^{nat}\text{Eu}(n,p)^{153}\text{Sm}$ reaction with fast d(Be) neutrons should also be evaluated. The two therapeutic radionuclides ^{153}Sm and ^{169}Yb are generally produced at a nuclear reactor via the (n, γ) process. This method leads to high production yields but allows only low specific radioactivity. In order to obtain ^{153}Sm in no-carrier-added form, the $^{nat}\text{Nd}(\alpha,n)$ reaction should be investigated up to 26.5 MeV. Similarly, in the case of ^{169}Yb the $^{169}\text{Tm}(p,n)^{169}\text{Yb}$ reaction should be studied with proton energies up to 19 MeV.

The third direction of this work should be towards cross section measurements concerning the production of the radionuclides ^{71}As , ^{72}As , ^{73}As and ^{74}As , the radionuclide ^{73}As being of interest in environmental research and the others in diagnostic nuclear medicine. Measurements should be done on the $^{\text{nat}}\text{Ge}(p,xn)^{71,72,73,74}\text{As}$ reactions with protons in the energy range up to 100 MeV. For analysis and validation of some data experiments on enriched ^{72}Ge should also be performed. The experimentally determined data should be compared with the results of nuclear model calculations. Furthermore, integral yields should be calculated and the possibilities of production of the four radionuclides should be discussed.

The radionuclide ^{82}Sr is the basis of the $^{82}\text{Sr}/^{82}\text{Rb}$ -generator system, which is of high interest for Positron Emission Tomography (PET). It is often produced via the $^{\text{nat}}\text{Rb}(p,xn)^{82}\text{Sr}$ reaction. It is planned to standardise the production data. Besides evaluation of the existing data, some measurements should be done on the excitation function of the $^{\text{nat}}\text{Rb}(p,xn)^{85}\text{Sr}$ reaction, which is the most significant radionuclidic impurity in this production route. Finally, the evaluated data should be validated by measuring thick target yield of ^{82}Sr and the percentage of the ^{85}Sr impurity for various energy ranges and comparing them with the values calculated from the excitation functions.

The last aspect of this thesis should deal with the production of n.c.a. ^{73}Se via the $^{75}\text{As}(p,xn)$ reaction using a novel target material. The presently used Cu_3As alloy can withstand high-current irradiations; however, it is difficult to prepare this alloy and due to the high proportion of copper, the activation of the target is high, leading to a high radiation exposure to the worker. For these reasons, the AlAs alloy should be investigated as a new target material. Besides its lesser activation by proton bombardment, it has a higher arsenic proportion of about 74 %, leading to higher possible yields. Production tests using AlAs should be performed and an effective radiochemical separation method should be developed.

3 Experimental

3.1 General

The experimental work was performed with the aim to determine energy dependent as well as spectrum averaged cross sections. Thus irradiations with fast spectral neutrons as well as with alpha particles and protons of different incident energies were done. All neutron irradiations were carried out at the compact cyclotron CV 28 of the Forschungszentrum Jülich GmbH. Proton beams with particle energies up to 20 MeV and alpha particle beams of energies up to 26.5 MeV were also available at the compact cyclotron CV 28. For irradiations with protons over the energy range of 20 to 45 MeV the injector cyclotron of the Cooler Synchrotron (COSY) of the Forschungszentrum Jülich was used. The experiments on the proton induced reactions on arsenic were done in collaboration with the Isotope Production section of the *Laboratory for Accelerator Based Sciences* (iThemba LABS) in Somerset West, South Africa. For those studies three different cyclotrons were used: the CV 28 and the injector of COSY of the Forschungszentrum Jülich, and the Separate Sector Cyclotron (SSC) of iThemba LABS. The investigation of the $^{169}\text{Tm}(p,n)^{169}\text{Yb}$ reaction was done in collaboration with the Institute of Nuclear Research (ATOMKI) of the Hungarian Academy of Sciences in Debrecen, Hungary, which was supported by a scholarship of the Deutsche Akademische Austauschdienst (DAAD). For this purpose irradiations were carried out at the CV 28 in Jülich and at the cyclotron MGC-20E in Debrecen. Table 3-1 gives an overview of all irradiations performed and nuclear reactions studied in the course of this work.

Table 3-1 Irradiations performed and nuclear reactions studied in this work

Target	Nuclear reaction	Irradiation facility
^{nat}S ,	$^{nat}\text{S}(n,x)^{32}\text{P}$	CV 28 *
^{nat}Ge , ^{72}Ge	$^{nat}\text{Ge}(p,xn)^{71,72,73,74}\text{As}$, $^{72}\text{Ge}(p,xn)^{71,72}\text{As}$	CV 28, COSY injector, SSC
^{nat}As	$^{75}\text{As}(p,3n)^{73}\text{Se}$	COSY injector
^{nat}Rb	$^{nat}\text{Rb}(p,xn)^{82,85}\text{Sr}$	COSY injector, SSC
^{nat}Zr	$^{90}\text{Zr}(n,p)^{90}\text{Y}$	CV 28 *
^{nat}Eu	$^{153}\text{Eu}(n,p)^{153}\text{Sm}$	CV 28 *
^{nat}Nd	$^{150}\text{Nd}(\alpha,n)^{153}\text{Sm}$	CV 28
^{nat}Tm	$^{169}\text{Tm}(p,n)^{169}\text{Yb}$	CV 28, MGC-20E, COSY injector

* Neutrons produced using a d(Be) target.

3.2 Target preparation

The procedure of target preparation depended on the kind of irradiation. In the case of neutron irradiations, energy degradation was not a point of concern; thus thicker targets could be prepared. For charged particle irradiations, on the other hand, usage of thin targets was mandatory in order to obtain differential cross section data.

3.2.1 Preparation of thin targets via sedimentation

For the preparation of thin targets needed in the investigations on the $^{nat}\text{Ge}(p,xn)$, $^{72}\text{Ge}(p,xn)$, $^{nat}\text{Rb}(p,xn)$, $^{nat}\text{Nd}(\alpha,n)$ and $^{169}\text{Tm}(p,n)$ reactions, the sedimentation technique was applied [Rösch et al., 1993]. In general, metal foils are established as effective and easily manageable target materials for irradiations. Since metal foils of Rb, Nd and Tm are hardly available and are quickly oxidised under normal conditions, target samples were prepared in the form of thin layers of their respective oxide or chloride. In the case of germanium, however, both metal foils and oxide sediments were irradiated. Table 3-2 shows a list of the utilised compounds.

Table 3-2 Compounds used for target preparation via the sedimentation technique

GeO ₂	99.999 %	ChemPur Feinchemikalien und Forschungsbedarf GmbH
RbCl	98.5 %	Koch-Light Laboratories Ltd.
	99.99 %	Aldrich Chemical Company Inc.
Nd ₂ O ₃	99.999 %	Koch-Light Laboratories Ltd.
Tm ₂ O ₃	99.99 %	Koch-Light Laboratories Ltd.

The sedimentation was done using a sedimentation cell made of Teflon, as it is shown in Figure 3-1. Inside the cell an aluminium backing foil (99.5 % pure) is fixed and the material meant for sedimentation is transferred on top in the form of a suspension. As solvent for the suspension of RbCl, Nd₂O₃ and Tm₂O₃, high-purity ethanol was used. In the case of GeO₂ a mixture of ethanol and water (2:1) was employed. The enriched ⁷²Ge (96.4 %) was obtained from Chemotrade Chemiehandelsgesellschaft mbH. The solvent was slowly evaporated, leading to the formation of thin sediments attached to the backing foil. In order to ensure good adhesion of the sedimented powder to the backing material, the Al foils were washed before use with diluted HCl and acetone. The homogeneity of the sample was verified using either a microscope or a strong magnifying lens (*LUXO Deutschland GmbH*). Due to the high fragility of the sediment, each sample was carefully covered with an aluminium foil of 10 µm thickness.

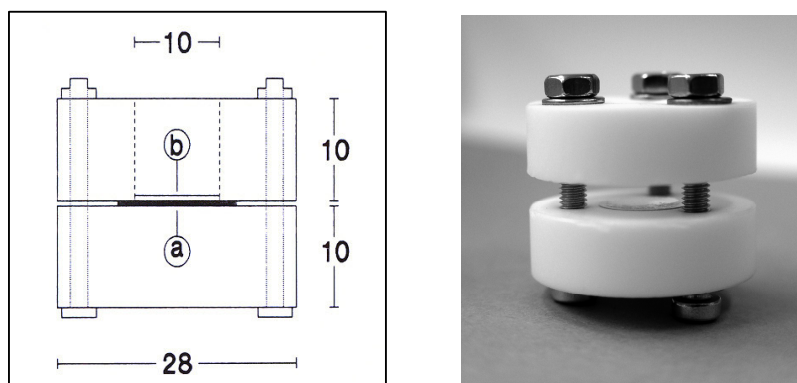


Fig. 3-1 Scheme and picture of a sedimentation cell containing a GeO₂ sediment (b) on an Al backing foil (a).

3.2.2 Preparation of targets for the production of ^{73}Se

Concerning experiments on the improved production of ^{73}Se , three different methods of target preparation were applied.

Firstly, aiming towards a reproducibility of the previously reported results on the production of radioselenium [Blessing et al., 1994, Blum, 2003], 0.5 to 1.0 mm thick samples of Cu_3As alloy were irradiated. Details on the preparation of these samples are given in previous publications from this institute [Blessing et al., 1982, Blessing and Qaim, 1984].

In the later irradiations, AIAs was tested as target material, aiming at improved yields and simpler target preparation. The compound was obtained from *Aldrich Chemical Company, Inc.* and was pressed into pellets of 13 mm diameter with weights of 0.6 to 1.4 g. The pellets were prepared under a pressure of 10 t/cm^2 and wrapped into 10 μm thick Al foil afterwards for protection. However, the compound proved to be badly compressible and decomposed under normal conditions within one day, thus being inappropriate for irradiation.

As a third method, AIAs pellets were prepared under vacuum at iThemba LABS. The pellets (16 mm diameter) were pressed into Al capsules with a wall thickness of 0.75 mm and sealed under vacuum.

3.2.3 Preparation of targets for neutron irradiations

For the preparation of the S, ZrO_2 and Eu_2O_3 samples, pellets of different thicknesses were pressed using high-purity materials. In the case of S and ZrO_2 very thin pellets of about 0.5 to 1.0 mm thickness were prepared and packed in a thin polyethylene film or 10 μm thick Al foil. The Eu_2O_3 irradiation samples were prepared by adding an equal amount of KCl powder to obtain higher stability of the pellets, which were about 3 mm thick and were placed inside Al capsules of 0.5 mm wall thickness and 20 mm diameter for irradiation.

3.3 Irradiation experiments

3.3.1 Irradiations with d(Be)-breakup neutrons

The experimental setup for all irradiations using the d(Be) neutron source of the Forschungszentrum Jülich (see 1.5.1) was the same for S, ZrO₂ and Eu₂O₃. The sample was placed between two stacks of monitor foils (see 3.3.1.2). Those targets were positioned at a distance of 1 cm from the d(Be) neutron source, in 0° direction of the incoming deuteron beam. Figure 3-2 shows a sketch of the experimental setup for neutron irradiations and the target stack.

For d(Be) neutron generation, irradiations were carried out using a 14 MeV deuteron beam of 5 μA beam current, which was determined using a Faraday Cup. The determination of the neutron flux in the target is explained in detail in section 3.3.1.2. The bombardment time varied according to the nuclear reaction under investigation between 1 and 5 hours. An overview of all the irradiation experiments done in this work is given in Table 3-7.

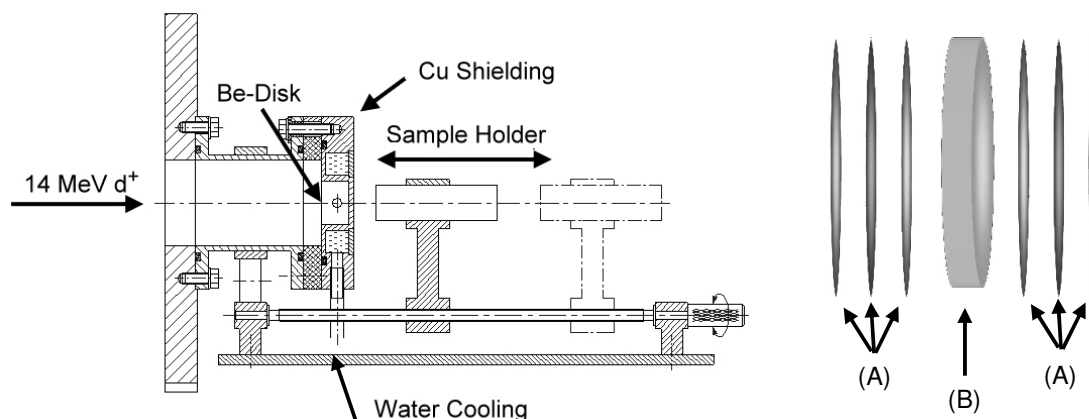


Fig. 3-2 *Left:* sketch of the d(Be) neutron target. The 5 μA deuteron beam comes from the left. *Right:* Target stack, containing the monitor foils (A) and the sample material (B), is placed on the adjustable sample holder at a distance of 1 cm from the copper shielding.

3.3.1.1 Characterisation of the neutron spectrum

The breakup neutrons generated at the 14 MeV d(Be) source at the CV 28 (see 1.5.1) show an energy distribution over a range of about 15 MeV. Precise information on this spectrum is essential for the calculation and validation of all cross section measurements.

The neutron spectrum characterisation was accomplished via the multiple-foil activation technique. The basic data for the calculation were obtained through the irradiation of different metal foils, inducing 11 different nuclear reactions with threshold energies between 0.4 and 12.4 MeV (see Table 3-3). The radioactivity of each product nuclide was determined via conventional high-resolution γ -ray spectrometry. For unfolding the neutron spectrum, the code **SULSA** [Sudár, 1989] was used. It is an iterative code based on the generalized least squares method and does not require any input spectrum. The calculation of the neutron energy distribution is based on the produced radioactivity on the one hand, and on the known cross section and covariance data of the induced reactions on the other. The deduced neutron spectrum in the 0° direction for a primary deuteron energy of 14 MeV on Be is given in Figure 3-3. This spectrum was adopted as the standard neutron field for integral measurements.

Table 3-3 Nuclear reactions and threshold energies in multiple foil activation

Nuclear reaction	Half-life	Threshold energy (MeV)
$^{58}\text{Ni}(n,p)^{58m+g}\text{Co}$	70.91 d	0.4
$^{115}\text{In}(n,n')^{115m}\text{In}$	4.48 h	0.4
$^{47}\text{Ti}(n,p)^{47}\text{Sc}$	3.34 d	1.0
$^{54}\text{Fe}(n,p)^{54}\text{Mn}$	312.2 d	1.5
$^{46}\text{Ti}(n,p)^{46m+g}\text{Sc}$	83.83 d	1.8
$^{56}\text{Fe}(n,p)^{56}\text{Mn}$	2.57 h	2.8
$^{27}\text{Al}(n,\alpha)^{24}\text{Na}$	15.03 h	3.2
$^{48}\text{Ti}(n,p)^{48}\text{Sc}$	1.82 d	3.2
$^{197}\text{Au}(n,2n)^{196}\text{Au}$	6.18 d	8.0
$^{93}\text{Nb}(n,2n)^{92m}\text{Nb}$	10.15 d	8.8
$^{58}\text{Ni}(n,2n)^{57}\text{Ni}$	1.50 d	12.4

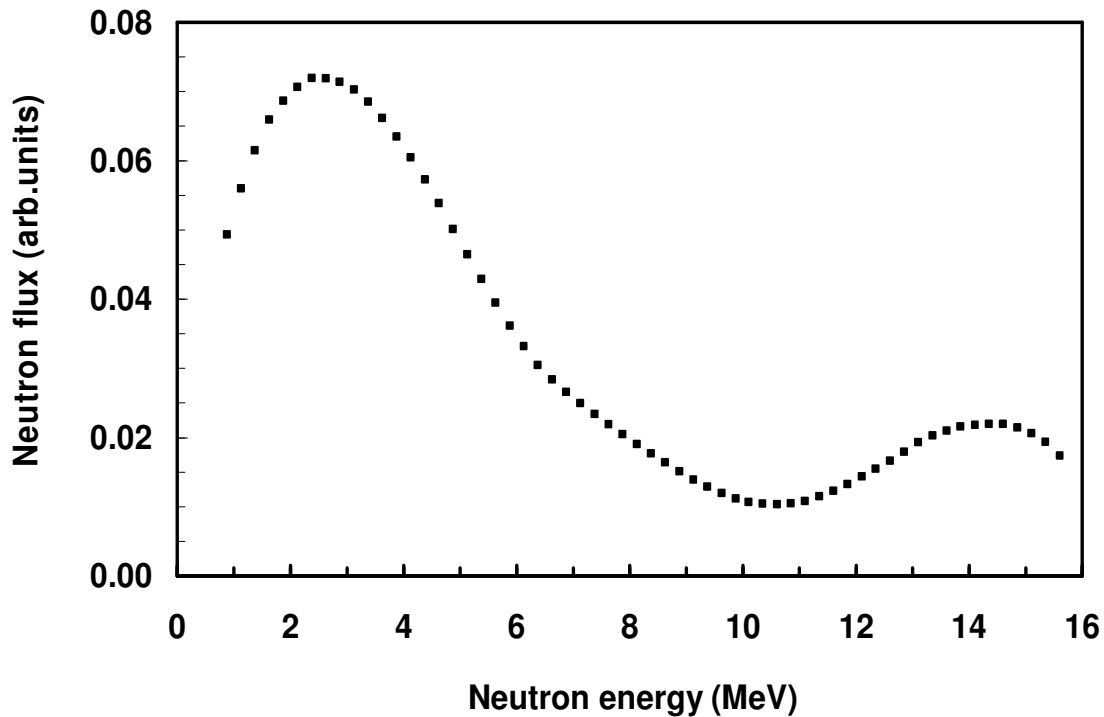


Fig. 3-3 Energy spectrum of 14 MeV d(Be) neutrons determined via multiple foil activation and the iterative computer code SULSA.

3.3.1.2 Determination of the neutron flux density

The determination of the neutron flux during irradiations was done through neutron induced nuclear reactions, whose reaction cross sections are well known and whose reaction products could be measured easily via γ -ray spectrometry. A list of these so-called *monitor reactions*, which were applied in this work, is given in Table 3-4 together with the decay data of interest. The monitor foils were introduced into the experiment (Fig. 3-2) in their natural isotopic composition. The produced activity was measured via γ -ray spectrometry, and the activity at the end of bombardment (EOB) was deduced from a decay curve analysis, utilising known half-lives. In the case of ^{58}Co , the γ -ray measurement was done after a waiting period of several days, in order to allow complete decay of $^{58\text{m}}\text{Co}$ ($T_{1/2} = 8.94$ h) to $^{58\text{g}}\text{Co}$.

Table 3-4 Monitor reactions and nuclear decay data important for the determination of neutron flux densities

Nuclide (abundance in %)	Nuclear reaction	Half-life [h]	E_γ [keV]	Intensity [%]
^{56}Fe (91.7)	$^{56}\text{Fe}(n,p)^{56}\text{Mn}$	2.58	846.8	98.87
			1810.8	27.20
			2113.12	14.3
^{27}Al (100)	$^{27}\text{Al}(n,\alpha)^{24}\text{Na}$	14.97	1368.6	100.00
			2754.0	100.00
^{58}Ni (68.27)	$^{58}\text{Ni}(n,p)^{58}\text{Co}$	1699.68	810.8	99.0
			863.9	68.3
			1674.7	51.8

Table 3-5 Spectrum averaged cross sections of the applied monitor reactions for the 14 MeV d(Be) neutron spectrum

Monitor reaction	$^{27}\text{Al}(n,\alpha)^{24}\text{Na}$	$^{56}\text{Fe}(n,p)^{56}\text{Mn}$	$^{58}\text{Ni}(n,p)^{58}\text{Co}$
Averaged cross section [mb]	16.31	16.51	343.42

On the basis of the measured radioactivity at EOB (see 3.6.1) and the known excitation function of the monitor reaction, which was taken from the Reference Neutron Activation Library (RNAL) [IAEA-TECDOC-1285], the neutron flux (Φ) during the irradiation could be calculated by converting Equation 6 to the following form:

$$\Phi = \frac{A_{\text{EOB}}}{\sigma \cdot N_x \cdot H \cdot (1 - e^{-\lambda \cdot t})} \quad (13)$$

The number of nuclei N_x was obtained from the mass of the respective foil corrected for the composition and the chemical purity of the material (see Appendix). In Equation 13, σ is the spectrum averaged cross section of the nuclear reaction, which is obtained by multiplying the characterised neutron energy spectrum (see 3.3.2) with the excitation function of the relevant monitor reaction (Figures 3-4 to 3-6). The resulting spectrum averaged cross sections of the used monitor reactions are given in Table 3-5. The average neutron flux generated through the $d(\text{Be})$ source during irradiations with 14 MeV deuterons and a beam current of 5 μA , was found to be about $7 \cdot 10^{10} \text{ n} \cdot \text{s}^{-1} \cdot \text{cm}^{-2}$.

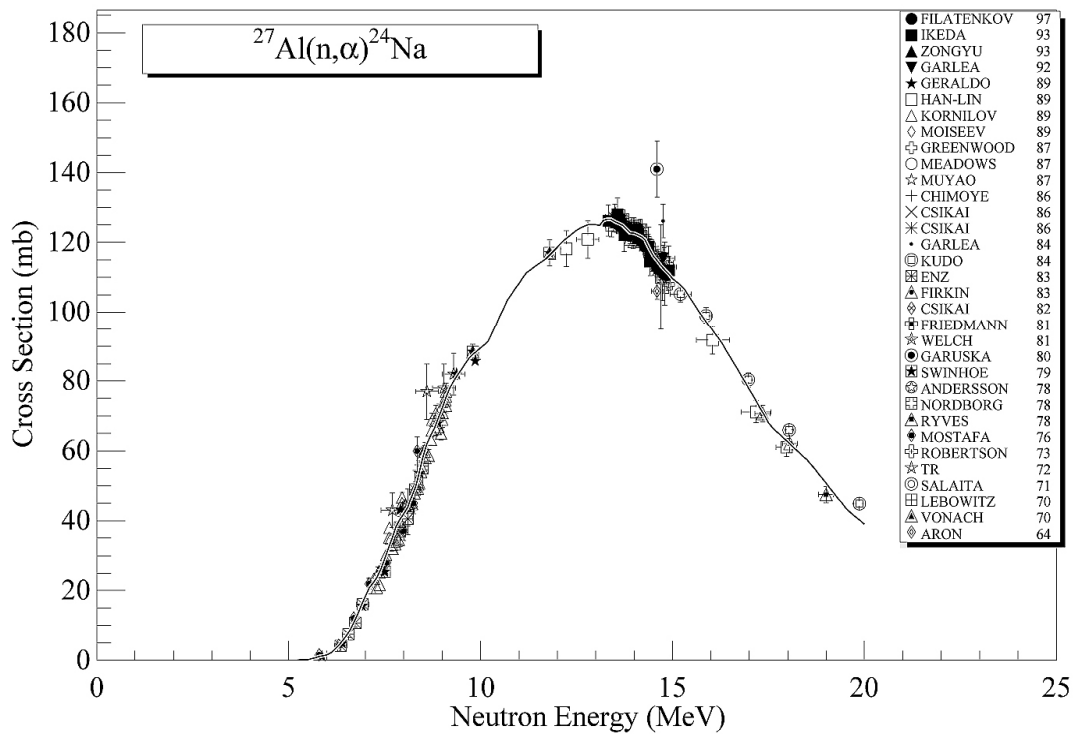


Fig. 3-4 Excitation function of the (n,α) reaction on ^{27}Al from RNAL used for the determination of the neutron flux density in the $d(\text{Be})$ neutron field.

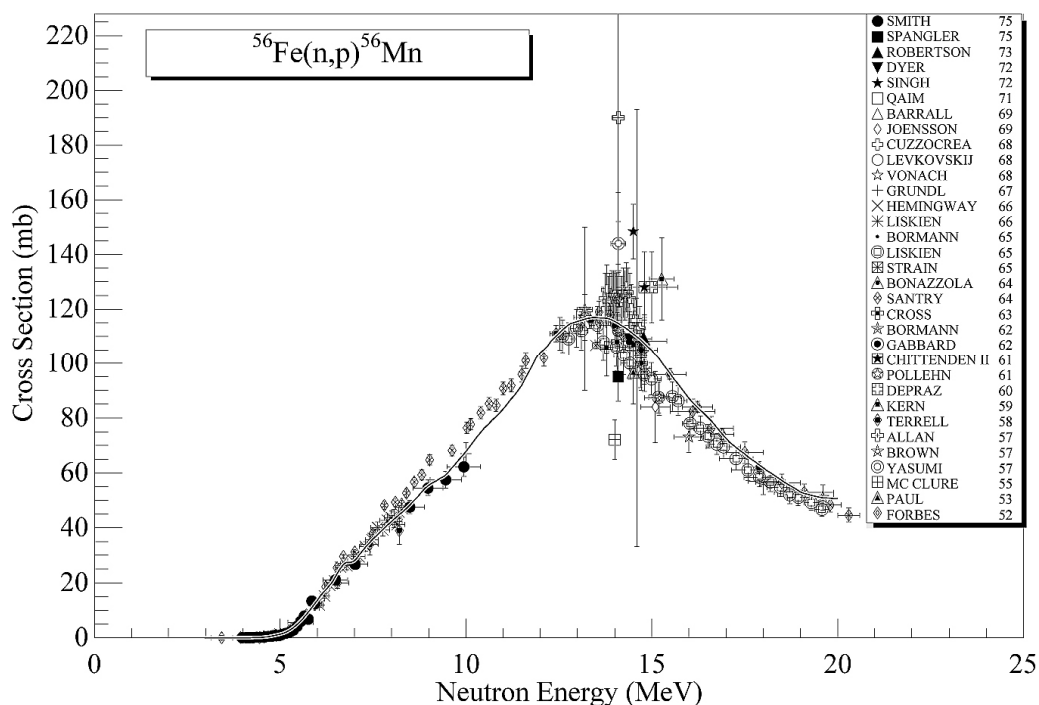


Fig. 3-5 Excitation function of the (n,p) reaction on ^{56}Fe from RNAL used for the determination of the neutron flux density in the d(Be) neutron field.

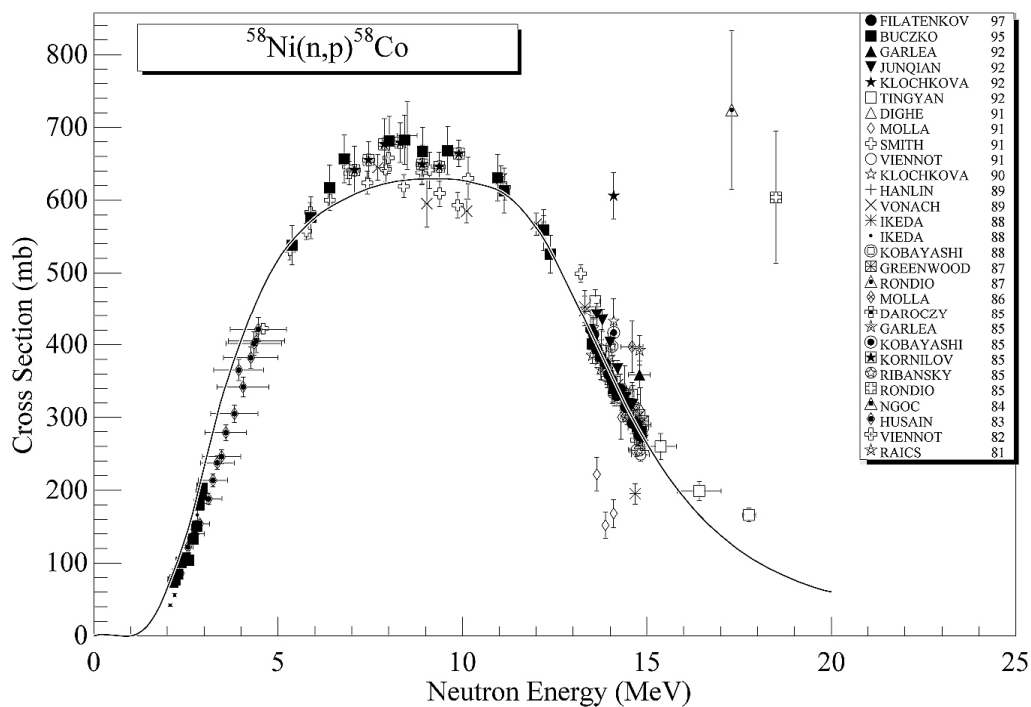


Fig. 3-6 Excitation function of the (n,p) reaction on ^{58}Ni from RNAL used for the determination of the neutron flux density in the d(Be) neutron field.

3.3.2 Irradiations with charged particles

3.3.2.1 Irradiation facilities

The charged particle irradiations required in this work were carried out at four different cyclotrons. In general, all proton irradiations with energies up to 20 MeV were done at the compact cyclotron CV 28 of the Forschungszentrum Jülich. In the case of $^{169}\text{Tm}(p,n)^{169}\text{Yb}$ reaction studies, experiments were also done at the MGC-20E cyclotron of the ATOMKI in Debrecen, whose technical parameters are similar to the parameters of the CV 28. All irradiations with α -particles were done at the CV 28. For irradiation at the CV 28 and the MGC-20E the sample stack (see 1.4.1) was put into an aluminium target holder and fastened to the beam line. The target holder had an inner diameter of 13 mm and was cooled by water from its backside (2π cooling). Figure 3-7 shows the arrangement of the target holder attached to the cyclotron beam line.

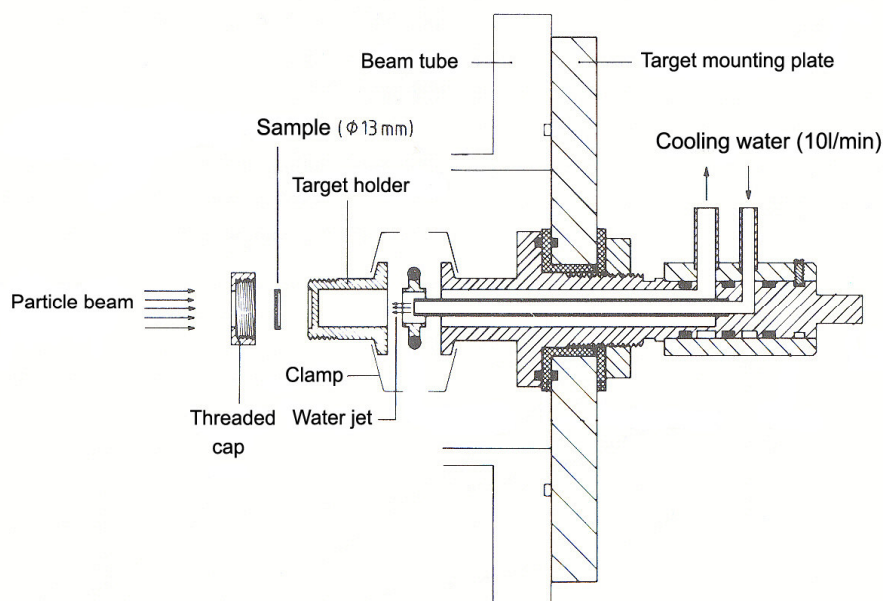


Fig. 3-7 Irradiation facility at the CV 28 [Blessing et al., 1982].

For irradiations with proton energies up to 45 MeV the injector cyclotron of the Cooler Synchrotron (COSY) of the Forschungszentrum Jülich was used. The target system at the injector includes an internal irradiation facility. The irradiation beam is extracted with a tungsten septum (Fig. 3-8). The energy adjustment of the proton beam was achieved by selecting an appropriate orbit of the extracted beam, having the

disadvantage of a rather poor separation of orbits. Therefore all cross section measurements were done using the maximum energy of 45 MeV, thus eliminating this problem. The energy adjustment in the target was done by introducing degrader foils into the stack (cf. Fig. 1-6). The target holder (Fig. 3-9), in which the stack was placed, consists of an Al body and an adjustable stack holder.

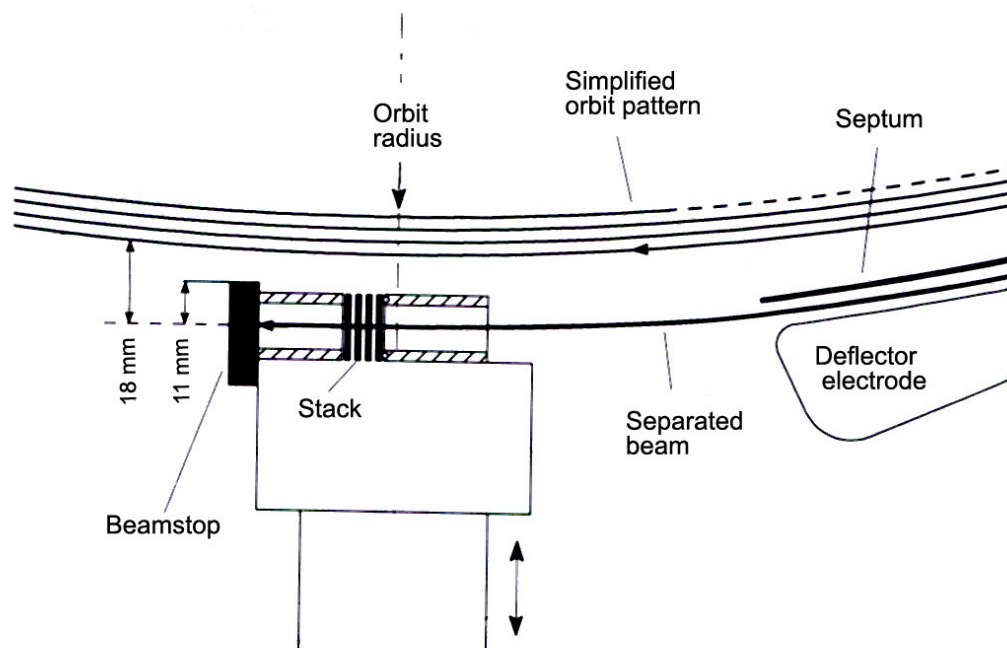


Fig. 3-8 Facility for beam extraction and sample irradiation at the injector of COSY [Blessing et al., 1995].

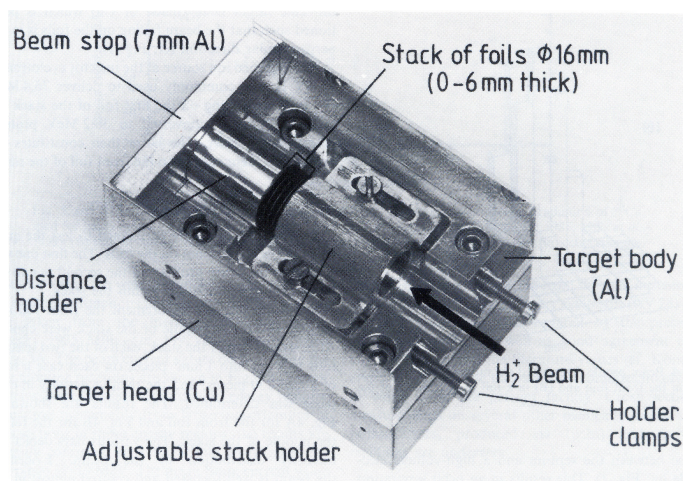


Fig. 3-9 Target holder for the irradiation of foil stacks at the injector of COSY [Blessing et al., 1995].

If necessary the stack was fixed additionally with an aluminium distance holder. At the end of the target system a 7mm thick Al beam stop is affixed.

In cooperation with iThemba LABS in Somerset West, South Africa, proton bombardments were carried out with incident particle energies of 66 and 99 MeV. Target samples were mounted onto metal frames, allowing sample diameters of 10 to 20 mm. These frames were irradiated in stacks according to the stacked-foil technique explained above (1.4.1), using degrader foils for energy adjustment. Activation experiments at iThemba LABS were performed in an electrically isolated irradiation chamber, which is a modified version of the *Recoil-Range-Measurements* facility (RERAME) installed at the *Laboratory Nazionale del Sud* (LNS) in Catania, Italy [Fresca Fantoni et al., 1994]. The chamber features a collimator assembly with electron suppression and acts as a Faraday chamber, allowing for accurate measurement of the integrated beam current. Due to a transparent front window the beam positioning and focussing can be done with a BeO viewer placed at the position of the target. Figure 3-10 shows a picture of the irradiation chamber. A detailed description of the facility is given by Szelecsényi et al. [2005].



Fig. 3-10 Modified RERAME irradiation chamber. The collimator and vice assemblies are mounted on the door. The beam enters the chamber from the left [Szelecsényi et al., 2005].

3.3.2.2 Determination of charged particle flux

Regarding the determination of particle flux during different irradiation experiments with protons and ^4He ions, it was possible to measure the particle fluence via the beam integrators, which are available at all the cyclotrons used. However, for all experiments monitor foils were inserted according to the procedure described for neutron irradiations (3.3.1.2). The proton beam currents were generally determined using Cu foils; however, for higher energies (>25 MeV) the cross sections of the $^{\text{nat}}\text{Cu}(p,xn)$ processes become rather low, making the use of Ni monitor foils more advantageous. The monitor reactions applied for the flux determinations are given in Table 3-6. The fluences were calculated analogous to section 3.3.1.2 using the absolute activity induced in the monitor foils and Equation 13. The reaction cross section at a particular projectile energy was taken from the literature [Tárkányi et al., 2001], and the monitor excitation functions are shown in Figures 3-11 to 3-14. For the determination of the proton or ^4He fluences, the results of the monitor measurements were favoured, due to the higher uncertainty of the beam integrator results. As regards the irradiations using the modified RERAME chamber at the SSC mentioned above, the results of the electronically determined fluxes were even slightly more accurate than the results of the monitor foil measurements, both agreeing within 5 % deviation. For those cases, averaged values were used for further calculations.

Table 3-6 Monitor reactions and nuclear decay data important for the determination of charged particle flux densities

Monitor foil	Nuclear reaction	Half-life	E_γ [keV]	Intensity [%]
Cu	$^{\text{nat}}\text{Cu}(p,xn)^{62}\text{Zn}$	9.19 h	596.56	26.2
	$^{\text{nat}}\text{Cu}(p,xn)^{63}\text{Zn}$	38.47 min	669.62	8.2
Ni	$^{\text{nat}}\text{Ni}(p,pn)^{57}\text{Ni}$	36.0 h	1377.63	81.7

Ti	$^{\text{nat}}\text{Ti}(\alpha,xn)^{51}\text{Cr}$	27.70 d	320.08	9.9

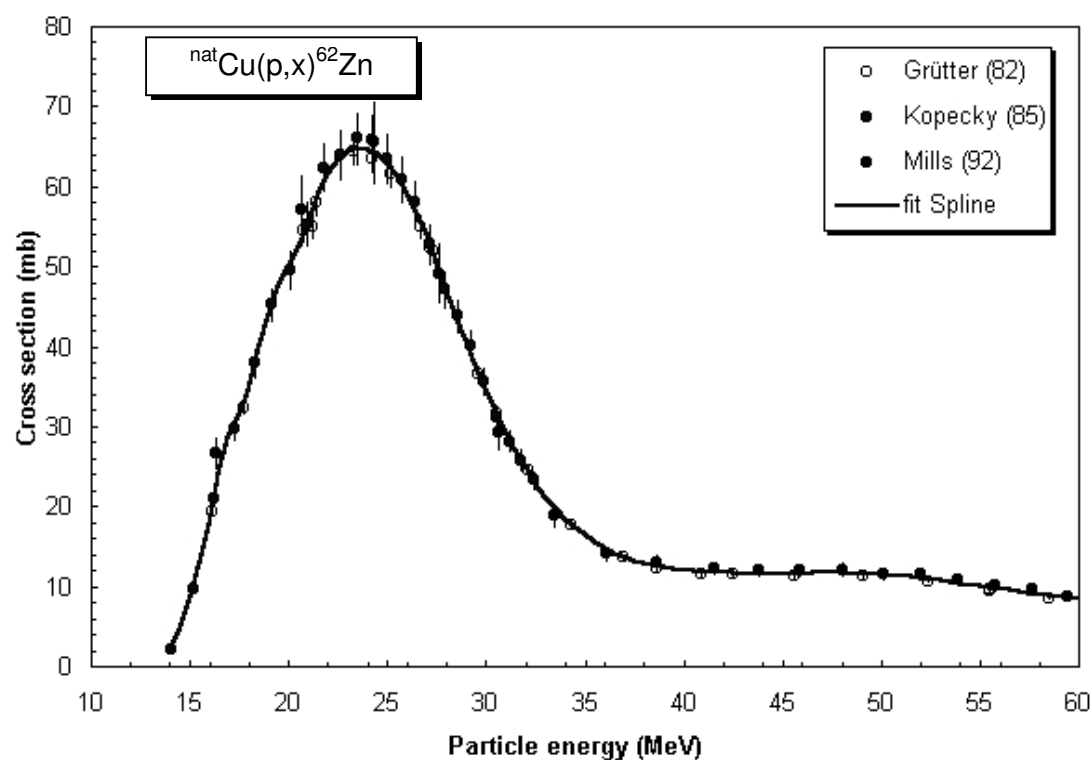


Fig. 3-11 Excitation function of the $^{nat}\text{Cu}(p,x)^{62}\text{Zn}$ reaction from IAEA-TECDOC-1211 used for the determination of the proton flux.

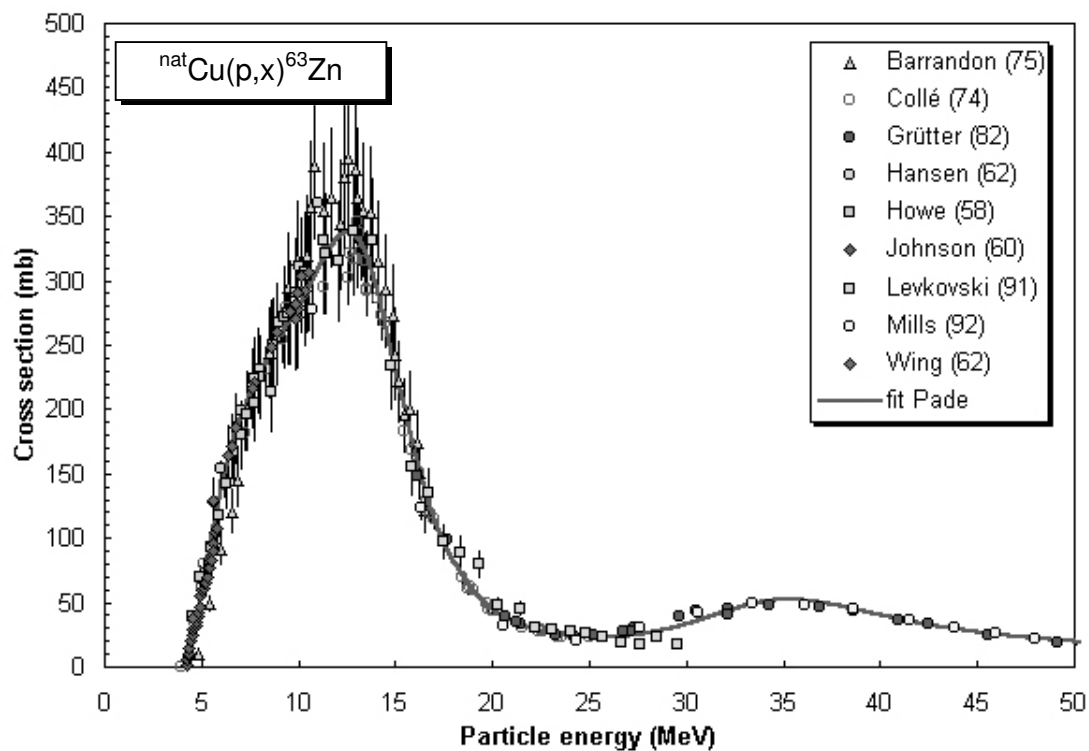


Fig. 3-12 Excitation function of the $^{nat}\text{Cu}(p,x)^{63}\text{Zn}$ reaction from IAEA-TECDOC-1211 used for the determination of the proton flux.

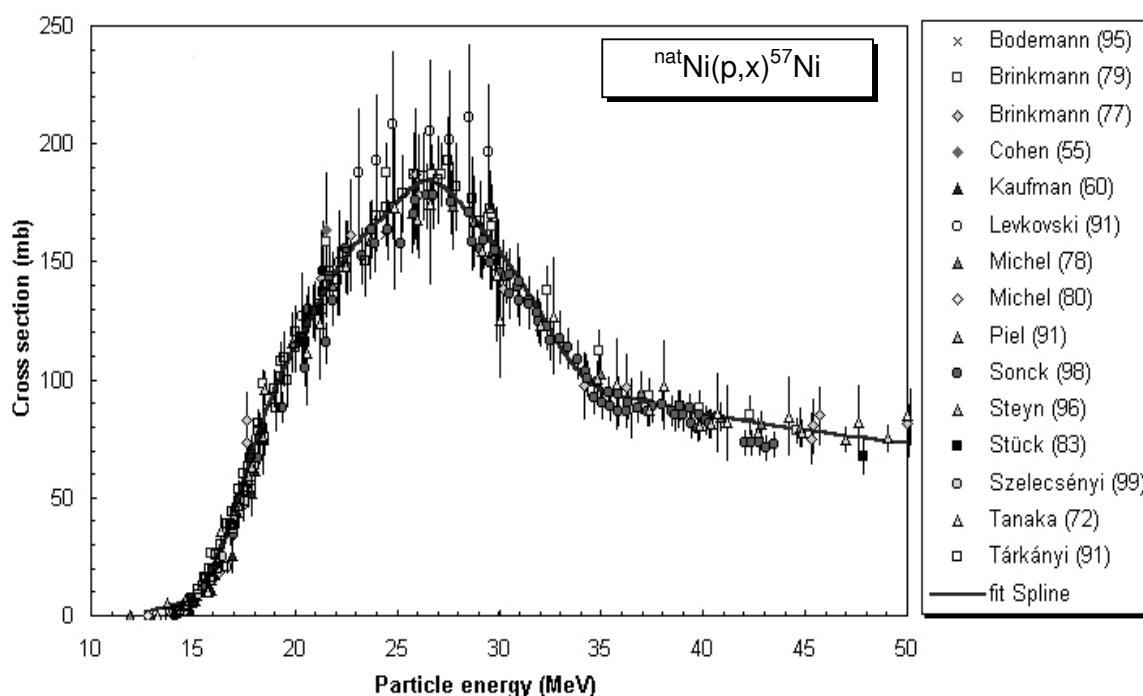


Fig. 3-13 Excitation function of the $^{nat}\text{Ni}(p,pn)^{57}\text{Ni}$ reaction from IAEA-TECDOC-1211 used for the determination of the proton flux.

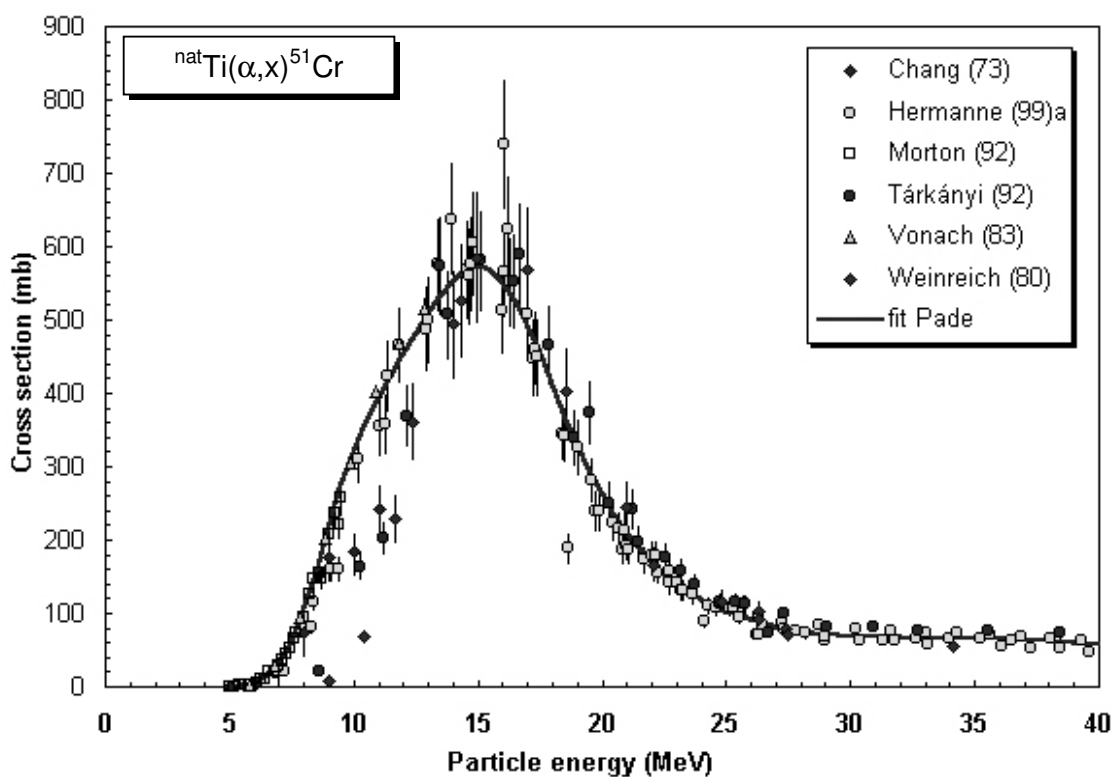


Fig. 3-14 Excitation function of the $^{nat}\text{Ti}(\alpha,xn)^{51}\text{Cr}$ reaction from IAEA-TECDOC-1211 used for the determination of the α -particle flux.

3.3.3 Irradiation experiments

In Table 3-7 an overview of the irradiation experiments performed within the scope of this work is given. Each nuclear reaction was investigated in repeated experiments to ensure the reproducibility of all results. The masses of the different samples are normalised to the respective target size and are given in the second column of Table 3-7 as g/cm².

Table 3-7 Overview of the performed irradiation experiments

Target	Mass (g/cm ²)	Type of irradiation
^{nat} S	0.0224 – 0.0290	d(Be)-neutron spectrum
^{nat} GeO ₂	0.0162 – 0.0458	18 MeV to 99 MeV, protons
⁷² GeO ₂	0.0039 – 0.0058	45 MeV and 66 MeV, protons
Cu ₃ As[^{nat} As]	0.2471 – 0.4697	45 MeV, protons
AlAs[^{nat} As]	0.2952 – 0.6999	45 MeV, 66 MeV, protons
^{nat} RbCl	0.0123 – 0.0401	45 MeV, protons
^{nat} ZrO ₂	0.0716 – 0.4866	d(Be)-neutron spectrum
^{nat} Eu ₂ O ₃	0.0365 – 0.8574	d(Be)-neutron spectrum
^{nat} Nd ₂ O ₃	0.0032 – 0.0102	26.5 MeV, ⁴ He
^{nat} Tm ₂ O ₃	0.0105 – 0.0322	10 MeV to 45 MeV, protons

Details on the target preparation and irradiation setup are given in the previous chapters. As mentioned above, the stacked-foil technique was applied for the irradiations with charged particles, allowing for the simultaneous activation of targets at different projectile energies (see 1.4.1). The adjustment of the respective particle energy was done with Al or Cu degrader foils if necessary. The projectile kinetic energy effective in each foil of the stack was calculated using the computer code STACK 2.3.

Target	atomic No. Target	Target-Data			Foil description	Grammage	average energy	Energy in	Energy out	Energy absorption	
		Molar weight	Weight	Diameter							
		[g/mol]	[g]	[mm]		[g/cm ²]	[MeV]	[MeV]	[MeV]	[MeV]	
Ni	28	58.700	0.04475	16.0	Monitor	1	2.226E-02	44.90	45.00	44.79	0.21
Al	13	26.982	0.00358	13.0	Cover	Al	2.700E-03	44.78	44.79	44.77	0.03
Ge	32	72.590	0.01097	10.0	Sample 1		1.397E-02	44.71	44.77	44.65	0.12
O	8	15.999	0.00483	10.0			6.150E-03	44.61	44.65	44.58	0.07
Al	13	26.982	0.03584	13.0		Backing	Al	2.700E-02	44.43	44.58	44.29
Al	13	26.982	0.32572	16.0	Absorber	0.6mm Al	1.620E-01	43.41	44.29	42.53	1.75
Ni	28	58.700	0.04475	16.0	Monitor	2	2.226E-02	42.43	42.53	42.32	0.22
Al	13	26.982	0.00358	13.0	Cover	Al	2.700E-03	42.30	42.32	42.29	0.03
Ge	32	72.590	0.01681	10.0	Sample 2		2.140E-02	42.19	42.29	42.10	0.19
O	8	15.999	0.00740	10.0			9.426E-03	42.04	42.10	41.98	0.12
Al	13	26.982	0.03584	13.0		Backing	Al	2.700E-02	41.83	41.98	41.68
Ni	28	58.700	0.04475	16.0	Monitor	3	2.226E-02	41.57	41.68	41.47	0.22
Al	13	26.982	0.43429	16.0	Absorber	0.8mm Al	2.160E-01	40.23	41.47	38.99	2.48
Al	13	26.982	0.00358	13.0	Cover	Al	2.700E-03	38.97	38.99	38.95	0.03
Ge	32	72.590	0.01013	10.0	Sample 3		1.290E-02	38.89	38.95	38.83	0.12
O	8	15.999	0.00447	10.0			5.691E-03	38.80	38.83	38.76	0.07
Al	13	26.982	0.03584	13.0		Backing	Al	2.700E-02	38.60	38.76	38.44
Ni	28	58.700	0.04475	16.0	Monitor	4	2.226E-02	38.32	38.44	38.21	0.23
Al	13	26.982	0.16286	16.0	Absorber	0.3mm Al	8.100E-02	37.72	38.21	37.23	0.98
Al	13	26.982	0.00358	13.0	Cover	Al	2.700E-03	37.21	37.23	37.20	0.03
Ge	32	72.590	0.02293	10.0	Sample 4		2.919E-02	37.06	37.20	36.92	0.28
O	8	15.999	0.01010	10.0			1.286E-02	36.83	36.92	36.74	0.18
Al	13	26.982	0.03584	13.0		Backing	Al	2.700E-02	36.57	36.74	36.41
Al	13	26.982	0.43429	16.0	Absorber	0.8mm Al	2.160E-01	35.03	36.41	33.65	2.76
Ni	28	58.700	0.04475	16.0	Monitor	5	2.226E-02	33.52	33.65	33.39	0.26
Al	13	26.982	0.00358	13.0	Cover	Al	2.700E-03	33.37	33.39	33.35	0.04
Ge	32	72.590	0.00993	10.0	Sample 5		1.264E-02	33.29	33.35	33.22	0.13
O	8	15.999	0.00437	10.0			5.564E-03	33.18	33.22	33.14	0.08
Al	13	26.982	0.03584	13.0		Backing	Al	2.700E-02	32.96	33.14	32.78
Cu	29	63.546	0.01801	16.0	Monitor	6	8.957E-03	32.73	32.78	32.68	0.10
Al	13	26.982	0.21715	16.0	Absorber	0.4mm Al	1.080E-01	31.94	32.68	31.20	1.48
Al	13	26.982	0.00358	13.0	Cover	Al	2.700E-03	31.18	31.20	31.16	0.04
Ge	32	72.590	0.02471	10.0	Sample 6		3.147E-02	30.99	31.16	30.81	0.35
O	8	15.999	0.01089	10.0			1.386E-02	30.70	30.81	30.59	0.22
Al	13	26.982	0.03584	13.0		Backing	Al	2.700E-02	30.40	30.59	30.21
Cu	29	63.546	0.01801	16.0	Monitor	7	8.957E-03	30.15	30.21	30.10	0.11
Al	13	26.982	0.00358	13.0	Cover	Al	2.700E-03	30.08	30.10	30.06	0.04
Ge	32	72.590	0.00632	10.0	Sample 7		8.047E-03	30.02	30.06	29.97	0.09
O	8	15.999	0.00278	10.0			3.540E-03	29.94	29.97	29.91	0.06
Al	13	26.982	0.03584	13.0		Backing	Al	2.700E-02	29.72	29.91	29.52
Al	13	26.982	0.10857	16.0	Absorber	0.2mm Al	5.400E-02	29.13	29.52	28.73	0.80
Al	13	26.982	0.00358	13.0	Cover	Al	2.700E-03	28.71	28.73	28.69	0.04
Ge	32	72.590	0.01384	10.0	Sample 8		1.762E-02	28.58	28.69	28.48	0.21
O	8	15.999	0.00610	10.0			7.764E-03	28.42	28.48	28.35	0.13
Al	13	26.982	0.03584	13.0		Backing	Al	2.700E-02	28.15	28.35	27.94
Cu	29	63.546	0.01801	16.0	Monitor	8	8.957E-03	27.89	27.94	27.83	0.11
Al	13	26.982	0.00358	13.0	Cover	Al	2.700E-03	27.81	27.83	27.79	0.04
Ge	32	72.590	0.00701	10.0	Sample 9		8.925E-03	27.73	27.79	27.68	0.11
O	8	15.999	0.00340	10.0			4.329E-03	27.64	27.68	27.61	0.07
Al	13	26.982	0.03584	13.0		Backing	Al	2.700E-02	27.40	27.61	27.19
Cu	29	63.546	0.01801	16.0	Monitor	9	8.957E-03	27.13	27.19	27.07	0.12
Al	13	26.982	0.10857	16.0	Absorber	0.2mm Al	5.400E-02	26.65	27.07	26.22	0.85
Al	13	26.982	0.00358	13.0	Cover	Al	2.700E-03	26.20	26.22	26.18	0.04
Ge	32	72.590	0.01458	10.0	Sample 10		1.856E-02	26.06	26.18	25.94	0.23
O	8	15.999	0.00642	10.0			8.177E-03	25.87	25.94	25.80	0.15
Al	13	26.982	0.03584	13.0		Backing	Al	2.700E-02	25.58	25.80	25.36
Cu	29	63.546	0.01801	16.0	Monitor	10	8.957E-03	25.30	25.36	25.23	0.12
Al	13	26.982	0.10857	16.0	Absorber	0.2mm Al	5.400E-02	24.78	25.23	24.33	0.90
Al	13	26.982	0.00358	13.0	Cover	Al	2.700E-03	24.31	24.33	24.29	0.05
Ge	32	72.590	0.01458	10.0	Sample 11		1.856E-02	24.16	24.29	24.04	0.25
O	8	15.999	0.00642	10.0			8.177E-03	23.96	24.04	23.88	0.16
Al	13	26.982	0.03584	13.0		Backing	Al	2.700E-02	23.65	23.88	23.41
Cu	29	63.546	0.01801	16.0	Monitor	11	8.957E-03	23.35	23.41	23.29	0.13

Figure 3-15 Screenshot from the computer code STACK showing a table for the calculation of the energy degradation in a target stack for the irradiation of GeO₂.

Figure 3-15 is taken from STACK and shows a typical stack of foils irradiated for the investigation of the $^{nat}\text{Ge}(p,x)$ processes, together with the proton energy effective at each part of the target stack, which was calculated by the program from the target parameters and the corresponding elemental data. Other charged particle irradiations were carried out in a similar way.

3.4 Radiochemical separation

While most of the cross section measurements in this work were done non-destructively, i.e. without chemical separations, in two cases extensive radiochemical work was involved. The first one was related to the separation of radioselenium from irradiated arsenic compounds, and the second one dealt with the study of the $^{153}\text{Eu}(n,p)^{153}\text{Sm}$ process. For investigating of the separation chemistry of ^{73}Se , the long-lived ^{75}Se ($T_{1/2} = 120$ d), which is co-produced during irradiation, was used as an analogue, thus reducing the radiation dose and the demand on speed during the separation process.

In the case of ^{153}Sm the produced activity was very low and was masked by the ^{152}Eu matrix activity, demanding a separation of the nuclide from the europium target bulk.

3.4.1 Radiochemical separation of n.c.a. $^{73, 75}\text{Se}$

The preparation of no-carrier added radioselenium is achieved via a two step process. The first step is the radiochemical separation via thermochromatography, followed by solvent extraction for purification. The method is based on established techniques [Blessing et al., 1994, Blum, 2003] and can be performed with ^{73}Se and ^{75}Se alike. The radiochemical investigation in this work focused on the thermochromatographic separation of the radionuclides.

The experimental setup of the thermochromatographic separation is shown in Figure 3-16. The irradiated arsenic alloy was placed in a quartz tube of 1.5 cm diameter and put into an electrical oven. An O_2 gas stream was used as purging gas, applying a flow rate of about 85 ml per minute. In the first step of the separation, the sample was heated to 660 °C for about 40 min leading to the formation of As_2O_3 , which was transported up to about 7 cm away from the end of the oven. Thereafter, the quartz

tube was shifted and the deposited As_2O_3 was positioned in the centre of the oven. The temperature was raised to $750\text{ }^\circ\text{C}$ for 10 min resulting in a shift of the deposit by further 12 cm. After moving the remaining target pellet to the centre of the oven again, the second step of the separation started. Therefore the temperature of the oven was raised stepwise to $900\text{ }^\circ\text{C}$ (10 min), $1000\text{ }^\circ\text{C}$ (15 min) and $1100\text{ }^\circ\text{C}$ (10 min). The produced radioselenium was deposited as $^{73}\text{SeO}_2$, or $^{75}\text{SeO}_2$ respectively, at about 11 cm distance from the end of the oven. After cooling to room temperature, the quartz tube was cut into pieces and the radioselenium was rinsed with a few ml of hot 6 M HCl. Radionuclidic purity and separation yield were determined via γ -ray spectrometry.

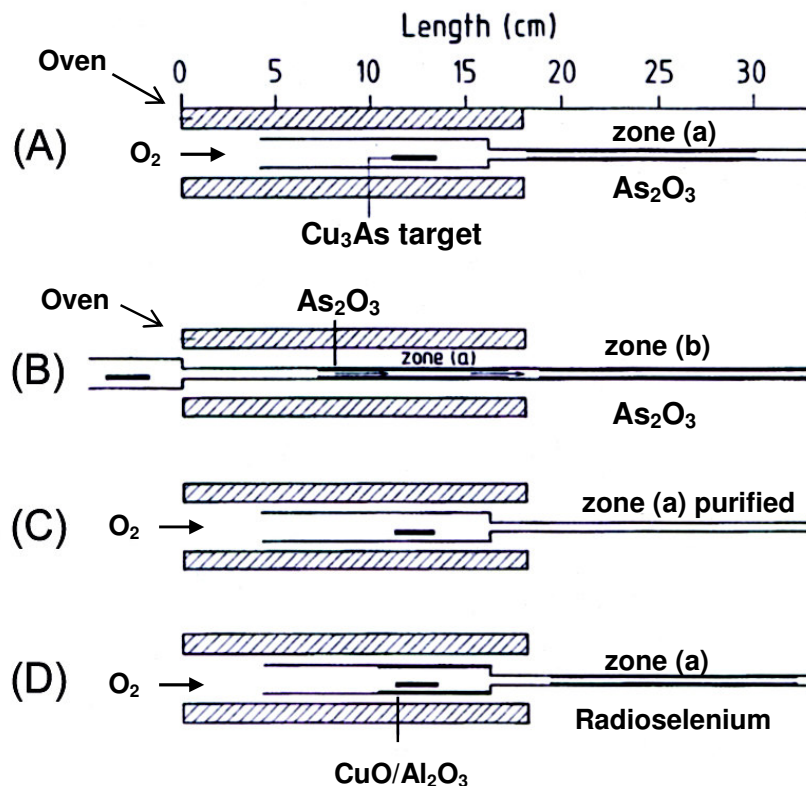


Fig. 3-16 Separation of $^{73}\text{Se}/^{75}\text{Se}$ via thermochromatography [adapted from Blessing et al., 1994]. The schemes (A) to (D) show the different steps of the process described above.

3.4.2 Radiochemical separation of ^{153}Sm

The radiochemical separation of ^{153}Sm from its Eu matrix was accomplished via column chromatography.

Firstly the irradiated sample was taken out of the Al capsule and shaken vigorously with 25 - 40 ml H_2O to dissolve the KCl. The suspension was then centrifuged at 7500 revolutions per minute and the water removed from the solid remaining at the bottom. About 100 mg of Sm_2O_3 carrier material was added and the precipitate dissolved in a volume of concentrated HNO_3 as small as possible. For chromatography a silica gel column of about 30 cm height and 3.5 cm diameter was set up. The silica gel was prepared with a 25 % solution of di-(2-ethylhexyl)phosphoric acid (HDEHP) in n-heptane. The dissolved Eu_2O_3 target was then eluted with a mixture of 0.5 M KNO_3 and 6 M HNO_3 at a flow rate of about 1.5 ml per minute. The eluate was caught in fractions of 10 to 20 ml.

After the γ -ray spectrometric analysis of the combined Sm fractions was completed, the material was investigated via Neutron Activation Analysis to ensure a quantitative washout of the Sm from the separation column. A flow sheet of the radiochemical separation is shown in Figure 3-17.

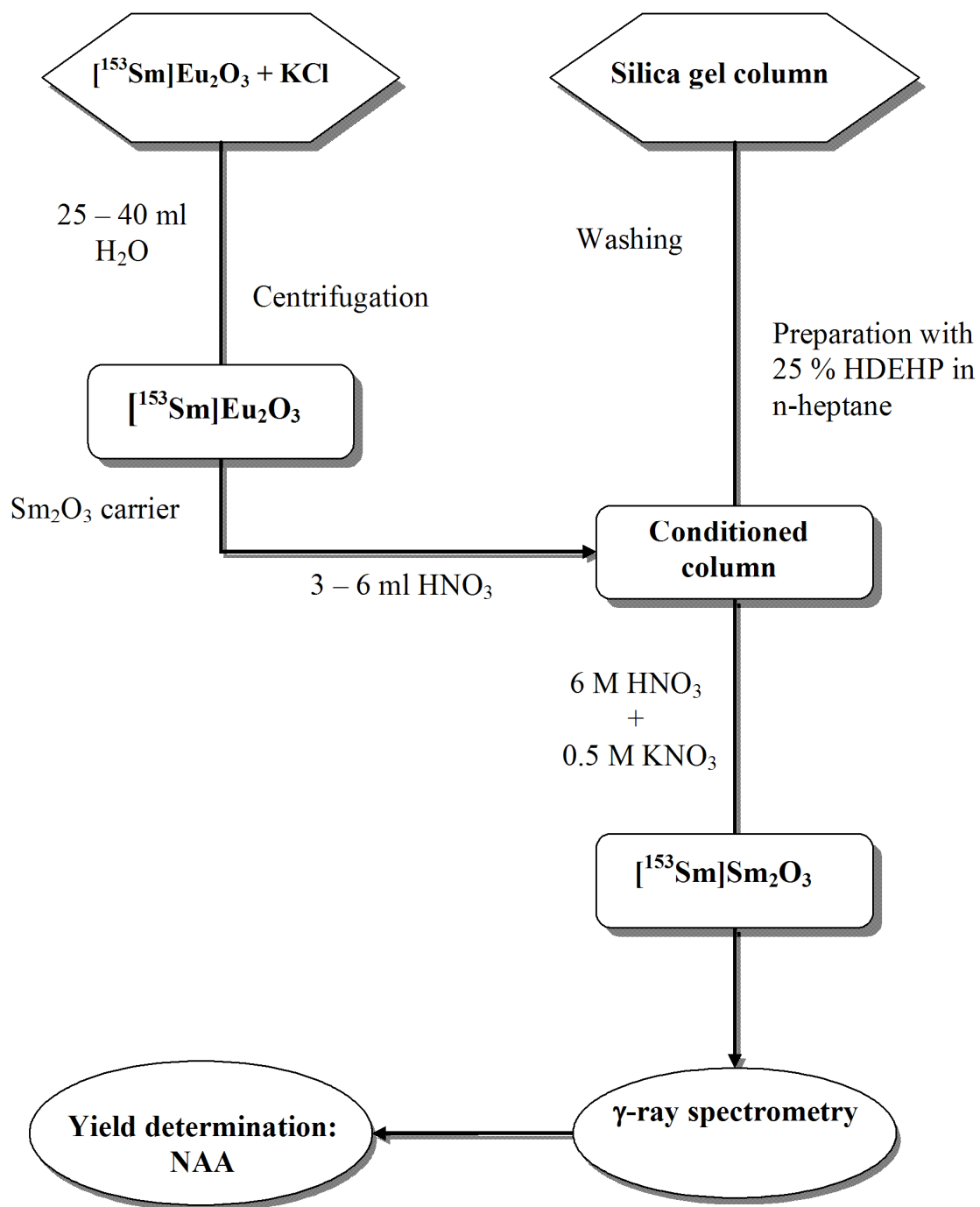


Fig. 3-17 Flow sheet of the radiochemical separation of ^{153}Sm from the irradiated Eu_2O_3 matrix.

3.5 Determination of radioactivity

Due to a variety of radionuclides under investigation, different counting techniques had to be applied for the determination of the produced absolute activities. The radioactivity of most of the therapeutic radionuclides and monitor products was determined via γ -ray spectrometry. In the case of ^{32}P and ^{90}Y , which lack any associated γ -rays, β^- -counting was used. All activated samples were measured repeatedly for subsequent decay curve analysis.

3.5.1 γ -ray spectrometry

The γ -ray spectrometry done at the experimental sites in Germany, Hungary and South Africa made use of high-purity germanium detectors (HPGe-detector) manufactured by EG&G Ortec and Silena International. Those detectors are compatible with IBM computers. In cross section work, except for the analysis of the produced ^{153}Sm , the radioactivity of each sample and monitor foil was determined non-destructively. The peak area analysis was done at the Forschungszentrum Jülich and the ATOMKI in Debrecen using the software *Gamma Vision 5.1* and *6.01* (EG&G Ortec). The program applies Gaussian fittings to the peaks of interest, whose search was done manually and not with Mariscotti type peak search that is embedded in the software. The distance of each sample to the detector was between 10 and 30 cm, so that the dead time was always lower than 5 % and the loss in count rate due to coincidence effects could be neglected (see 1.5.1). At iThemba LABS in Somerset West the spectrum analysis was done using the programs *Emcaplus* and *Emca 2000 vers. 2.03.0* of SILENA Int. The counting efficiency (ϵ) was determined at several distances from the detector using calibrated standard sources from PTB Braunschweig and Amersham International. In Figure 3-18 an example of the correlation of counting efficiency and γ -ray energy can be observed. Although the efficiency curve is individual for each detector, the curve shape is typical, displaying a maximum at about 150 keV γ -ray energy. The groups of radionuclides investigated are treated below separately.

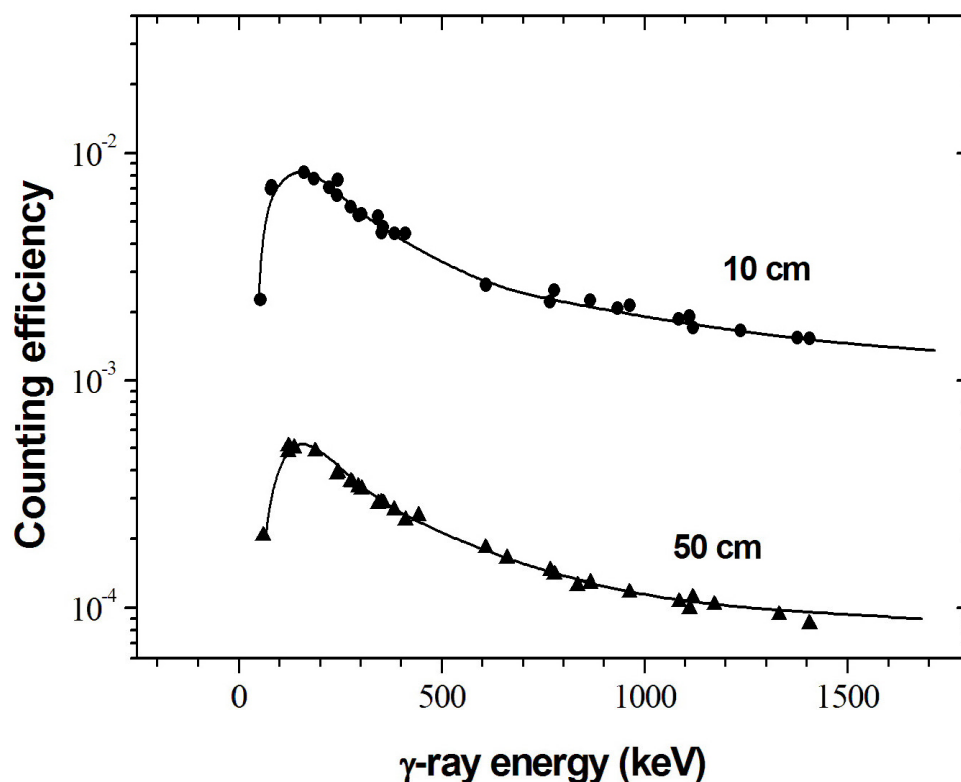


Fig. 3-18 Counting efficiency of a HPGe-detector as function of the γ -ray energy at 10 and 50 cm distance from the top of the detector.

^{71}As , ^{72}As , ^{73}As and ^{74}As

All investigated radioisotopes of arsenic possess clear and relatively intense γ -rays: ^{71}As ($E_\gamma = 174.95$ keV, 82 %), ^{72}As ($E_\gamma = 834.01$ keV, 80 %; 629.95 keV, 7.9 %), ^{73}As ($E_\gamma = 53.44$ keV, 10.3 %) and ^{74}As ($E_\gamma = 595.85$ keV, 59 %).

The low energy γ -ray (53 keV) of ^{73}As demanded a suitably prepared thin sample and a well calibrated detector. Its measurement possibly entails a higher uncertainty in the efficiency due to a less precisely defined calibration curve. In the case of ^{72}As , the formation of ^{72}Ga ($T_{1/2} = 14.1$ h) via (p, α n) and (p,2p3n) processes on ^{76}Ge must be taken into consideration, because of its interference with both the significant γ -lines of ^{72}As . However, since the abundance of the target nuclide ^{76}Ge is low (7.44 %) and the cross section for the (p, α n) + (p,2p3n) processes are also low as compared to (p,xn) processes, it was possible to subtract the disturbance from ^{72}Ga .

^{73}Se , (^{75}Se)

The investigation of the radionuclide ^{73}Se could be done by the use of its intense γ -rays of 361.23 keV (97 %) and 67.03 keV ($I_\gamma = 67$ %). In this case the formation of the isomeric state $^{73\text{m}}\text{Se}$ ($T_{1/2} = 39.8$ min) had to be considered. For the radiochemical processing the short-lived radionuclides were permitted to decay out, thus for the determination of the yield and quality of the radiochemical separation the long-lived ^{75}Se ($E_\gamma = 264.66$ keV, 58.5 %) was investigated.

 ^{82}Sr , ^{85}Sr

The PET nuclide ^{82}Sr does not emit any measurable γ -rays. Thus its radioactivity was determined through the analysis of its radioactive daughter nuclide ^{82}Rb ($T_{1/2} = 1.3$ min) that could be measured by its 776.52 keV γ -ray ($I_\gamma = 84$ %). The radioactivity of ^{85}Sr could only be analysed via its dominant 514.00 keV γ -line ($I_\gamma = 96$ %), which, however, could have strong interference from the 511 keV annihilation peak in the γ -ray spectrum. To overcome this disturbance, the measurements on ^{85}Sr were started about 9 months after the irradiation, thus reducing the background activity and enabling a better separation of the two neighbouring peaks.

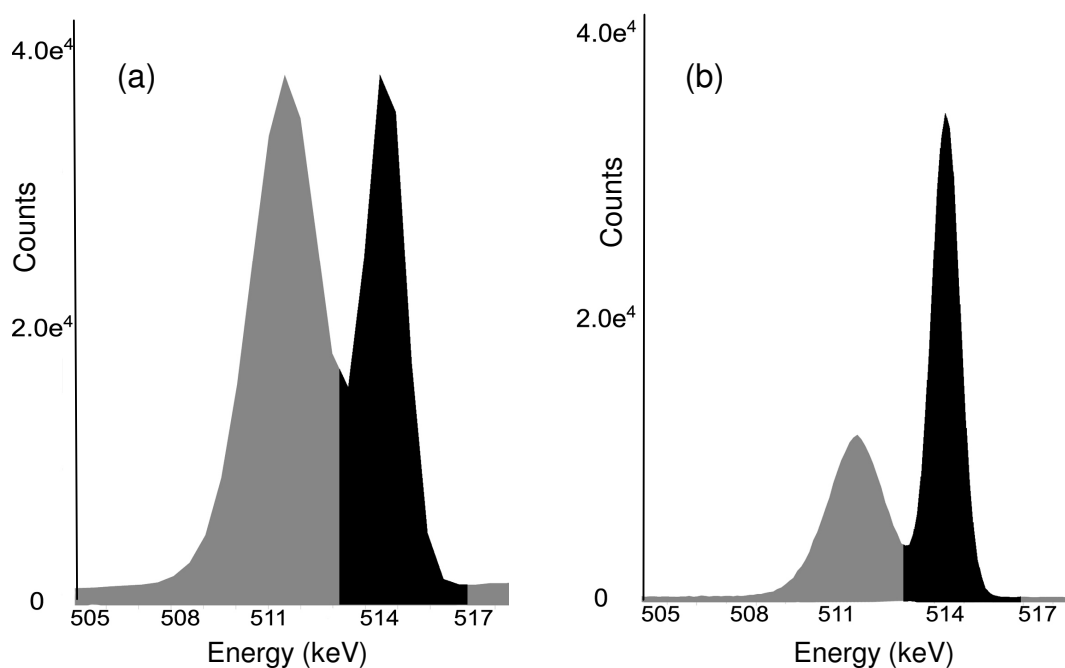


Fig. 3-19 Comparison of γ -ray spectra of ^{85}Sr , on the day of irradiation (a) and 9 months later (b). Counting times are 10000 s (a) and 72000 s (b).

In Figure 3-19 two different ^{85}Sr spectra can be seen, measured on the day of irradiation and 9 months later. In the latter case there is considerable improvement in the peak resolution.

^{153}Sm

The total radioactivity of the produced ^{153}Sm was determined using the 103.18 keV γ -ray ($I_\gamma = 31.4\%$). This γ -ray energy is on the rising part of the efficiency curve of the HPGe-detectors used in this work (cf. Fig. 3-18). Although this leads to high counting rates, it implies a greater uncertainty in the radioactivity values determined this way. As a result a greater overall uncertainty is associated with the cross section values related to the production of ^{153}Sm .

^{169}Yb

For the determination of the ^{169}Yb activity several strong γ -rays, namely 63.12 keV (43.7 %), 109.78 keV (17.4 %), 177.21 keV (21.5 %), 197.96 keV (34.9 %) and 307.74 keV (10.1 %) were available. However, a careful choice of the γ -rays had to be made, since several interfering factors needed to be considered. Thus the 109.78 keV γ -ray was disregarded in data processing, because this energy is located at about the maximum of the efficiency curve that shows considerable uncertainties, leading to strong deviations from the other γ -lines. Furthermore, at proton energies above 15 MeV the $^{169}\text{Tm}(p,pn)^{168}\text{Tm}$ reaction also takes place, the product of which has a 198.25 keV γ -ray, thus interfering with the 197.96 keV γ -ray of ^{169}Yb . In this work therefore use was made of the 177.21 keV γ -ray for the assay of ^{169}Yb .

3.5.2 β^- -counting

The pure β^- emitters ^{32}P and ^{90}Y were analysed using an anticoincidence gas-flow proportional counter of Berthold Technologies. The counting gas used was an argon/methane mixture (*P-10* gas). The anticoincidence array of the detector only causes the registration of an incidence, if an impulse is not recorded in the detection volume and on the detector shield simultaneously. This reduced the background radioactivity to 2 – 3 counts per minute (cpm), which then had to be subtracted manually. In Figure 3-20 a sketch of a 2π geometry proportional counter is shown.

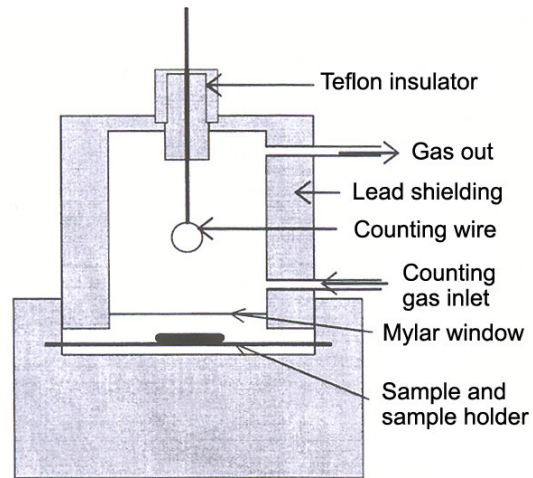


Fig. 3-20 Sketch of a 2π geometry proportional counter.

The counting efficiency of the detector could be determined in a similar way as done for the γ -ray detectors, using five different standard samples obtained from New England Nuclear Corporation (NEN). Due to the 2π arrangement of the proportional counter, the maximum efficiency of the detector was 50 %. Figure 3-21 shows the efficiency curve of the gas-flow proportional β^- -detector, determined experimentally.

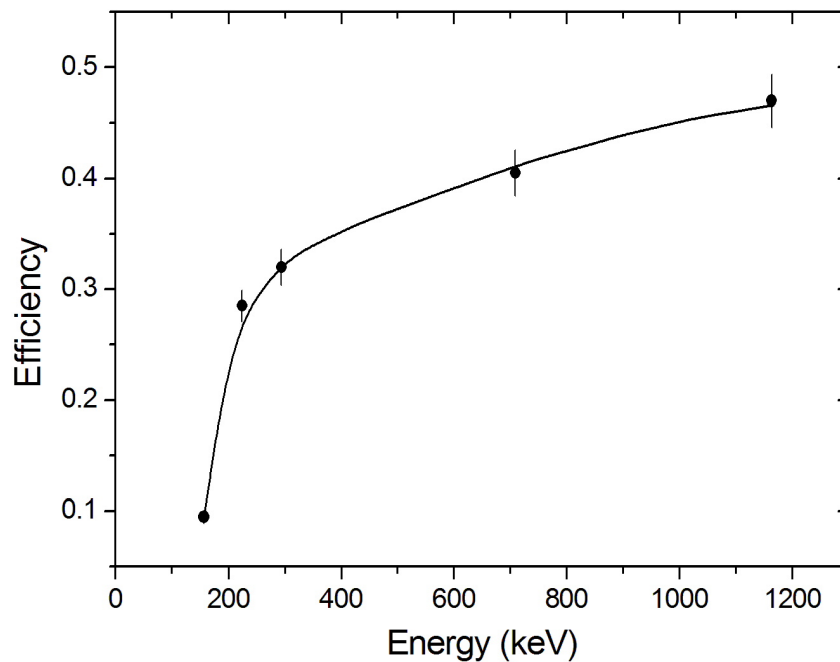


Fig. 3-21 Counting efficiency of the anticoincidence gas-flow proportional counter as a function of the β^- -ray energy.

For the determination of the produced radioactivity via β^- counting, it had to be considered that the used gas-flow proportional detector cannot analyse the kinetic energy of a registered β^- particle. Therefore accurate decay curve analysis had to be done, in order to verify the identity of the analysed radionuclide and to evaluate its nuclidic purity. For further validation of the detection results, absorption measurements were done to determine the end-point energy of the detected β^- particles. As absorbers Al foils were used. The required layer thicknesses of the Al absorbers were calculated using the ESTAR code of Berger et al. [2005].

In the case of β^- counting, the self-absorption within the analysed sample can not be neglected. Absorption measurements were therefore done using ^{32}P from PerkinElmer[®] as a reference sample. Due to the rather high energetic β^- particles emitted by ^{32}P ($E_\beta = 1.7$ MeV) and ^{90}Y ($E_\beta = 2.3$ MeV), the self-absorption was found to be rather low in the thin pellets.

3.6 Determination of nuclear reaction cross sections and their uncertainties

3.6.1 Determination of the absolute activity

For the interpretation of the experimental results, the measured radioactivity of all samples and monitor foils was converted to the radioactivity at the end of bombardment (EOB). The basis for the determination of the radioactivity from the measured γ -ray spectra is the counted number of decay incidents, represented by the peak area P of a specific γ -ray energy. This peak area is summed over the period of the measuring time T_{live} , thus the radioactive decay of the analysed sample during this time has to be considered and a corresponding decay correction has to be made. Therefore, for the calculation of the absolute radioactivity A at the beginning of the measurement, equation 8 is supplemented with the appropriate decay term.

$$A = \frac{\lambda \cdot P}{\varepsilon \cdot I_{\gamma} \cdot (1 - e^{-\lambda T_{\text{live}}})} \quad (14)$$

The dead time correction was included automatically in the registration of the measurement time. Due to the relatively large distance of the sample to the detector, the correction for coincidence effects could be neglected.

The radioactivity A_{EOB} at the end of bombardment can then be calculated according to the equation of the radioactive decay.

$$A_{\text{EOB}} = A \cdot e^{\lambda t} \quad (15)$$

t : time until the beginning of measurement

Another way of determining A_{EOB} is the decay curve analysis. All activated samples were measured repeatedly. The corresponding radioactivity values (A) were logarithmically plotted in correlation to the time elapsed since EOB, what complies with a conversion of equation 15 into the following term.

$$\ln(A) = \ln(A_{\text{EOB}}) + \lambda \cdot t, \text{ with } \lambda = \frac{\ln(2)}{T_{1/2}} \quad (16)$$

The extrapolation of this straight line results in the absolute radioactivity at EOB (A_{EOB}). This method allows for the additional control of the half-life of the radionuclide under investigation, thus giving information on its radionuclidic purity.

The latter is especially important for the evaluation of the β^- counting, since this type of detection did not allow for the proper identification of a radionuclide via its radiation energy. As mentioned above (3.5.2), the *Berthold* system used in this work, registered counts per minute instead of the conventional counts per second (Bq), demanding the appropriate conversion before subsequent data processing. In addition the counting background had to be subtracted manually and the measured absolute activity had to be corrected for the self-absorption effect.

3.6.2 Calculation of nuclear cross sections

By using the measured absolute radioactivity of a sample, described in the previous section, the reaction cross section of the investigated nuclear reaction could be calculated. Based on the known half-life $T_{1/2}$, the bombardment time t_B and the number of nuclei N_X in the sample, the reaction cross section is calculated by reformulating the activation equation (Equ. 6) as follows.

$$\sigma = A_{\text{EOB}} \cdot \left(\Phi \cdot N_X \cdot H \cdot \left(1 - e^{-\frac{\ln(2)}{T_{1/2}} \cdot t_B} \right) \right)^{-1} \quad (17)$$

The projectile flux Φ was deduced as described in the sections 3.3.1.2 and 3.3.2.2 applying the measured radioactivity at EOB produced in the monitor foils.

3.6.3 Calculation of differential and integral yield

As described in section 1.6 the differential radionuclidic yield of the investigated nuclear reaction at a given projectile energy can be calculated with equation 6. To do so, the mass of the target material N_x had to be calculated, which was required to degrade the projectile energy according to the energy interval that was chosen. This was achieved using the computer code STACK. As corresponding σ value, the average nuclear cross section, deduced from the excitation function fitted to the experimentally determined cross sections, was taken. The calculation of the integral, thick target yield was done by summing the calculated differential yields of each energy interval according to equation 11. The integral yields determined in the scope of this work are generally plotted as a function of the projectile energy and refer to the application of a pure element as target.

3.6.4 Uncertainties of the results

In all the experimental procedures described above, the possible sources of various uncertainties are implied. For the determination of the overall uncertainty, a deliberate analysis of all steps of the experiment and the evaluation are necessary to validate the quality of the determined results. Uncertainties are based to a high degree on the preparation and radiochemical processing of the investigated samples, but develop as well from the technical framework. The determination of the radioactivity and the related calculated data deduced from it, comprise further uncertainties, which cannot be avoided. The most significant uncertainties and their sources are discussed in detail in the following and are summarised in Table 3-8.

3.6.4.1 *Uncertainties of mass determination*

The uncertainties included in weighing affect the procedures of target preparation as well as the later radiochemical processing. For the determination of all significant masses a precision balance of the type AT 261 made by *Mettler Toledo* was used. This device enables the determination of masses with an accuracy of ± 0.1 mg. Therefore the uncertainty of most mass determinations is lower than 1 %, except for the experiments including very light samples.

Concerning the homogeneity of the target samples the uncertainty is estimated to be 5 %. The uncertainty of the chemical separations is based on those of the mass determination and amounts to 2 – 3 %.

3.6.4.2 *Uncertainties in particle energies*

All incident projectile energies possess an uncertainty of ± 0.2 MeV due to the accuracy of the technical parameters of the utilised accelerators. Concerning the irradiations using the d(Be) target, it has been shown by Olah et al. [1998], that the deviation in the incident particle energy only has a significant effect on the produced neutron spectrum at higher dimensions. With regard to charged particle irradiations the uncertainty in the projectile energy, however, is more significant, due to the application of the stacked foil technique. In the calculation of the energy degradation this uncertainty is propagated in addition to the uncertainty that is implied in the applied mathematical formalisms. Thus the energy uncertainty increases with the increasing number of samples in an irradiated foil stack, amounting up to 1 MeV uncertainty for large stacks.

3.6.4.3 *Uncertainties in the determination of radioactivity*

The uncertainty in the determination of the absolute radioactivity (see 3.6.1) is affected by several factors. Firstly there is the statistical uncertainty in the peak area analysis. When dealing with most radioactive samples, this statistical error is smaller than 1 % and can be neglected; however, considering weak samples, e.g. ^{153}Sm samples, the uncertainty could amount to 5 - 10 %.

Another source of uncertainty is the determination of the detector efficiency, which itself is affected by several factors. The uncertainty due to the peak area analysis could be reduced to less than 1 % by a suitable adjustment of the counting time. The uncertainty of the used standard samples amounts to 3 – 6 %, in addition to a deviation of 2 – 5 % due to the fitting procedure of the efficiency curves. These colluding uncertainties can, however, be reduced by plotting an accurate decay curve and calculating its standard deviation, whose accuracy is dependent on the above mentioned factors, and generally amounts to 4 to 7 %.

A further significant source of uncertainty is the determination of the particle flux. Here all the uncertainties discussed above collude together with the uncertainty

included in the recommended excitation function of the applied monitor reactions, resulting in an uncertainty of about 9 - 10 %. In the cases, where the Faraday chamber could be used during irradiation, this uncertainty declines to 5 – 6 %. The accuracy of the decay data used for the calculation covered a range of 0.1 – 1 %.

3.6.4.4 Overall uncertainty of the results

The overall uncertainty of the determined nuclear cross sections is deduced from the individual uncertainties discussed above using the error propagation according to Gauss, adding up to a value of 11 % to 19 %.

Table 3-8 Overview of the uncertainties significant for this work.

	Source of uncertainty	Magnitude in %
Experimental uncertainties	Weighing	1
	Detector efficiency	4 – 7
	Homogeneity of samples	5
	Separation yield	2 – 3
Calculational uncertainties	Decay data	0.1 – 1
	Peak area analysis	4 -7
	Particle flux	5 – 10
Overall uncertainty	Determination of radioactivity	7 – 14
	Determination of reaction cross section	11 – 19

4 Nuclear model calculations

Within the scope of this work the experimentally determined nuclear data have been compared with cross section data obtained from nuclear model calculations. Such a comparison is of considerable significance. Nuclear model calculations are very helpful in the validation of experimental data, which lack reference data in the literature or which are in disagreement with the existing data. On the other hand, reliable experimental cross section data are necessary to prove and improve the results of model calculations. Furthermore, a comparison of experimentally determined cross section values with nuclear model calculations may give information on the mechanism of the nuclear reaction under investigation.

The theoretical data shown in this work were calculated using the precompound model code ALICE-IPPE [Dityuk et al., 1998], which is an enhancement of the ALICE code developed by Blann [1975]. In this code the pre-equilibrium emission of particles was considered for the first time, and was combined with the model of nucleon evaporation for nuclear modelling. The pre-equilibrium emission model provided a consistently good description of experimental data including nuclear reactions, that include direct, intermediate and equilibrium components. A feature of ALICE-IPPE is that, instead of the Fermi gas model, it makes use of the generalised superfluid model for calculation of nuclear level densities of all nuclei formed in the evaporation cascade. Based on the geometry dependent hybrid model the cluster emission is described [Blann, 1972]. The code considers “knock-out” and “pick-up” processes, i.e. for the α -particle emission, as well as nucleon pairing and nuclear shell effects. Furthermore ALICE-IPPE takes into account the γ -emission of the residual nucleus as well. In addition spectra of ^3H and ^3He can be calculated according to the coalescence pick-up model. The emission of deuterons can be described using the phenomenological approach.

ALICE-IPPE has been quite successful in describing the (p,xn) and (p,pxn) excitation functions [cf. Faßbender et al., 1997, Hohn et al., 2001, Kastleiner et al., 2004] but not more complex reactions like (p,2p), etc. [Faßbender et al., 1999, Stoll, 2002]. Concerning nuclear reactions induced by more complex particles, fairly good

agreement with experimental data could be obtained for ^3He induced reactions [Hilgers et al. 2005]. The calculation of deuteron induced reactions using ALICE-IPPE, on the other hand, has been shown to lead to rather poor results [Tárkányi et al., 2006]. A disadvantage of the code is that it cannot describe the formation of isomeric states. The theoretical cross section data calculated with the ALICE-IPPE code given in this work are taken from the MENDL-2P data file [Shubin et al., 1998]. The ALICE-IPPE code can only calculate excitation functions for individual reaction channels. Therefore the theoretical cross section data were converted for the description of nuclear reactions on target material with natural isotopic composition, summing up overlapping reaction channels and considering isotopic abundances.

5 Results and discussion

5.1 Integral tests of differential data

5.1.1 Measurement of integral cross sections

The fast neutron field used in this work was generated via the breakup reaction of 14 MeV deuterons on a beryllium target and was characterised by multiple foil activation and spectrum unfolding technique (see section 3.3.1.1). The maximum flux density occurs at about 2.5 to 3.5 MeV neutron energy, and a low but significant intensity is also observed in the higher energy range. The neutron flux intensity in the investigated 0° direction at 1 cm from the Be-target was found to be about 10^{10} neutrons/cm²s.

The spectrum averaged cross sections of the nuclear reactions $^{nat}\text{S}(n,x)^{32}\text{P}$, $^{nat}\text{Zr}(n,p)^{90}\text{Y}$ and $^{nat}\text{Eu}(n,p)^{153}\text{Sm}$ were experimentally measured. Concerning the radionuclides ^{32}P and ^{90}Y , β^- -counting was applied and accurate decay curve analyses were done to determine the produced radioactivity. Figures 5-1 and 5-2 show examples of the decay curves of ^{32}P and ^{90}Y .

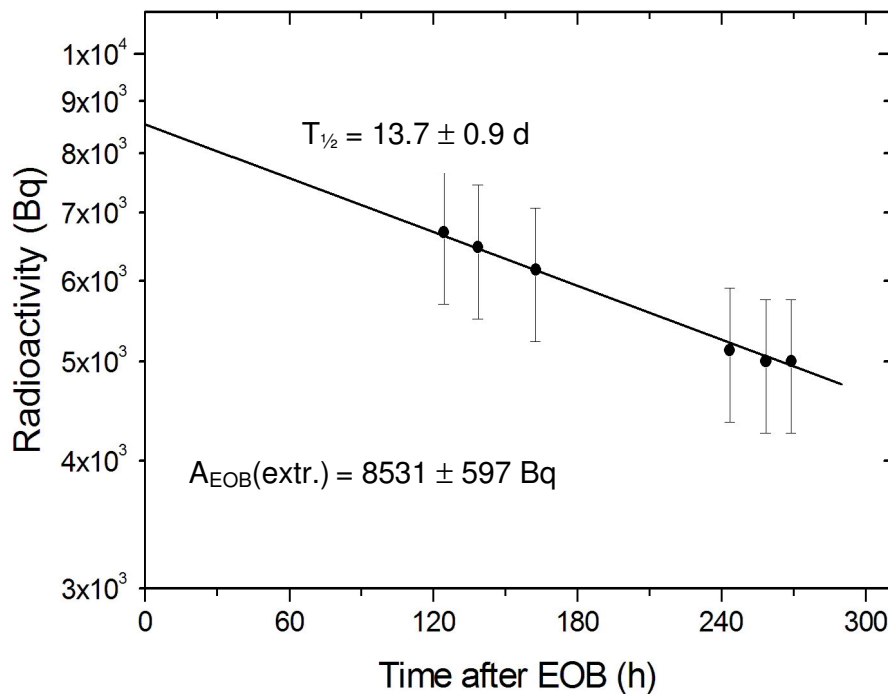


Fig. 5-1 Decay curve of ^{32}P together with the experimentally determined half-life of the radionuclide and the resulting extrapolated radioactivity at EOB.

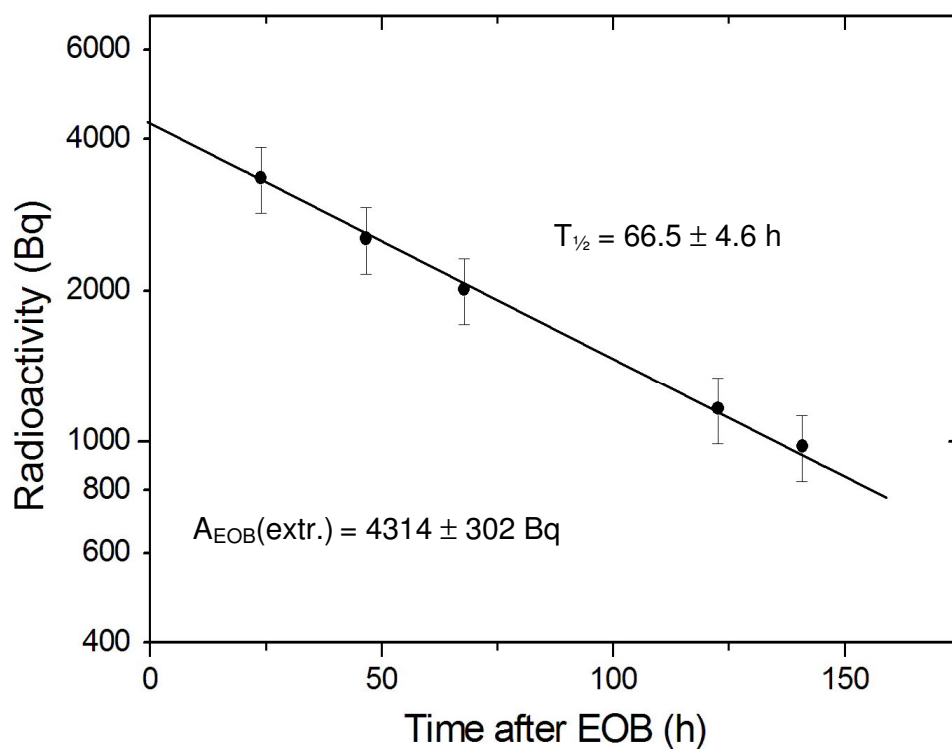


Fig. 5-2 Decay curve of ^{90}Y together with the experimentally determined half-life of the radionuclide and the resulting extrapolated radioactivity at EOB.

In the case of ^{153}Sm the absolute radioactivity at EOB was determined via measurement of the 103.18 keV γ -ray and performing decay curve analysis. The analysis using this γ -line is associated with a higher uncertainty, due to the larger uncertainty in the detector efficiency in this energy region. However, fitting a decay curve of known half-life to the measured points, analogous to the examples shown above, allowed a quite accurate extrapolation of the radioactivity to EOB with an uncertainty of about 15 %. The determination of radioactivity using a γ -ray in a more suitable energy range is, however, not recommended due to the very low intensities (< 1 %) of all other γ -rays.

The results of the integral cross section measurements are given in Table 5-1 together with their uncertainties. These experimentally determined spectrum averaged cross sections can be used to validate the differential data of the nuclear reactions under investigation. The calculated spectrum averaged cross sections were obtained as described in section 1.7. It can be seen that the (n,p) reaction channel becomes less distinctive with increasing mass and charge of the target nucleus.

Table 5-1 Neutron spectrum averaged cross sections determined experimentally via integral measurements in this work

Nuclear reaction	Cross section (mb)
$^{32}\text{S}(n,p)^{32}\text{P}$	152 ± 27
$^{90}\text{Zr}(n,p)^{90g}\text{Y}$	2.7 ± 0.50
$^{153}\text{Eu}(n,p)^{153}\text{Sm}$	0.26 ± 0.04

5.1.2 Comparison of integral and integrated data

The uncertainty of a calculated spectrum averaged cross section is dependent on the uncertainty of the respective recommended excitation function and the accuracy of the measured neutron spectrum as discussed above. A comparison of the measured cross sections with the calculated values is given in Table 5-2. Keeping the uncertainties of both the experimental and calculated cross section values in mind, the data show a good agreement within 10 - 15 % deviation. Based on this validation it is possible to recommend evaluated excitation functions for these three nuclear processes, which can be used as standard for future calculations [Al-Abyad et al., 2006]. There has been a lack of such evaluated and recommended data and the integral tests using a d(Be) neutron spectrum comply with a request of the IAEA in connection with the standardisation of data for the production of therapeutic radionuclides.

Table 5-2 Comparison of measured integral spectrum averaged cross sections with the calculated data

Nuclear reaction	Spectrum averaged cross section (mb)		
	Integral	Integrated	σ (Integral)/ σ (Integrated)
$^{32}\text{S}(n,p)^{32}\text{P}$	152 ± 27	167	0.91
$^{90}\text{Zr}(n,p)^{90g}\text{Y}$	2.7 ± 0.50	3.20	0.85
$^{153}\text{Eu}(n,p)^{153}\text{Sm}$	0.26 ± 0.04	0.30	0.87

5.2 New production routes of the therapeutic radionuclides ^{32}P , ^{90}Y , ^{153}Sm and ^{169}Yb

Alternative methods for the production of the therapeutic radionuclides ^{32}P , ^{90}Y , ^{153}Sm and ^{169}Yb have been investigated, using on the one hand 14 MeV d(Be) breakup neutrons and, on the other, charged particle induced reactions, which had not been at all or insufficiently investigated earlier. The results of the individual cases are discussed in the following.

5.2.1 Possibility of production of ^{32}P , ^{90}Y and ^{153}Sm with fast d(Be) neutrons

Beside its significance in the development of nuclear data, the measurement of the neutron spectrum cross section of the $^{\text{nat}}\text{S}(n,p)^{32}\text{P}$ reaction is of high interest for the large scale production of this important therapeutic radionuclide in no-carrier-added form. Up to now, the fission neutron induced (n,p) reaction on sulphur is the only way of producing ^{32}P with high specific radioactivity. The cross section measurement of the same reaction with d(Be) neutrons leads to a value three times higher than the value for a fission neutron field. In Table 5-3 a comparison is given, showing the cross section data determined for the formation of the three radionuclides, viz. ^{32}P , ^{90}Y and ^{153}Sm , via irradiations with 14 MeV d(Be) neutrons measured in this work, and the data for the production in a nuclear reactor. Concerning the (n,p) process, the higher efficacy of fast neutron spectra has been shown for other nuclides earlier [Spahn et al., 2004]. Thus it can be concluded, that for production of radionuclides via the (n,p) process, the use of high-intensity fast neutron spectral sources (e.g. a fusion or a spallation source) would be more effective than the present day fission reactors.

Table 5-3 Comparison of (n,p) cross sections induced by d(Be) and fission spectral neutrons [Calamand, 1974]

Radionuclide	(n,p) reaction cross section (mb)		Ratio
	d(Be) neutrons	Fission neutrons	
^{32}P	152	69	2.2
^{90}Y	2.7	0.18	15.0
^{153}Sm	0.26	0.015	17.3

As regards the production of ^{90}Y , it should be mentioned that the $^{90}\text{Zr}(n,p)^{90g}\text{Y}$ reaction does not have a reaction cross section high enough to compete with the well established $^{90}\text{Sr}/^{90}\text{Y}$ generator system. The generator system is based on ^{90}Sr , which is available in large quantities via the fission process. It is relatively inexpensive and, furthermore, is available in form of generator kits for simple and fast application of radiopharmaceuticals. Thus the alternative production route of ^{90}Y , i.e. via the (n,p) process investigated in this work, can not be recommended for application.

Concerning the production of the therapeutic radionuclide ^{153}Sm , the investigation of an alternative production route is very important. This radionuclide is of increasing significance for internal radiotherapy and has hitherto been produced mainly via the (n, γ) reaction on 98 % enriched ^{152}Sm at a nuclear reactor. This method leads to high production yields, but delivers a product of only limited specific radioactivity. Although co-ordinated attempts have been underway [cf. IAEA-TECDOC-1114] to optimise its production, the no-carrier-added form of the radionuclide has not been obtained so far. In this regard two new production routes, viz. the $^{153}\text{Eu}(n,p)^{153}\text{Sm}$ and the $^{\text{nat}}\text{Nd}(\alpha,n)^{153}\text{Sm}$ reaction, were investigated in this work. The former reaction is considered here and the latter in the next section. The application of the (n,p) reaction at a nuclear reactor is not very efficient due to the very low cross section of this process (0.015 mb [Calamand, 1974] with the fission neutrons. The reaction cross section determined in this work using d(Be) spectral neutrons is significantly higher (0.26 ± 0.4 mb). A 5 g sample of Eu_2O_3 , irradiated at our facility for 100 h with a neutron flux of $10^{10} \text{ cm}^{-2} \cdot \text{s}^{-1}$, would result in a radionuclide yield of about 11.5 kBq of no-carrier-added ^{153}Sm . The use of enriched ^{153}Eu could increase the yield to about 22 kBq but the total ^{153}Sm activity would, nevertheless, be rather low. However, newer concepts of spallation neutron sources, which aim at fast neutron flux densities of $10^{14} \text{ n} \cdot \text{cm}^{-2} \cdot \text{s}^{-1}$ and more, would enable ^{153}Sm yields of up to 180 MBq combined with quite a high specific radioactivity.

5.2.2 Production of ^{153}Sm and ^{169}Yb using charged particle induced reactions

Due to the declining reaction cross sections of the (n,p) process with the increasing mass and charge of the target element, alternative production routes via charged particle induced reactions have been studied within the scope of this work, in order to obtain two high mass therapeutic radionuclides under investigation with high specific activity.

The cross section data of the charged particle induced production of ^{153}Sm via the $^{150}\text{Nd}(\alpha,n)^{153}\text{Sm}$ reaction have been measured for the first time in this work. Those data are up to two hundred times larger than (n,p) reaction data. As target material for this study natural Nd_2O_3 was employed, however, only the isotope ^{150}Nd is effective as target for the formation of ^{153}Sm with α -particles, which in natural neodymium possess an abundance of only 5.64 %. The cross section data given in Table 5-4 have been normalised to 100 % abundance of ^{150}Nd .

Table 5-4 Measured cross sections of the $^{150}\text{Nd}(\alpha,n)^{153}\text{Sm}$ reaction corrected for the abundance of ^{150}Nd

α -particle energy (MeV)	Cross section (mb)
10.9 ± 0.8	2 ± 0.3
14.2 ± 0.7	19 ± 9
14.8 ± 0.7	29 ± 10
15.4 ± 0.6	34 ± 3
17.8 ± 0.6	40 ± 2
18.7 ± 0.5	48 ± 5
20.4 ± 0.5	49 ± 17
21.8 ± 0.5	49 ± 6
22.7 ± 0.4	44 ± 4
23.8 ± 0.4	45 ± 15
24.6 ± 0.4	44 ± 6
25.6 ± 0.3	36 ± 4
26.2 ± 0.3	42 ± 4

Reproducing these results, Figure 5-3 shows the normalised cross section values and a first excitation function fitted to the experimental data. The maximum cross section of about 45 mb occurs at about 20 MeV. Since over the α -particle energy range investigated in this work no other Sm radionuclide can be formed from ^{150}Nd , this nuclear reaction can be considered as a possible production route of high-purity ^{153}Sm . The differential and integral yields of the $^{150}\text{Nd}(\alpha,n)^{153}\text{Sm}$ reaction were calculated according to section 3.6.3 based on the excitation function given in Fig. 5-3 and the integral yield is shown in Figure 5-4 as a function of the α -particle energy. The basic conditions presumed for this calculation are 1 h irradiation, a beam current of 1 μA and the abundance of ^{150}Nd as 100 %.

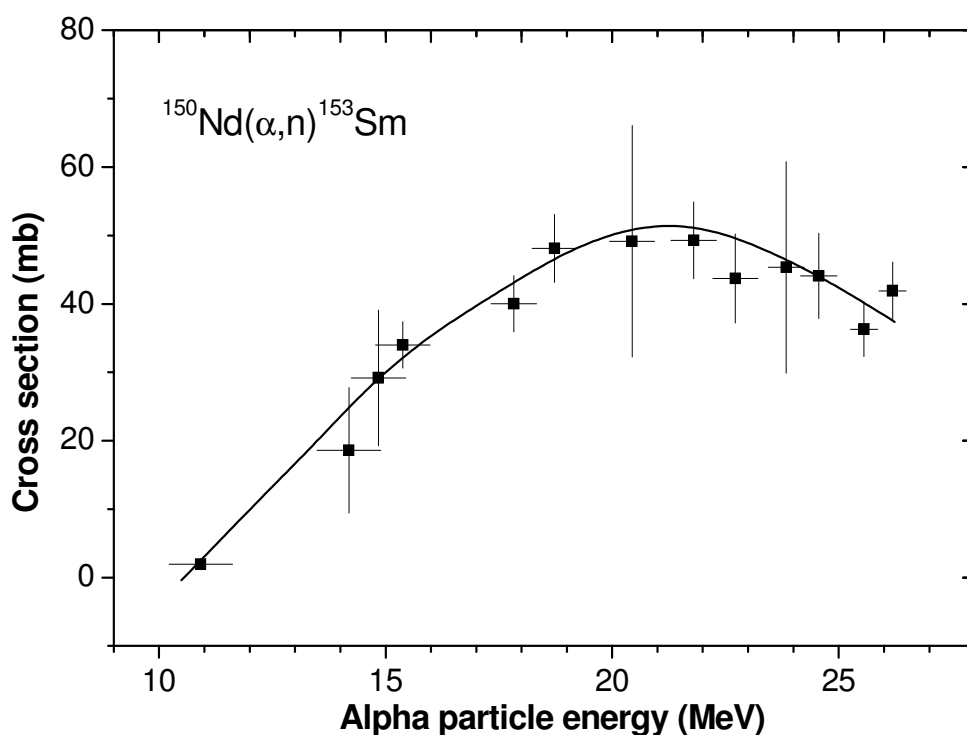


Fig. 5-3 Excitation function of the $^{150}\text{Nd}(\alpha,n)^{153}\text{Sm}$ reaction. The curve gives an eye guide through the data points.

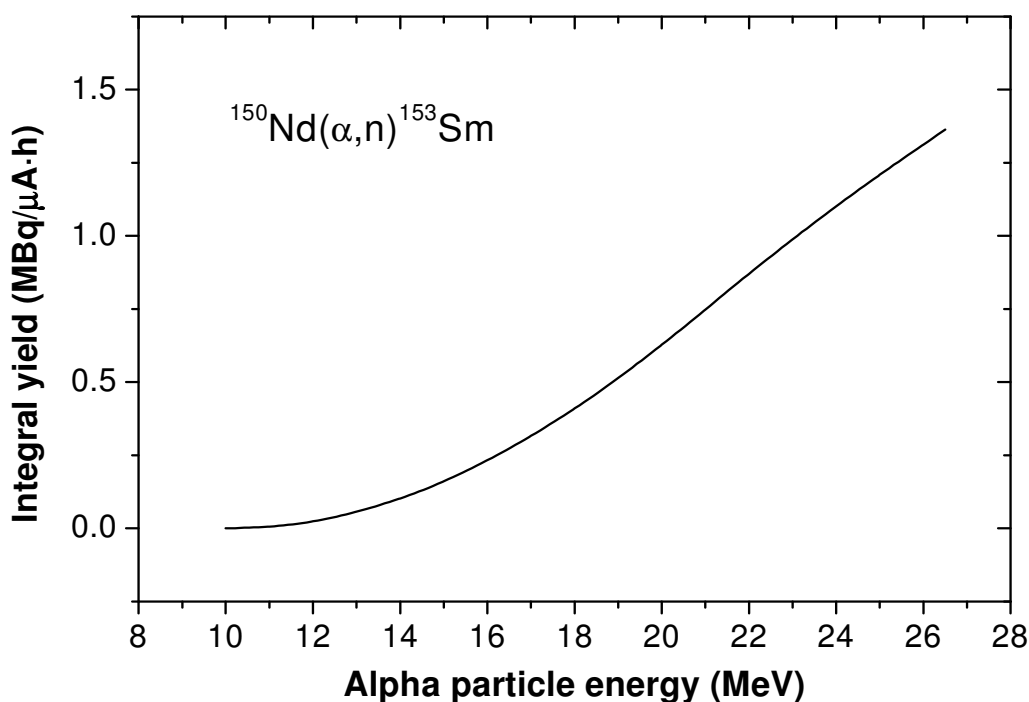


Fig. 5-4 Integral yield of ^{153}Sm calculated from the excitation function given in Fig. 5-3 (assuming a 100 % enriched ^{150}Nd metal target).

Considering the suitable energy range of $E_\alpha = 25 \rightarrow 15$ MeV, the ^{153}Sm yield amounts to 1.1 MBq/μA·h. Thus the possible batch yield using the α -particle induced reaction may amount up to about 2 GBq of n.c.a ^{153}Sm , if a high-current target of enriched ^{150}Nd is available. Although this total yield would still be much lower than that via the (n,γ) reaction on ^{152}Sm at a nuclear reactor, the advantage of the no-carrier-added form may justify the costs. In Table 5-5 a comparison of production yields of no-carrier-added ^{153}Sm via the investigated (n,p) and (α,n) reactions under the given production conditions is given.

Table 5-5 Comparison of the different production routes of ^{153}Sm in n.c.a form

Nuclear reaction	Production route	Calculated yield (MBq)
$^{153}\text{Eu}(n,p)^{153}\text{Sm}$	Fission neutrons ^{a)}	10.3
	14 MeV d(Be) neutrons ^{b)}	0.022
	Spallation neutrons ^{c)}	180
$^{150}\text{Nd}(\alpha,n)^{153}\text{Sm}$	^4He -beam (25 → 15 MeV) ^{d)}	2.1×10^3

Production conditions:

a) 5 g Eu_2O_3 , $\sigma_{(n,p)} = 0.015 \text{ mb}$, $\Phi = 10^{14} \text{ ncm}^{-2}\text{s}^{-1}$, irradiation time = 100 h

b) 5 g Eu_2O_3 , $\sigma_{(n,p)} = 0.26 \text{ mb}$, $\Phi = 1.2 \times 10^{10} \text{ ncm}^{-2}\text{s}^{-1}$, irradiation time = 100 h

c) 5 g Eu_2O_3 , $\sigma_{(n,p)} = 0.26 \text{ mb}$, $\Phi = 10^{14} \text{ ncm}^{-2}\text{s}^{-1}$, irradiation time = 100 h

d) 100 % enriched $^{150}\text{Nd}_2\text{O}_3$, $I_\alpha = 100 \mu\text{A}$, irradiation time = 30 h

For the production of no-carrier-added ^{169}Yb the proton induced $^{\text{nat}}\text{Tm}(p,n)^{169}\text{Yb}$ process was investigated. The existing information on this nuclear reaction provided by Birattari et al. [1973] were found to be inadequate. In this work the proton energy range from threshold up to 45 MeV was investigated. The resulting cross section data were compared with the results of nuclear model calculations.

The measured cross sections of the $^{169}\text{Tm}(p,n)^{169}\text{Yb}$ reaction together with their uncertainties are given in Table 5-6. They are shown in Figure 5-5 as a function of the proton energy. Since Tm is a monoisotopic element, any correction for isotopic abundance of the target was not necessary. As described above, the experimental data were obtained using three different accelerators. They all exhibit good consistency. Fig. 5-5 shows a distinct maximum cross section, amounting to about 285 mb at 11 MeV proton energy. In general, our excitation function agrees with the results of Birattari et al. [1973], but shows a significant deviation around the maximum, which was determined in more detail in this work. The total uncertainty was calculated according to section 3.6.4 and amounted to about 13 % in general. For validation of the data, theoretical cross section values taken from the MENDL-2P data file [Shubin et al., 1998] are also shown in Fig. 5-5. The uncertainty in the calculation of theoretical cross sections is estimated to be about 15 %. The

agreement between the theoretical values and the experimental data appears to be good. The calculated maximum of the excitation function is slightly lower than the measured one, but considering the uncertainties of both, the agreement is regarded as good.

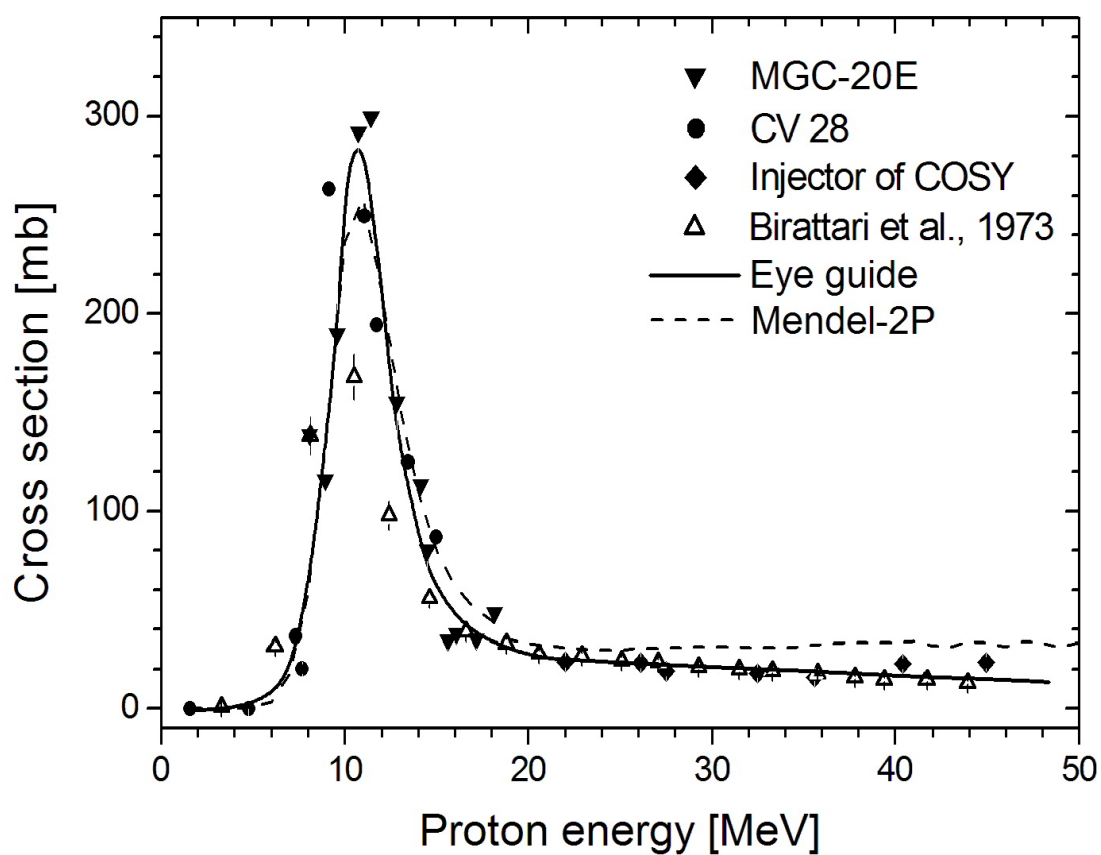


Fig. 5-5 Excitation function of the $^{169}\text{Tm}(p,n)^{169}\text{Yb}$ reaction. Experimental data were measured using three different cyclotrons (MGC-20E, CV 28, Injector of COSY). MENDL-2P is the activation data file based on ALICE-IPPE calculations [Shubin et al., 1998].

Table 5-6 Measured cross sections of the $^{169}\text{Tm}(p,n)^{169}\text{Yb}$ reaction and the estimated mean uncertainties

Proton energy (MeV)	Cross section (mb)
4.8 ± 0.6	0.2 ± 0.1
7.3 ± 0.5	37 ± 5
7.7 ± 0.5	20 ± 3
8.1 ± 0.4	134 ± 17
8.9 ± 0.4	112 ± 15
9.1 ± 0.4	263 ± 34
9.6 ± 0.4	184 ± 24
10.7 ± 0.3	284 ± 37
11.1 ± 0.3	250 ± 33
11.4 ± 0.3	291 ± 38
11.8 ± 0.4	194 ± 25
12.8 ± 0.3	151 ± 20
13.4 ± 0.4	125 ± 16
14.1 ± 0.3	110 ± 14
14.5 ± 0.4	78 ± 10
15.0 ± 0.3	87 ± 11
15.6 ± 0.3	33 ± 4
16.1 ± 0.3	37 ± 5
17.2 ± 0.3	34 ± 5
18.2 ± 0.3	47 ± 6
22.0 ± 0.8	36 ± 5
26.1 ± 0.7	34 ± 4
27.5 ± 0.7	28 ± 4
32.5 ± 0.5	27 ± 4
35.6 ± 0.4	25 ± 3
40.4 ± 0.4	23 ± 3
44.9 ± 0.2	22 ± 3

Based on the experimentally determined cross sections it is possible to calculate the differential and integral yields of the produced radioisotope, thus enabling the estimation of batch yields and their comparison with yields obtained via other routes. In this work the yields were calculated from the eye-guide curve in Fig. 5-5. The calculated integral yield of ^{169}Yb is shown in Figure 5-6 as a function of the proton energy. It refers to a pure ^{169}Tm target, an irradiation time of 1 h and a beam current of $1\ \mu\text{A}$. Evidently, the yield increases significantly with the increasing proton energy up to about 16 MeV, and only marginally thereafter. This suggests that the use of protons of energies above 16 MeV for the production of ^{169}Yb via the (p,n) reaction is not very meaningful. The optimum energy range appears to be $E_p = 16 \rightarrow 7\ \text{MeV}$, the integral yield of ^{169}Yb amounting to $1.5\ \text{MBq}/\mu\text{A}\cdot\text{h}$.

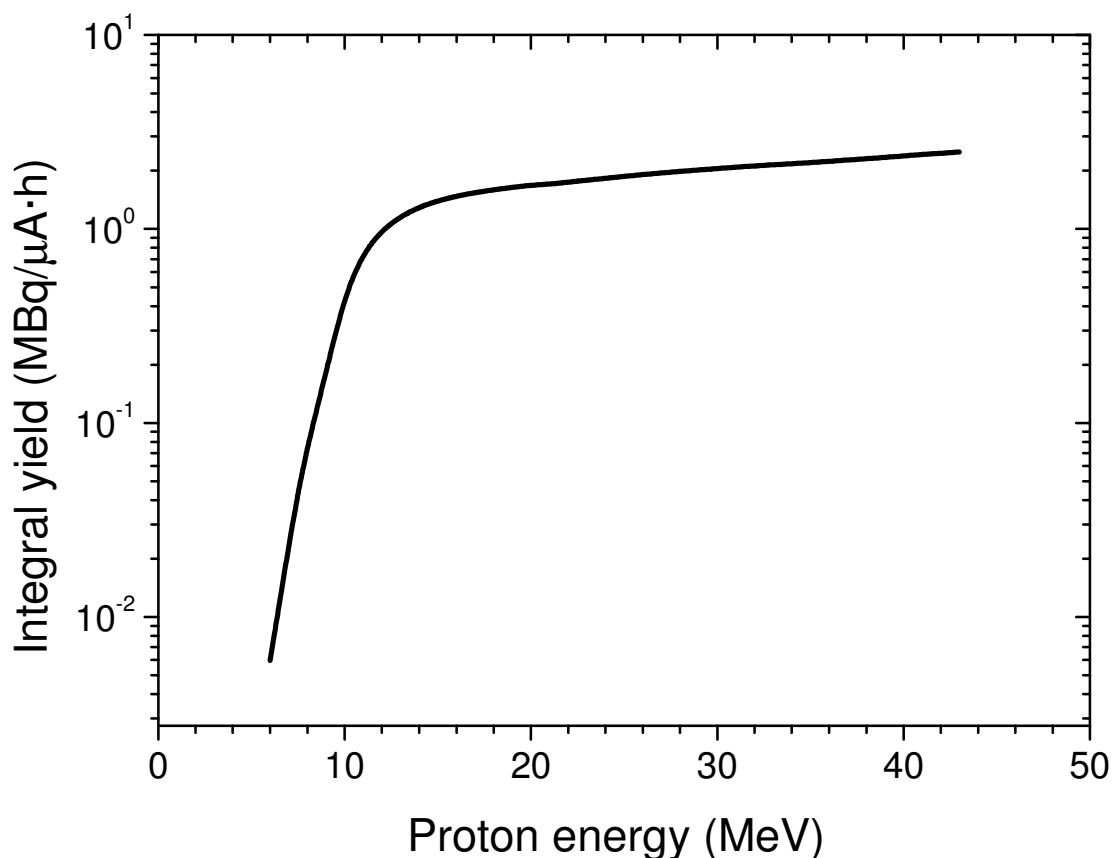


Fig. 5-6 Calculated integral yield of ^{169}Yb from the measured excitation function of the $^{169}\text{Tm}(p,n)^{169}\text{Yb}$ reaction.

A comparison of the data relevant to the reactor and cyclotron production of ^{169}Yb is given in Table 5-7. The average cross section of the $^{168}\text{Yb}(n,\gamma)^{169}\text{Yb}$ process is very high as compared to that of the $^{169}\text{Tm}(p,n)^{169}\text{Yb}$ reaction. However, the abundance of ^{168}Yb in natural ytterbium is only 0.13 %. In practice, therefore, a 17.1 % enriched ^{168}Yb in natural ytterbium is only 0.13 %. In practice, therefore, a 17.1 % enriched ^{168}Yb in natural ytterbium is only 0.13 %. In practice, therefore, a 17.1 % enriched ^{168}Yb in natural ytterbium is only 0.13 %. In practice, therefore, a 17.1 % enriched ^{168}Yb in natural ytterbium is only 0.13 %.

Table 5-7 Comparison of reactor and cyclotron based production of ^{169}Yb

Parameter	Nuclear reactor*	Cyclotron†
Reaction	$^{168}\text{Yb}(n,\gamma)^{169}\text{Yb}$	$^{169}\text{Tm}(p,n)^{169}\text{Yb}$
Cross section	$\langle\sigma\rangle = 2300 \text{ b}$	excitation function up to 45 MeV ($\sigma_{\text{max}} = 285 \text{ mb}$ at 11 MeV)
Target	^{168}Yb in Yb_2O_3 (17 % enriched)	Tm_2O_3
Flux	$2 \cdot 10^{14} \text{ n}\cdot\text{cm}^{-2}\cdot\text{s}^{-1}$	$1.87 \cdot 10^{15} \text{ p}\cdot\text{s}^{-1}$
Irradiation	100 h	30 h
Yield	10.63 TBq‡	13.42 GBq ($E_p = 16 \rightarrow 7 \text{ MeV}$) 21.46 GBq ($E_p = 40 \rightarrow 7 \text{ MeV}$)
Specific activity	12.11 TBq/g(Yb)	no-carrier-added

* Assuming the conditions described in the IAEA-TECDOC-1340 [cf. Környei, 2003].

† Estimates based on cross section measurements and assumptions made in this work.

‡ Irradiation of 1g of the enriched target using the whole neutron spectrum.

However, the reactor produced ^{169}Yb is only of low specific activity containing, besides “cold” ^{168}Yb , radioactive ^{175}Yb and ^{177}Yb as impurities, resulting in the necessity of a 30 days cooling period. Furthermore, the use of isotopically enriched ^{168}Yb leads to an increase in costs. On the other hand, cyclotron irradiations are also expensive. At a cyclotron ^{169}Yb is, however, obtained in “no-carrier added” form and the quantities that can be produced are sufficient for medical application without relying on the availability of enriched ^{168}Yb .

Recent studies on the production of no-carrier-added ^{169}Yb using the $^{169}\text{Tm}(d,2n)^{169}\text{Yb}$ process have shown that in the heavy-mass region this reaction is more suitable [Tárkányi et al., 2006]. The excitation function showing a maximum of about 580 mb at 13.5 MeV deuteron energy, leading to a thick target yield of about 3.8 MBq/ $\mu\text{A}\cdot\text{h}$ of n.c.a. ^{169}Yb in the investigated energy range of 20 \rightarrow 9 MeV. Thus, in case a suitable deuteron beam is available, the production of ^{169}Yb can be done more effectively via the $^{169}\text{Tm}(d,2n)^{169}\text{Yb}$ process than via the $^{169}\text{Tm}(p,n)^{169}\text{Yb}$ reaction.

5.3 Cross sections for the formation of the radionuclides ^{71}As , ^{72}As , ^{73}As and ^{74}As

The diagnostic β^+ -emitters ^{71}As ($T_{1/2} = 65.28$ h), ^{72}As ($T_{1/2} = 26.01$ h) and ^{74}As ($T_{1/2} = 17.77$ d) are potential analytical tools in nuclear medicine, and ^{73}As ($T_{1/2} = 80.30$ d) is of interest in environmental research. Their production via the (p,xn) processes has been reported [Basile et al., 1981, Horiguchi et al. 1983], but a reliable cross section data base is missing. In this work the reactions $^{\text{nat}}\text{Ge}(p,\text{xn})^{71,72,73,74}\text{As}$ within the proton energy range of 100 MeV down to the threshold energy of the corresponding nuclear reaction were studied.

5.3.1 Cross section measurements using $^{\text{nat}}\text{Ge}$ as target

Table 5-8 shows the measured cross sections and corresponding uncertainties for the formation of ^{71}As , ^{72}As , ^{73}As and ^{74}As via the (p,xn) processes on natural germanium. The measured cross section values thus refer to elemental germanium. The data were acquired using three different accelerators (cf. section 3). In general, all experiments show good consistency. However, the data resulting from irradiations at the injector of COSY are slightly lower. The total uncertainty was calculated with error propagation according to Gauss. In general, it amounts to 8 to 13 % but may be larger in case of very small cross sections. The mean uncertainty of the proton energy is estimated as ± 0.2 to 0.5 MeV but may in individual cases exceed this limit, when the proton beam energy is degraded over a very large range.

Table 5-8 Measured cross section data for the formation of ^{71}As , ^{72}As , ^{73}As and ^{74}As via the $^{\text{nat}}\text{Ge}(p,xn)$ reaction

Energy [MeV]	Formation cross section (mb)			
	^{71}As	^{72}As	^{73}As	^{74}As
4.9 ± 1.7		105.2 ± 8.9	35.7 ± 3.2	181.4 ± 15.4
6.7 ± 0.8		70.0 ± 10.1		135.2 ± 9.9
8.6 ± 0.7	0.4 ± 0.1	113.3 ± 10.8		164.8 ± 16.5
10.2 ± 0.6		208.2 ± 9.9		336.9 ± 33.4
11.0 ± 1.5	1.1 ± 0.1	212.0 ± 18.0	113.7 ± 9.6	275.4 ± 23.4
12.7 ± 0.4	0.5 ± 0.1			115.2 ± 10.9
12.8 ± 0.6				193.4 ± 10.1
13.4 ± 0.5		165.8 ± 15.1		180.8 ± 12.4
13.8 ± 0.5	1.4 ± 0.2	246.4 ± 14.9		280.7 ± 8.7
14.0 ± 0.5		161.9 ± 10.7		256.6 ± 15.0
14.9 ± 1.4	55.8 ± 7.5	184.7 ± 15.7	298.9 ± 25.4	104.0 ± 8.9
15.2 ± 0.5	10.4 ± 0.9			
15.5 ± 0.5	31.6 ± 2.4	162.2 ± 10.1		90.9 ± 9.8
15.6 ± 0.5	37.1 ± 2.6	144.1 ± 12.4		74.1 ± 15.2
16.1 ± 0.5	35.9 ± 3.4	143.8 ± 8.2		78.7 ± 11.9
18.1 ± 1.2	144.7 ± 15.9	107.0 ± 9.1	349.3 ± 29.7	56.8 ± 8.9
18.3 ± 0.5	85.0 ± 11.9	77.0 ± 14.1		30.0 ± 7.4
18.6 ± 0.5	115.6 ± 8.7	88.7 ± 11.1		34.2 ± 7.1
18.9 ± 0.5	77.8 ± 7.3	64.1 ± 6.3		25.8 ± 12.1
20.0 ± 0.5	126.0 ± 12.7	75.5 ± 11.1		26.1 ± 8.1
22.2 ± 1.2	159.2 ± 16.9	74.2 ± 6.3	330.8 ± 28.1	35.4 ± 3.0
22.7 ± 0.9	139.1 ± 12.8	64.3 ± 5.5		33.2 ± 8.4
26.0 ± 0.9	85.7 ± 7.7	89.3 ± 7.6	252.2 ± 21.4	55.7 ± 3.7
26.4 ± 0.7	100.1 ± 11.2	123.1 ± 10.9		53.1 ± 15.8
27.1 ± 0.7	99.9 ± 9.0	70.9 ± 6.5		45.2 ± 3.4
27.8 ± 0.5	75.8 ± 9.9	156.6 ± 15.4		53.4 ± 12.1
29.1 ± 0.5	101.9 ± 12.1	147.6 ± 12.5	142.7 ± 12.1	65.2 ± 5.5
30.0 ± 0.6	80.3 ± 7.2	135.1 ± 5.9		53.9 ± 6.4
30.7 ± 0.6	70.6 ± 12.9	175.2 ± 15.8		
30.8 ± 0.6	116.4 ± 22.2			53.1 ± 16.1
30.9 ± 0.6				27.7 ± 6.7
32.1 ± 0.5	67.3 ± 5.4	173.5 ± 14.8	86.9 ± 7.4	62.6 ± 5.3
32.5 ± 0.5	61.3 ± 5.5			51.0 ± 10.4
33.6 ± 0.4	52.6 ± 4.8			57.9 ± 9.1
33.6 ± 0.4	43.1 ± 4.7			
35.8 ± 0.4		164.6 ± 14.0		50.0 ± 4.3

Energy [MeV]	Formation cross section (mb)			
	⁷¹ As	⁷² As	⁷³ As	⁷⁴ As
35.9 ± 0.3	55.7 ± 6.8	142.6 ± 11.8	62.7 ± 5.3	61.9 ± 13.8
36.9 ± 0.3	34.6 ± 3.1	84.5 ± 9.7		38.9 ± 2.7
37.1 ± 0.3	45.4 ± 4.7	97.4 ± 20.1		24.7 ± 12.0
37.2 ± 0.2	34.6 ± 3.1	73.3 ± 11.1		24.3 ± 12.1
38.6 ± 0.2	58.9 ± 6.6	131.3 ± 12.3		32.0 ± 8.3
39.2 ± 0.2		137.7 ± 11.7	62.3 ± 5.3	38.5 ± 3.3
39.7 ± 0.2	53.6 ± 4.4	86.8 ± 8.6		20.5 ± 3.4
40.5 ± 0.2	52.6 ± 8.9	72.2 ± 12.5		18.3 ± 14.0
40.8 ± 0.2	38.8 ± 2.9	68.1 ± 6.6		22.0 ± 5.5
42.1 ± 0.2	40.4 ± 3.6	50.9 ± 4.1		16.3 ± 13.4
42.4 ± 0.2	75.6 ± 9.2	94.3 ± 13.9		24.3 ± 16.5
42.5 ± 0.2	53.8 ± 6.7	63.8 ± 20.0	65.3 ± 11.3	17.0 ± 8.1
43.3 ± 0.2	72.9 ± 3.1	76.4 ± 8.3		23.3 ± 3.8
44.3 ± 0.2	54.9 ± 6.2	52.6 ± 10.8		24.2 ± 10.8
45.9 ± 0.2	78.3 ± 6.4	70.0 ± 6.0	60.4 ± 10.5	21.6 ± 1.8
52.0 ± 0.2	66.0 ± 5.6	48.3 ± 4.1	38.8 ± 9.1	16.3 ± 1.4
52.5 ± 0.2	72.5 ± 6.2			
54.9 ± 0.2	55.7 ± 4.7	44.1 ± 3.8	35.1 ± 8.2	13.8 ± 1.4
58.6 ± 0.2	44.8 ± 3.8	40.7 ± 3.5	30.9 ± 9.2	14.3 ± 1.2
62.1 ± 0.2	36.9 ± 3.1	38.8 ± 3.3	45.9 ± 8.1	11.6 ± 1.0
62.9 ± 0.2	28.9 ± 2.5	28.6 ± 5.6		9.7 ± 05.9
63.7 ± 0.2	33.0 ± 2.5	36.7 ± 6.4		10.9 ± 3.0
63.8 ± 0.2	32.4 ± 2.7	34.3 ± 3.7		10.7 ± 2.5
64.3 ± 0.2	37.9 ± 3.2	39.1 ± 6.4		12.9 ± 4.7
64.5 ± 0.2	27.0 ± 2.3	28.5 ± 3.8	35.1 ± 10.3	9.2 ± 2.2
65.0 ± 0.2	27.8 ± 2.4	30.2 ± 6.7	38.8 ± 23.2	9.6 ± 7.7
65.9 ± 0.2	22.2 ± 1.9	23.4 ± 3.3	30.8 ± 18.1	7.5 ± 5.2
66.6 ± 0.2	20.2 ± 1.7	21.5 ± 6.2		6.8 ± 5.2
69.7 ± 0.2	29.3 ± 2.5	29.1 ± 2.5	24.6 ± 17.1	10.6 ± 0.9
74.2 ± 0.2	25.9 ± 2.2	25.3 ± 2.2	24.9 ± 18.5	9.8 ± 0.8
78.5 ± 0.2	23.2 ± 1.9	24.3 ± 2.1	25.4 ± 19.9	9.8 ± 0.8
82.6 ± 0.2	21.8 ± 1.9	20.9 ± 1.8	24.5 ± 20.2	7.7 ± 0.7
86.6 ± 0.2	19.7 ± 1.7	19.3 ± 1.6	22.2 ± 19.3	7.7 ± 0.6
90.5 ± 0.2	18.2 ± 1.5	18.0 ± 1.5	13.4 ± 12.2	7.7 ± 0.7
94.3 ± 0.2	17.0 ± 1.4	17.9 ± 1.5	19.9 ± 18.8	7.4 ± 0.6
97.9 ± 0.2	16.4 ± 1.4	16.1 ± 1.4	14.9 ± 14.6	6.5 ± 0.5

Figures 5-8 to 5-11 show the cross section data determined in this work as a function of proton energy. Besides our data, for comparison the literature experimental results [Basile et al., 1981; Horiguchi et al., 1983] as well as the theoretical curves deduced from the MENDL 2P data file, are also given. Fig. 5-8 shows the cross sections for the formation of ^{71}As . The data measured at FZJ and iThemba LABS are shown separately. Two distinct maxima at about 22 and 48 MeV proton energy, corresponding to the $^{72}\text{Ge}(p,2n)^{71}\text{As}$ and $^{74}\text{Ge}(p,4n)^{71}\text{As}$ reaction channels, respectively, are visible. A maximum for the $^{73}\text{Ge}(p,3n)^{71}\text{As}$ reaction channel cannot be distinguished due to the relatively low abundance (7.73 %) of the target nucleus ^{73}Ge in natural germanium. Our values show very good agreement with the data of Basile et al. [1981] from 15 up to about 40 MeV. The data of Horiguchi et al. [1983] from 20 up to 65 MeV are slightly higher but still agree with the values determined in this work within the limits of uncertainty. Beyond 65 MeV the new data constitute the first measurement. The ALICE-IPPE calculation generally gives the proper form of the excitation function but overestimates the cross sections around the maxima.

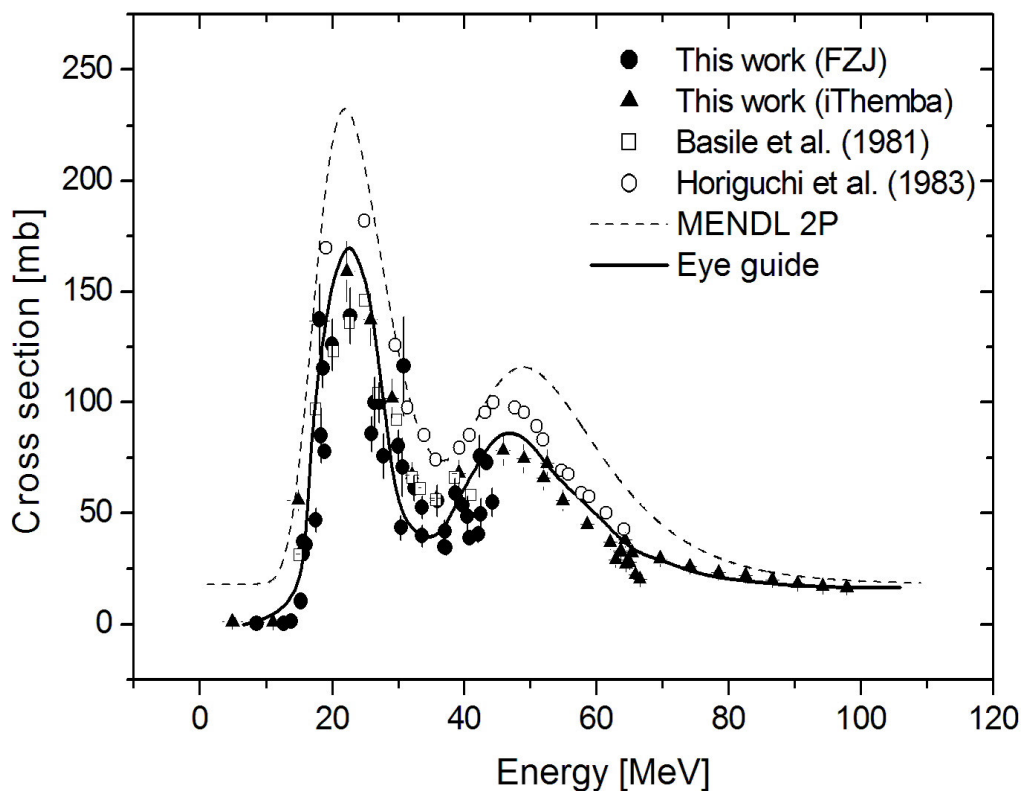


Fig. 5-8 Excitation function of the $^{\text{nat}}\text{Ge}(p,xn)^{71}\text{As}$ reaction in comparison to data from the literature and nuclear model calculation.

The cross section data of the $^{\text{nat}}\text{Ge}(p,xn)^{72}\text{As}$ reaction are given in Fig. 5-9. Again two maxima at about 18 and 45 MeV are observed. They correspond to the $^{73}\text{Ge}(p,2n)^{72}\text{As}$ and $^{75}\text{Ge}(p,4n)^{72}\text{As}$ reactions, respectively. The measured excitation function shows good agreement with the literature data, although the data of Horiguchi et al. [1983] show higher tendency here as well. Also for this reaction the measurements below 9 MeV and above 65 MeV have been done for the first time in this work. The theoretical curve resulting from the ALICE-IPPE calculation agrees well with the experimental results, except for an energy shift in the second maximum. However, with an estimated uncertainty of about 15 % for the theoretical data this deviation is not significant.

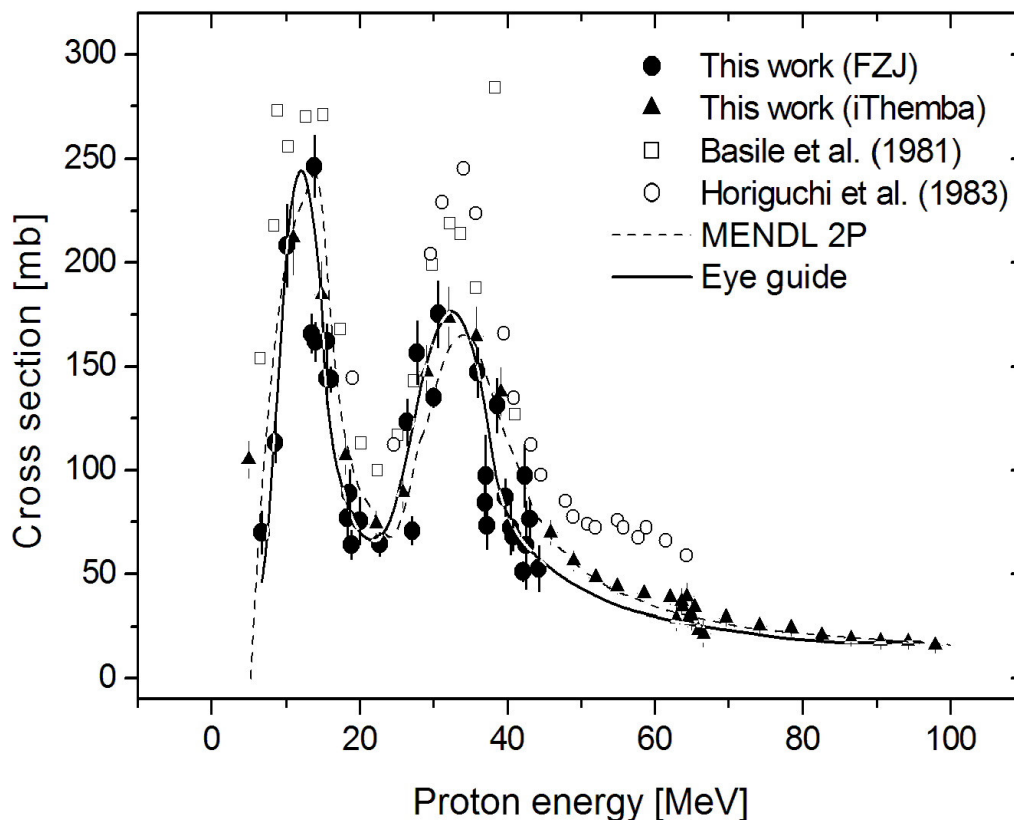


Fig. 5-9 Excitation function of the $^{\text{nat}}\text{Ge}(p,xn)^{72}\text{As}$ reaction in comparison to data from the literature and nuclear model calculation.

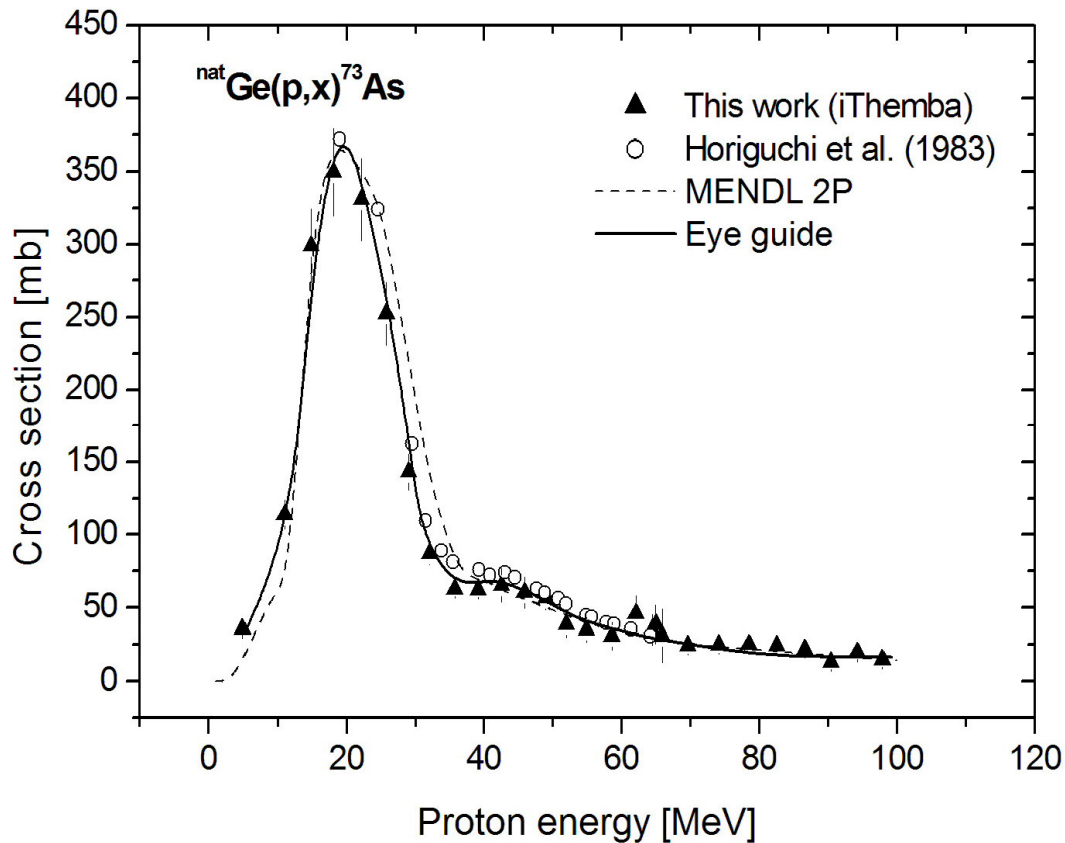


Fig. 5-10 Excitation function of the $^{\text{nat}}\text{Ge}(p,x)^{73}\text{As}$ reaction in comparison to data from the literature and nuclear model calculation.

The excitation function of the $^{\text{nat}}\text{Ge}(p,x)^{73}\text{As}$ reaction is given in Fig. 5-10. In this case a major peak due to the $^{74}\text{Ge}(p,2n)^{73}\text{As}$ reaction at about 20 MeV is observed. The peak is, however, rather broad due to some possible contribution from the low-abundance ^{73}Ge (7.73 %) via the $^{73}\text{Ge}(p,n)^{73}\text{As}$ process. A small bump due to the $^{76}\text{Ge}(p,4n)^{73}\text{As}$ reaction at about 44 MeV is also visible. Due to the low abundance of the ^{76}Ge (7.44 %) the contribution of this nuclear process is small. In the literature only the experimental data of Horiguchi et al. [1983] are available for comparison. Those data from 20 to 65 MeV as well as the calculated excitation function agree very well with our data. The database for the production of ^{73}As is thus strengthened.

Fig. 5-11 shows the results for the $^{\text{nat}}\text{Ge}(p,xn)^{74}\text{As}$ reaction. In this case a conspicuous peak at about 10 MeV is observed and is attributed to the $^{74}\text{Ge}(p,n)^{74}\text{As}$ reaction. A bump at about 31 MeV is due to the occurrence of the $^{76}\text{Ge}(p,3n)^{74}\text{As}$ reaction on the relatively less-abundant ^{76}Ge (7.44 %). The results are compared with the data from the literature. There appears to be good agreement. The data beyond 66 MeV are new. The ALICE code clearly underestimates the height of the maximum. In the area of the second maximum at about 30 MeV the present measurements show good agreement with the calculated data, depicting a slightly smaller maximum than indicated by the results of Basile et al. [1981] and Horiguchi et al. [1983].

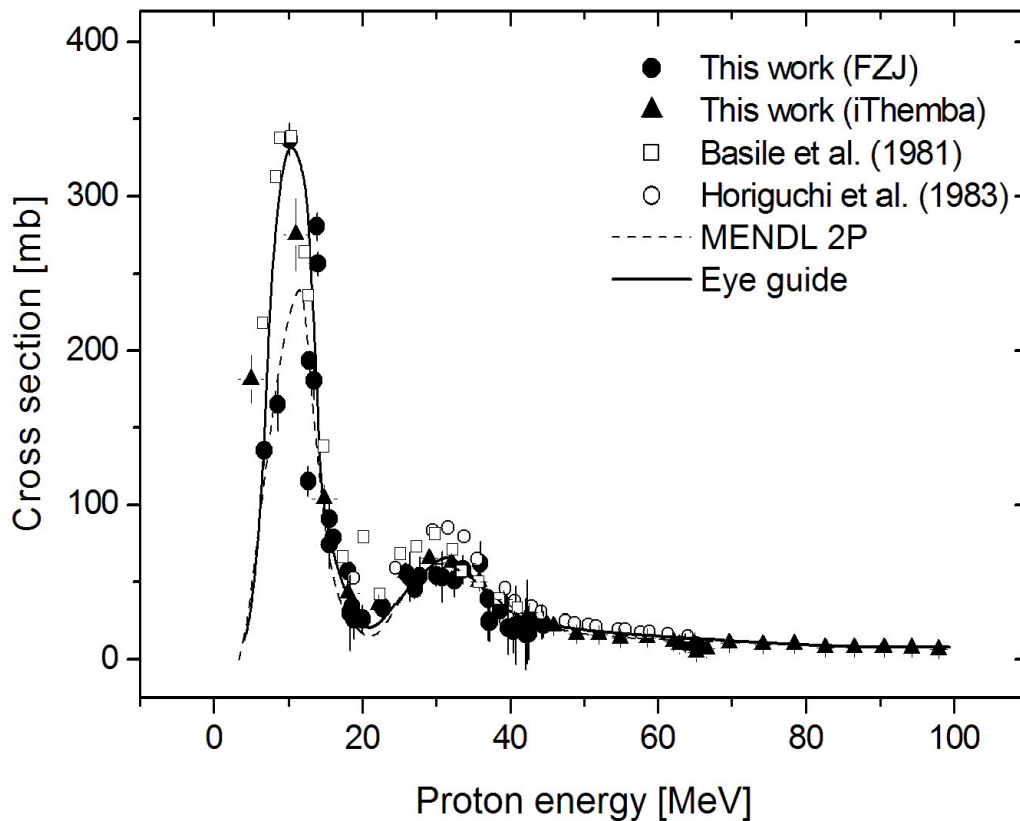


Fig. 5-11 Excitation function of the $^{\text{nat}}\text{Ge}(p,xn)^{74}\text{As}$ reaction in comparison to data from the literature and nuclear model calculation.

5.3.2 Investigation on the production possibilities of ^{71}As , ^{72}As , ^{73}As and ^{74}As

From the excitation functions measured in this work, differential and integral yields of the four radionuclides, namely ^{71}As , ^{72}As , ^{73}As and ^{74}As , were calculated assuming the irradiation time as 1 h and the proton beam current as 1 μA . The integral results are shown in Figure 5-12 as a function of proton energy. Evidently, the yields of the shorter-lived radionuclides ^{71}As and ^{72}As are high and those of the relatively long-lived radionuclides ^{73}As and ^{74}As are low.

It should be interesting to compare the yields calculated from the excitation functions with those measured experimentally using a thick target. Dmitriev and Molin [1981] reported yields for 22 MeV protons on $^{\text{nat}}\text{Ge}$. A comparison of those yields with the results obtained in this work for the same proton energy is given in Table 5-9, generally showing good agreement within the limits of the uncertainties. Regarding the integral yield of ^{73}As the deviation is about 40 % and thus significantly larger. This may be due to the difficulties in the accurate detection of the radioactivity of this radionuclide (cf. 3.5.1). The value of Dmitriev and Molin is estimated to be too low.

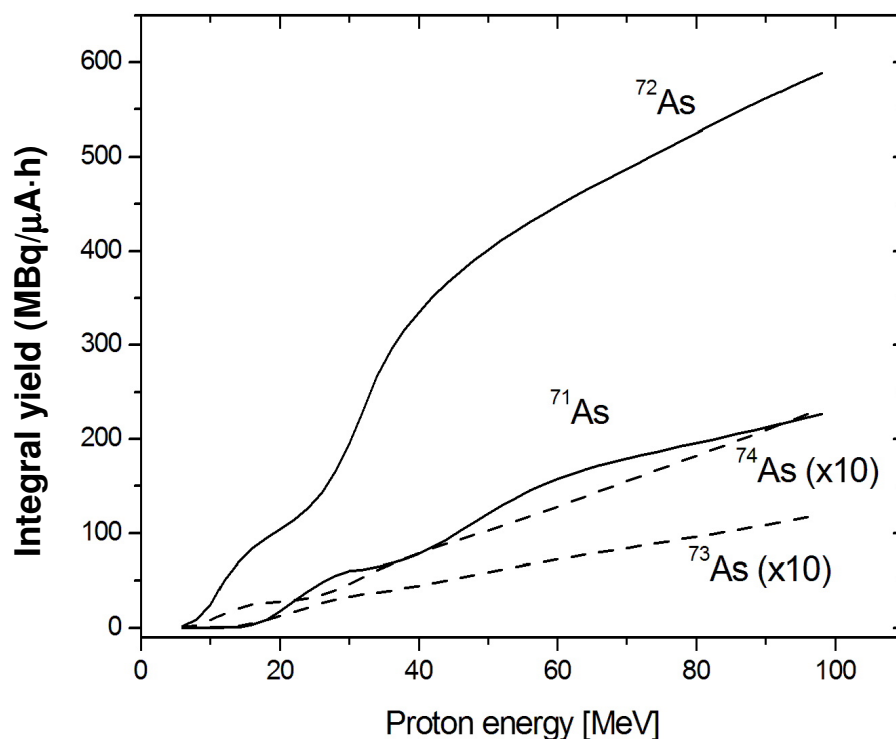


Fig. 5-12 Comparison of the integral yields calculated from the excitation functions. The data of the ^{73}As and ^{74}As curves have been multiplied by a factor of 10 for better demonstration.

Table 5-9 Comparison of thick target yields in the interaction of 22 MeV protons with ^{nat}Ge

Product radionuclide	Thick target yield (MBq/μA·h)	
	This work [*]	Dmitriev et al. [1981] [†]
⁷¹ As	28.1	32
⁷² As	114.4	135
⁷³ As	3.1	1.9
⁷⁴ As	7.4	7.0

* calculated from the excitation function (uncertainty: ± 10 %)

† measured experimentally (uncertainty: 11 – 15 %)

On the basis of the yield curves given in Fig. 5-12, a few general remarks concerning the production possibilities of the four diagnostic radionuclides of arsenic can be made.

From Fig. 5-12 it is obvious that the radionuclide ⁷²As can be produced in relatively large amounts. However, it will contain a large proportion of the somewhat longer-lived ⁷¹As and small amounts of the long-lived radionuclides ⁷³As and ⁷⁴As as impurities. The long-lived ⁷³As, on the other hand, could possibly be produced in a relatively pure form if a decay time of about 60 days is allowed. In Table 5-10 a few suitable energy regions for production of the four radionuclides are given and the conditions under which a reasonable purity could be achieved are considered.

The radionuclide ⁷¹As can be produced over the energy range of $E_p = 50 \rightarrow 18$ MeV with a yield of 118 MBq/μA·h but the level of ⁷²As would be very high. Even after a decay time of 50 h i.e. about two half-lives of ⁷²As, the purity of ⁷¹As would not be very high. Using a higher or lower energy range would not alter the situation; in the higher energy range the level of the long-lived impurities would even increase.

Table 5-10 Possible production yields of arsenic radionuclides and potential impurities produced via the $^{nat}\text{Ge}(p,xn)$ reactions

Radio-nuclide	Energy range [MeV]	Product yield [MBq/ $\mu\text{A}\cdot\text{h}$]	Impurities [%]			
			^{71}As	^{72}As	^{73}As	^{74}As
^{71}As	50 \rightarrow 18	117.6 ^{a)}	†	73 ^{a)}	5.0 ^{a)}	6.1 ^{a)}
		65.16 ^{b)}	†	56 ^{b)}	4.9 ^{b)}	5.7 ^{b)}
^{72}As	18 \rightarrow 8	92.8 ^{a)}	8.6 ^{a)}	†	1.8 ^{a)}	6.3 ^{a)}
	50 \rightarrow 8	399.1 ^{a)}	23 ^{a)}	†	1.8 ^{a)}	3.2 ^{a)}
^{73}As	30 \rightarrow 18	4.0 ^{a)}	93.4 ^{a)}	111.8 ^{a)}	†	41.2 ^{a)}
		2.4 ^{c)}	--	--	†	11.1 ^{c)}
^{74}As	18 \rightarrow 8	6.2 ^{a)}	58.4 ^{a)}	93.7 ^{a)}	21.5 ^{a)}	†
		3.5 ^{d)}	5.4 ^{d)}	0.2 ^{d)}	30.0 ^{d)}	†

a) at EOB b) 50 h after EOB c) 60 days after EOB d) 15 days after EOB
 †) radionuclide of interest

The radionuclide ^{72}As can be produced over the energy range of $E_p = 18 \rightarrow 8$ MeV with about 9 % ^{71}As impurity and the yield (93 MBq/ $\mu\text{A}\cdot\text{h}$) is rather low. Using a higher energy range of $E_p = 50 \rightarrow 8$ MeV would lead to a higher yield of ^{72}As (399 MBq/ $\mu\text{A}\cdot\text{h}$) but the level of ^{71}As impurity would also increase. A certain waiting time after EOB would not improve the situation; on the contrary, due to the longer half-lives of the three other radionuclides under study as compared to ^{72}As , the level of impurity will increase with the decay time.

From the above discussion it is concluded that neither ^{71}As nor ^{72}As , i.e. the two radionuclides of interest in PET studies, can be produced in large yield, and with high radionuclidic purity via the (p,xn) reactions on ^{nat}Ge . If a mixture of the two could be tolerated, then the production would be meaningful. The radionuclide ^{72}As , on the other hand, could be produced in small quantities with a reasonable radionuclidic purity (^{71}As level: < 10 %) if the low-energy range of $E_p = 18 \rightarrow 8$ MeV is utilised. For better production, however, a highly enriched ^{72}Ge target would be advantageous; the yield of ^{72}As would then become almost four times higher.

The production of ^{74}As has been discussed in detail by Basile et al. [1981] in connection with its application in environmental studies. The present measurements reveal that the most suitable energy range for the production of this radionuclide is $E_p = 18 \rightarrow 8$ MeV. The yield is relatively low (6.2 MBq/ $\mu\text{A}\cdot\text{h}$) and the level of the impurities high at EOB. However, if a waiting time of 15 days is allowed (i.e. till ^{71}As and ^{72}As have decayed out), then the only impurity would be ^{73}As at a level of about 30 %.

The radionuclide ^{73}As , which we consider more suitable for environmental studies, can be produced over the energy range of $E_p = 30 \rightarrow 18$ MeV with a yield of 4 MBq/ $\mu\text{A}\cdot\text{h}$. The level of radionuclidic impurities at EOB is rather high but within a decay time of about 60 days, it will decrease drastically, the only impurity then being ^{74}As at a level of about 11 %. Assuming that a $^{\text{nat}}\text{Ge}$ target can withstand 30 MeV proton beam currents of about 100 μA and that the irradiation time is 30 h, about 7 GBq of ^{73}As of high-radionuclidic purity could be obtained at 60 d after EOB. This quantity should be sufficient for environmental studies.

5.3.3 Cross section measurements using enriched ^{72}Ge as target

While using natural target material, the identification and quantification of individual nuclear reaction channels is difficult and may in some cases be impossible, due to several overlapping peaks in an excitation function. The use of enriched target material may help in resolving such overlapping regions.

Within the scope of this work some preliminary experiments have been done using enriched ^{72}Ge (96.4 %). The aim was to separate the various contributing processes to the formation of ^{71}As via the $^{\text{nat}}\text{Ge}(p,xn)^{71}\text{As}$ reaction. To achieve this, cross section measurements were done on the interaction of $^{72}\text{GeO}_2$ with protons in the energy range between 66.5 MeV and 23 MeV. The measured cross sections are given in Table 5-11 and are reproduced in Figure 5-13 as a function of proton energy together with a fitted curve. In order to compare these results with those on natural Ge, these data were corrected by a factor of 0.274 to represent the abundance of ^{72}Ge in the natural target material. By subtracting these corrected cross section values from the fitted excitation function of the $^{\text{nat}}\text{Ge}(p,xn)^{71}\text{As}$ reaction shown in Fig. 5-8, the cross section data of the $^{73}\text{Ge}(p,3n)^{71}\text{As}$ and $^{74}\text{Ge}(p,4n)^{71}\text{As}$ processes could

be calculated. The thus extracted nuclear data were then corrected to 100 % isotopic abundance of ^{73}Ge and ^{74}Ge and the results obtained are shown in Figure 5-14 as a function of proton energy. Two distinctive maxima can be observed. The first peak at 24.7 MeV corresponds to the (p,3n) reaction on ^{73}Ge and shows a maximum cross section of about 840 mb. The cross section of the (p,4n) reaction on pure ^{74}Ge amounts to about 200 mb at 47.2 MeV proton energy.

On the basis of these results further analysis of data seems to be promising. Further irradiations within an extended proton energy range would allow for a better evaluation of the production routes of the other diagnostic radionuclides ^{72}As , ^{73}As and ^{74}As , and thus may be interesting topics for further research projects.

Table 5-11 Measured cross sections of the $^{72}\text{Ge}(p,2n)^{71}\text{As}$ reaction using enriched target material

Proton energy (MeV)	Cross section (mb)
23.2 ± 0.9	466.5 ± 46.6
26.3 ± 0.7	254.7 ± 25.5
27.0 ± 0.7	282.3 ± 21.82
30.7 ± 0.6	161.6 ± 16.2
33.3 ± 0.4	91.0 ± 15.2
33.9 ± 0.4	100.8 ± 25.0
39.5 ± 0.3	68.6 ± 12.1
46.6 ± 0.3	64.0 ± 14.0
54.9 ± 0.3	49.3 ± 15.0
63.2 ± 0.4	13.5 ± 1.4
63.9 ± 0.2	12.1 ± 1.2
64.5 ± 0.2	24.2 ± 2.4
65.2 ± 0.2	19.8 ± 2.0
65.9 ± 0.2	16.6 ± 1.7
66.5 ± 0.2	19.2 ± 1.9

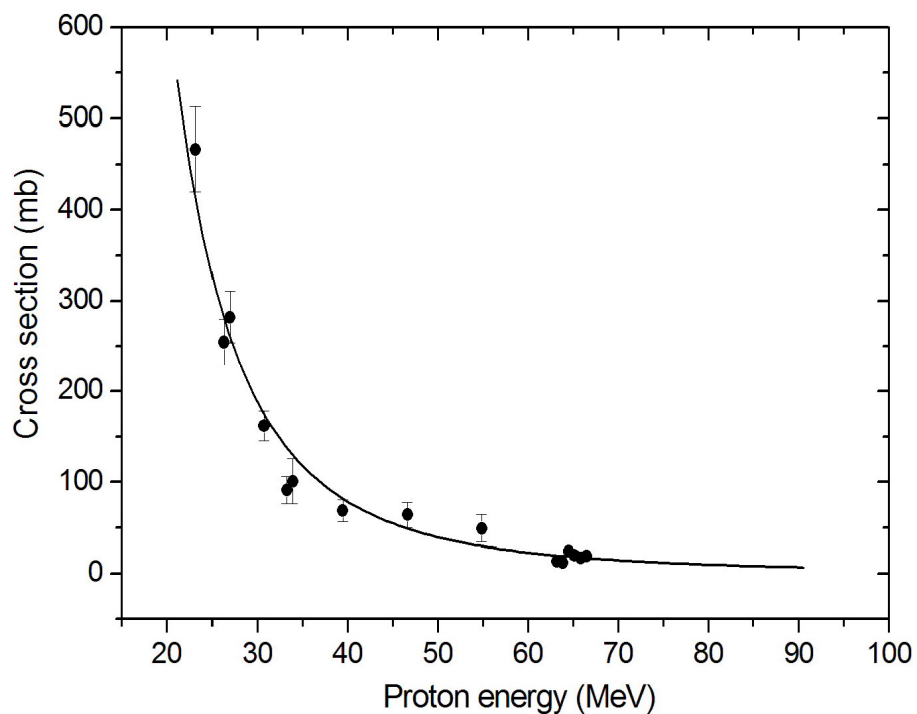


Fig. 5-13 Cross sections of the $^{72}\text{Ge}(p,2n)^{71}\text{As}$ nuclear reaction on 96.4 % enriched ^{72}Ge , plotted as a function of proton energy.

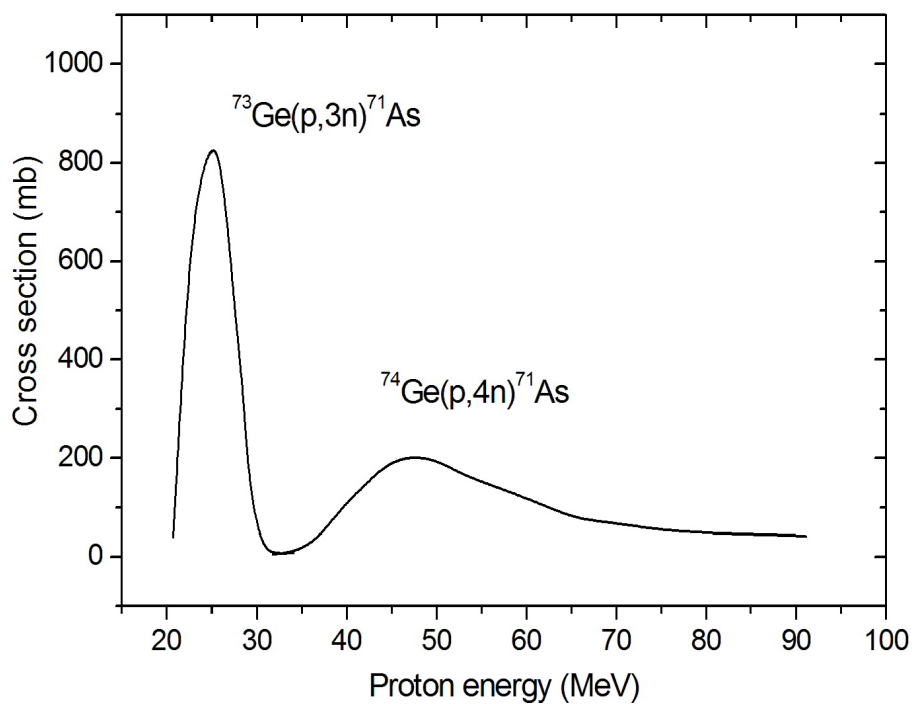


Fig. 5-14 Excitation functions of the $^{73}\text{Ge}(p,3n)^{71}\text{As}$ and $^{74}\text{Ge}(p,4n)^{71}\text{As}$ processes, calculated from the results on ^{72}Ge and $^{\text{nat}}\text{Ge}$ and extrapolated to 100 % isotopic abundance.

5.4 Standardisation and validation of data for the production of ^{82}Sr via the $^{\text{nat}}\text{Rb}(p,xn)$ process

Concerning the important radionuclide ^{82}Sr , an accurate knowledge of the ideal production conditions is desired. The available information on the excitation functions of nuclear processes on ^{85}Rb and $^{\text{nat}}\text{Rb}$ leading to the formation of ^{82}Sr was recently evaluated under the auspices of the IAEA [Qaim et al., 2001]. With a view to resolving some discrepancies in the data, two independent measurements were performed over the last four years: one on highly enriched ^{85}Rb under a German - South African collaboration [Kastleiner et al., 2002] and the other one on $^{\text{nat}}\text{Rb}$ under a Hungarian-Japanese collaboration [Ido et al., 2002]. A third measurement on $^{\text{nat}}\text{Rb}$ has recently been reported by Buthelezi et al. [2006], though with somewhat undefined uncertainties. There were also discrepancies in the data for the formation of the long-lived activity ^{85}Sr . These have hitherto not been resolved. Therefore, an aim of this work was also to measure cross sections of the $^{\text{nat}}\text{Rb}(p,x)^{85}\text{Sr}$ process in the energy range where the database is especially weak. The final goal was to present standardised data for the formation of ^{82}Sr .

The cross section measurements in the present work were done via the well-known stacked-foil technique over the limited energy range of 25 to 45 MeV. The ^{85}Sr activity was determined using the 514 keV γ -ray. Counting was started about three months after the end of irradiation so that many of the positron emitters had decayed out. Decay curve analyses were done for all samples. Due to the close proximity of the 514 keV γ -line to the broad 511 keV annihilation peak, the use of a high resolution detector and good software for spectrum analysis was essential. The agreement between the cross section data determined in this work and those of Buthelezi et al. [2006] is not good. We consider that the uncertainties given in the latter publication are too small. Those authors used RbCl samples of 100 – 200 mg/cm^2 (in contrast to thin samples employed by us) and so each point had a rather large energy spread. Secondly, it is not clear how in that work the 514.0 keV γ -ray of ^{85}Sr was analysed from the annihilation radiation. In any case the total uncertainty of about 14 % reported by them appears to be too low. The experimentally determined cross section values for the formation of the radionuclide ^{85}Sr via the $^{\text{nat}}\text{Rb}(p,xn)^{85}\text{Sr}$ process are given in Table 5-12. The total uncertainty in the data amounts to about

20 %. The measured reaction cross sections are shown in Figure 5-15 as a function of proton energy. The curve given in Fig. 5-15 is fitted to the most concordant data points. This was achieved by a fitting curve, which was drawn through the averaged values of the concordant sets of data using the program *Table Curve 2D*. Cross section values which showed large deviations were discarded. In the region of 25 to 45 MeV a Gaussian shape was adopted. The fitted curve in Fig. 5-15 is now recommended as the standard curve for the formation of ^{85}Sr from $^{\text{nat}}\text{Rb}$.

The existing data from Sakamoto et al. [1984], Ido et al. [2002], and Buthelezi et al. [2006] are also shown in Fig. 5-15. The data of Kastleiner et al. [2002] up to 20 MeV, normalised to $^{\text{nat}}\text{Rb}$, are also given. They could not be normalised to $^{\text{nat}}\text{Rb}$ at proton energies above 20 MeV (as in the case of ^{82}Sr production) since out of the two contributing processes, viz. $^{85}\text{Rb}(p,n)^{85}\text{Sr}$ and $^{87}\text{Rb}(p,3n)^{85}\text{Sr}$, the relative contribution of the (p,3n) process is expected to be appreciable but cannot be estimated from measurements on ^{85}Rb .

Table 5-12 Experimental cross section values of the $^{\text{nat}}\text{Rb}(p,xn)^{85}\text{Sr}$ reaction

Energy (MeV)			Cross section (mb)		
24.5	±	0.4	34.4	±	6.9
27.7	±	0.4	86.6	±	17.3
28.1	±	0.3	81.2	±	16.2
30.6	±	0.3	98.7	±	19.7
32.7	±	0.3	102.4	±	20.5
33.0	±	0.3	120.7	±	24.1
36.7	±	0.3	127.8	±	25.6
41.3	±	0.2	63.6	±	12.7
44.7	±	0.2	45.4	±	9.1

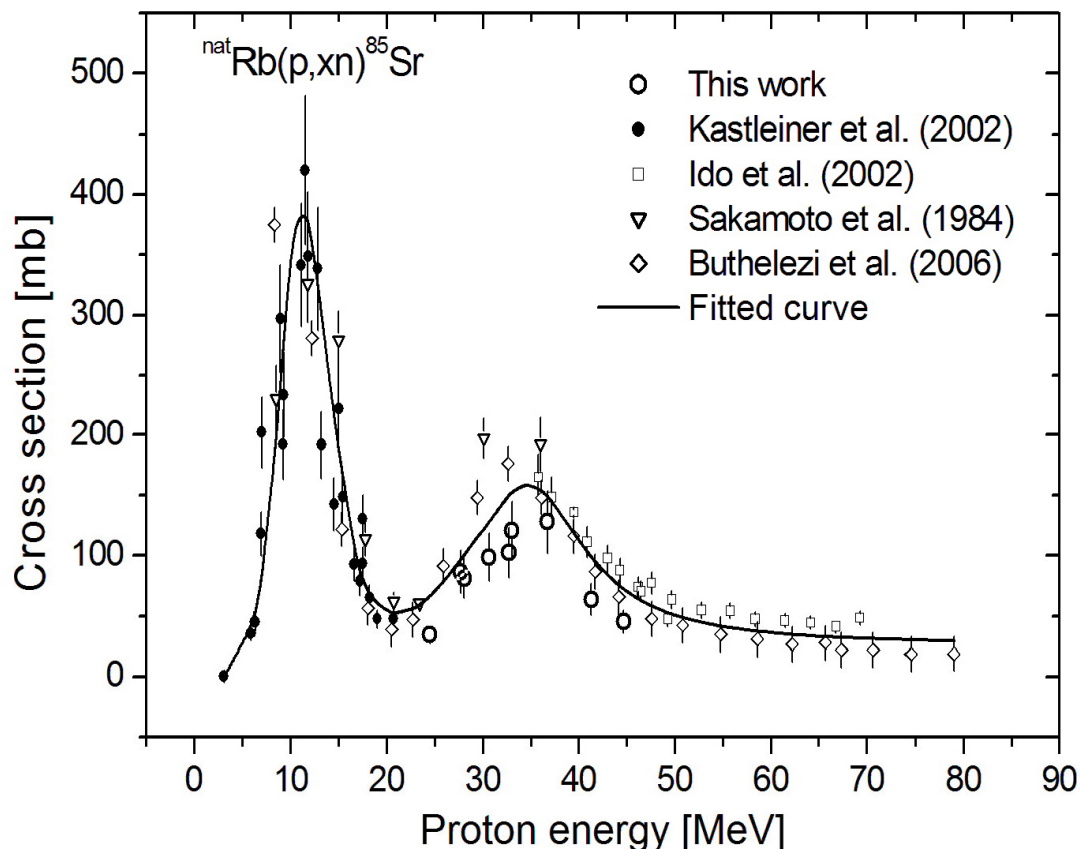


Fig. 5-15 Evaluated excitation function of the $^{nat}\text{Rb}(p,xn)^{85}\text{Sr}$ process. The data by Kastleiner et al. (2002) for the $^{85}\text{Rb}(p,n)^{85}\text{Sr}$ reaction were normalised to ^{nat}Rb up to 20 MeV.

Based on the fitted excitation function the integral yield of the $^{nat}\text{Rb}(p,xn)^{85}\text{Sr}$ reaction was calculated as described above. The result is shown in Figure 5-16 as a function of proton energy together with the yield curve of ^{82}Sr , which was calculated from the evaluated excitation function. Beyond 65 MeV the yield of ^{82}Sr is still increasing but that of ^{85}Sr does not show any significant increase anymore. Considering the spread of the measured data, the uncertainty of the yield calculations is estimated to be about 10 %. According to these calculations the ^{82}Sr obtained is of high radionuclidic purity (over the energy range of 70 to 40 MeV), the level of ^{85}Sr impurity being below 12 %.

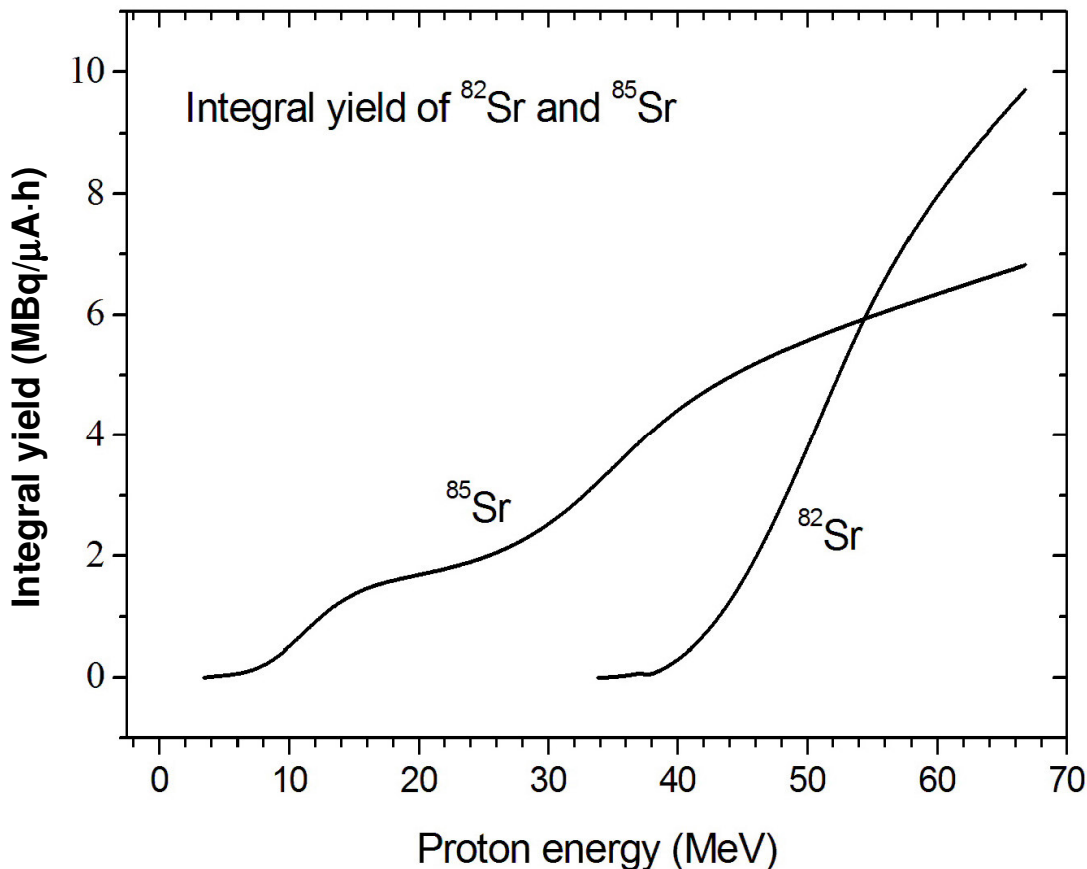


Fig. 5-16 Integral yields of ⁸⁵Sr and ⁸²Sr in proton irradiation of ^{nat}RbCl, calculated using the evaluated excitation curves given in Fig. 5-15 and in [Qaim et al., 2007].

For the validation of the evaluated cross section data, the calculated production yields were compared with the experimentally determined values. The production yields of ⁸²Sr and ⁸⁵Sr were measured using thick ^{nat}RbCl targets. Such targets are commonly employed at iThemba LABS for producing large quantities of ⁸²Sr on a routine basis. A comparison of the calculated and experimental yields for several energy ranges is given in Table 5-13. The uncertainty in the experimentally determined absolute radioactivity of ⁸²Sr and ⁸⁵Sr is estimated to be about 12 % and that in the beam current measurement about 7 %; the total uncertainty thus amounts to about 14 %.

Table 5-13 Yield comparison of ^{82}Sr and ^{85}Sr in proton irradiation of $^{\text{nat}}\text{RbCl}$

Energy range (MeV)	Yield ^{82}Sr (MBq/ μAh)		Yield ^{85}Sr (MBq/ μAh)		Ratio $^{85}\text{Sr}/^{82}\text{Sr}$	
	Calc.	Experimental	Calc.	Experimental	Calc.	Experimental
65 \rightarrow 44.2	8.06	8.67 \pm 0.92	1.73	1.54 \pm 0.22	0.21	0.18
61.5 \rightarrow 39.4	8.18	9.02 \pm 0.95	2.18	---	0.27	---
60 \rightarrow 37.4	7.92	9.07 \pm 0.92	2.47	2.15 \pm 0.32	0.27	0.24
55 \rightarrow 29.9	6.20	7.13 \pm 0.73	3.52	3.11 \pm 0.46	0.57	0.44
50 \rightarrow 21.4	3.78	4.41 \pm 0.42	3.83	3.60 \pm 0.50	1.01	0.82
45 \rightarrow 9.7	1.59	1.86 \pm 0.20	4.81	5.15 \pm 0.72	3.03	2.77

Evidently, the agreement between experiment and calculation concerning the production yields of both ^{82}Sr and the impurity ^{85}Sr is good (between 7 and 15 %). These integral measurements thus confirm the reliability of the evaluated excitation functions. Whereas in the field of neutron data such integral tests of differential data have been often performed, regarding charged particle data very few such tests have been carried out. With the standardisation of data and yield measurements under well-defined conditions, the recommended sets of data have been validated. The last column in Table 5-13 gives the experimentally obtained ratio of ^{85}Sr to ^{82}Sr . For each energy range, it is very close to that calculated from Fig. 5-16. Evidently, the amount of the ^{85}Sr impurity is relatively high. Although it is not as high as in the spallation of molybdenum, it is much higher than that when enriched ^{85}Rb is used as the target material. Thus in an actual production process, the advantages and disadvantages of the use of the highly enriched target material need to be analysed. If $^{\text{nat}}\text{Rb}$ is used as the target material, an incident proton energy of 60 MeV or above is recommended. The ^{85}Sr impurity would then correspond to $< 20\%$.

5.5 Preliminary tests on the production of n.c.a. ^{73}Se via the $^{75}\text{As}(p,3n)^{73}\text{Se}$ reaction using novel targetry

Concerning the PET radionuclide ^{73}Se ($T_{1/2} = 7.1$ h), the aim of this work was not to study an alternative production reaction, since this question has been discussed in several previous publications [Mushtaq et al., 1988, Mushtaq and Qaim, 1990], leading to the establishment of the $^{75}\text{As}(p,3n)^{73}\text{Se}$ reaction as the most applicable production process. The effort of this work was therefore devoted to improvement in targetry and radiochemical separation of no-carrier-added ^{73}Se .

To this end a new target material was introduced. The copper-arsenic alloy (Cu_3As) which has been used before [Blessing et al., 1982], bears several disadvantages. First of all, this metal alloy is not commercially available to date and requires an extensive laboratory effort for its preparation [Blessing et al., 1982, Blessing and Qaim, 1984], with an arsenic ratio, which is limited to about 30 % at maximum in the compound. Higher ratio is possible, but leads to the formation of inhomogeneities and may also lead to decomposition at higher temperatures [Heyding and Despault, 1960]. Furthermore, the alloy contains a high fraction of copper, which, though advantageous concerning the heat transport and the processability of the material, leads to a very high activation during proton irradiations, due to the generation of ^{62}Zn ($T_{1/2} = 9.19$ h), ^{63}Zn ($T_{1/2} = 38.47$ min) and ^{65}Zn ($T_{1/2} = 244.26$ d). The use of the suggested AIAs alloy as target material may remedy these disadvantages. The fraction of Al in pure Cu_3As is only about 25 % [Heyding and Despault, 1960] and the generation of the radioactive by-products ^{22}Na ($T_{1/2} = 2.60$ a) and ^{24}Na ($T_{1/2} = 14.96$ h) is less of a problem. In Table 5-14 a comparison of both target materials is given. The AIAs used in this work is commercially available and was bought from Aldrich Chemical Company Inc.

Table 5-14 Comparison of the target materials Cu_3As and AIAs

	Molar weight (g/mol)	As content (%)	Melting point (°C)
Cu_3As	265.560	31	830
AIAs	101.903	73.5	1740

However, the utilisation of AIAs for high-current irradiations shows some drawbacks as well. As mentioned above (3.2.2) the compound is badly compressible and has to be capsuled for irradiation, thus implying the necessity of mechanically removing the material from the capsule prior to the radiochemical separation. Furthermore, it cannot withstand very high currents. Several of such capsuled AIAs samples were irradiated at the SSC of iThemba LABS. The radioactivity of ^{73}Se produced was determined via non-destructive γ -ray spectrometry. The average production yields per gram of AIAs are given in Table 5-15 for different proton energy ranges dealt with in this work. In the third column the corresponding integral yields calculated from the results of Mushtaq et al. [1988] are given, showing a rather large deviation at high and low proton energies. Concerning the energy range from 19.7 to 25.8 MeV, it should be mentioned that Mushtaq et al. did not calculate values below 24.5 MeV, where they supposed the threshold of the reaction to be. The difference between experimental and integral data is most likely due to uncertainties in the (p,3n) reaction cross sections in the area of the reaction threshold.

Table 5-15 Thick target yields of ^{73}Se from the irradiation of AIAs

Energy range (MeV)	Thick target yield (MBq/ $\mu\text{A}\cdot\text{h}$)	Integral yield (MBq/ $\mu\text{A}\cdot\text{h}$)
42.5 → 39.8	43.4	87
40.3 → 31.9	325.3	355
25.8 → 19.7	48.1	16

For investigations on the separation of radioselenium, ^{75}Se ($T_{1/2} = 119.8$ d) was applied as a marker during the radiochemical processing. It was produced via the $^{75}\text{As}(p,n)^{75}\text{Se}$ reaction. This way the radiochemical studies could be performed after a cooling time of several months, thus reducing the radiation exposure during the processing.

The main focus concerning the radiochemical separation of no-carrier-added radioselenium was the thermochromatographic step of the separation, leading to the removal of the bulk As for a subsequent separation via liquid extraction. The separation of radioselenium from the irradiated target was done analogous to the processing of radioselenium from a Cu_3As target as described in section 3.4.1. The

procedure was applied to the new target material without much change in the experimental setup. However, due to the reaction of Al with the O₂ gas during the process, it was converted quantitatively into Al₂O₃, which had to be taken into account. Therefore the irradiated sample was put into a ceramic vessel for the chromatography to avoid the transport of Al₂O₃ powder in the gas stream. A potential problem that had to be investigated was the passivation due to the formation of Al₂O₃, which may lead to the retention of arsenic and radioselenium. A γ -ray spectrometric analysis of the remaining material after the separation showed, that less than 10 % of radioselenium remained in the target. However, it was found that the bulk of arsenic (about 70 %) was not removed from the target. A consequence of this phenomenon is a delayed removal of arsenic from the target, thus leading to an incomplete separation of the radioselenium from the As matrix. Figure 5-17 shows a γ -ray spectrum of a ⁷⁵Se fraction resulting from a thermochromatographic separation.

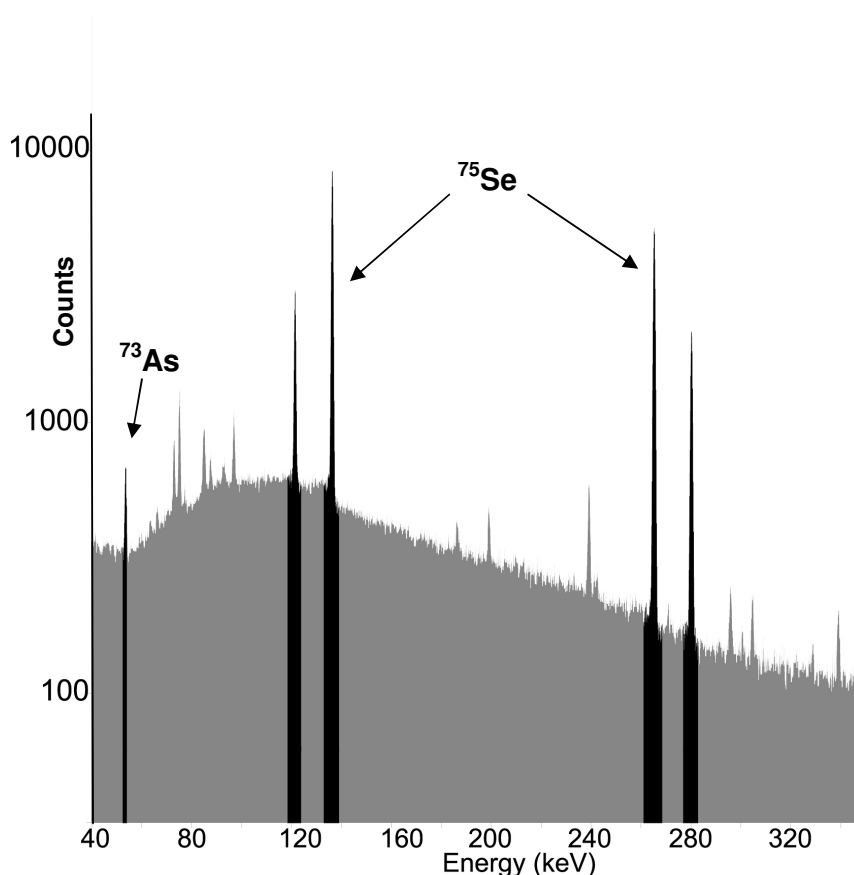


Fig. 5-17 γ -ray spectrum of a ⁷⁵Se fraction showing the separated ⁷⁵Se and the impurity of radioarsenic at 53 keV.

Further difference in the separation chemistry, as compared to the use of a conventional Cu_3As target, was the appearance of radioselenium in the first fraction of the thermochromatographic separation. This may either be due to an improved transport of $[\text{}^{75}\text{Se}]\text{SeO}_2$, or to an increased carry over of radioselenium with As_2O_3 .

From the difficulties mentioned, it can be concluded that for the separation of radioselenium from irradiated AIAs, a single thermochromatographic separation step is not sufficient, demanding an additional separation cycle when using this type of target material. Nevertheless, the advantages of the compound may justify the prolonged separation procedure. However, further radiochemical studies concerning the optimisation of the process are needed.

6 Summary

Nuclear reaction cross section data are of considerable importance for the production of medically interesting radionuclides and the optimisation of existing methods. Within the scope of this work integral and differential cross section measurements were done and new routes relevant to the production of some therapeutic and diagnostic radionuclides were investigated. Concerning n.c.a. ^{73}Se , preliminary experiments were done on its production via the $^{75}\text{As}(p,3n)^{73}\text{Se}$ reaction using novel targetry. Irradiations were done using four different cyclotrons. As projectiles protons of energies up to 100 MeV, α -particles of 26.5 MeV incident energy and fast spectral neutrons generated with a 14 MeV d(Be) source were employed. The beam currents were measured via monitor reactions and in some cases using a Faraday Cup. In most cases, the produced radioactivity was determined non-destructively via γ -ray spectrometry or via β^- -counting using a gas-flow proportional counter. In the case of ^{153}Sm a radiochemical separation was done prior to the determination of radioactivity. For the validation of data the measured values were compared with the results of nuclear model calculations wherever possible. Based on the measured excitation functions, possible production yields were calculated and discussed.

Integral cross section measurements on the nuclear reactions $^{\text{nat}}\text{S}(n,p)^{32}\text{P}$, $^{\text{nat}}\text{Zr}(n,p)^{90}\text{Y}$ and $^{\text{nat}}\text{Eu}(n,p)^{153}\text{Sm}$ were performed using 14 MeV d(Be) neutrons. The spectral distribution of the breakup neutrons was analysed using multiple foil activation and the iterative computer code SULSA. The spectrum averaged reaction cross sections were compared with the integrated values calculated from the known excitation functions. The integrated data could be validated within 10 - 15 % deviation, thereby supporting the evaluated and recommended excitation functions of the three nuclear processes. The measured data were also considered in terms of large scale production of ^{32}P , ^{90}Y and ^{153}Sm with high specific radioactivity. It could be shown that the use of high-intensity fast neutron spectral sources (i.e. a fusion or a spallation source) would be more effective for production of the therapeutic radionuclides via the (n,p) process than through the use of present day fission reactors. Due to their increasing significance in internal radiotherapy, alternative routes for production of ^{153}Sm and ^{169}Yb in no-carrier-added form were investigated.

Both radionuclides are presently produced via the (n,γ) reaction, and hence with low specific activity. In the case of ^{153}Sm the $^{nat}\text{Nd}(\alpha,n)^{153}\text{Sm}$ process was studied. The cross section data for this reaction have been measured for the first time in this study. The possible yield of ^{153}Sm calculated on the basis of those data amounted to $1.1 \text{ MBq}/\mu\text{A}\cdot\text{h}$ considering the suitable energy range of $E_\alpha = 25 \rightarrow 15 \text{ MeV}$. Thus the batch yield of no-carrier-added ^{153}Sm using the α -particle induced reaction may amount up to about 2 GBq , if a high-current target of enriched ^{150}Nd is available.

For the production of n.c.a. ^{169}Yb the proton induced $^{nat}\text{Tm}(p,n)^{169}\text{Yb}$ process was investigated. The measured excitation function shows a distinct maximum cross section, amounting to about 285 mb at 11 MeV proton energy. A comparison with the results of nuclear model calculations showed good agreement within the limits of uncertainties. The optimum energy range for production of the radionuclide appears to be $E_p = 16 \rightarrow 7 \text{ MeV}$, the integral yield of ^{169}Yb amounting to $1.5 \text{ MBq}/\mu\text{A}\cdot\text{h}$. The batch yield expected in the (p,n) reaction on ^{nat}Tm is, however, much lower than via the reactor based production route. At a cyclotron ^{169}Yb can, however, be produced in “no-carrier added” form and in still sufficient quantities for medical application.

Cross section measurements were also done on the production of ^{71}As , ^{72}As , ^{73}As and ^{74}As via the $^{nat}\text{Ge}(p,xn)$ reaction using proton energies from threshold up to 100 MeV . The data showed good consistency with total uncertainties of 8 to 13% . Excitation functions were fitted for all four nuclear reactions and compared with the results of nuclear model calculations with generally good agreement. Based on the fitted excitation function, possible production yields were calculated and were found to be in good agreement with data from the literature, wherever available. On the basis of the integrated yield curves, optimum production conditions and possible radionuclidic impurities could be assessed. The formation of radioarsenic via the proton induced reaction on natural Ge is affected by different simultaneous nuclear reaction channels. In the case of ^{71}As , the contribution of the (p,n) , $(p,2n)$ and $(p,3n)$ reactions could be documented by doing measurements on 96.4% enriched ^{72}Ge .

Related to the standardisation and validation of data for the production of ^{82}Sr via the $^{nat}\text{Rb}(p,xn)$ process, cross section measurements on the formation of the long-lived impurity ^{85}Sr via the $^{nat}\text{Rb}(p,xn)^{85}\text{Sr}$ reaction were done. Based on the measured excitation function, the integral yield was calculated, allowing for an evaluation of the

best production conditions of ^{82}Sr . For production of ^{82}Sr via the (p,xn) reaction on natural Rb, an incident proton energy of 60 MeV or above is recommended to obtain a ^{85}Sr impurity of less than 20 %.

With the production of n.c.a. ^{73}Se via the $^{75}\text{As}(p,xn)$ reaction in view, preliminary experiments were done using AIA's alloy as novel target material. Thick target yields were determined using different proton energy ranges. For investigation of the thermochromatographic separation of radioselenium from the target, ^{75}Se was used as marker. The separation proved to be incomplete and an increased effort is necessary to obtain better results. However, considering the 7.1 h half-life of ^{73}Se , the advantages of the novel target material, like better availability and reduced radiation exposure to the worker, a longer separation procedure may be justified. Further radiochemical studies concerning the optimisation of the process are needed.

In short, this work deals with several aspects of radionuclide development for medical applications. The measurement of integral cross sections and yields of some diagnostic and therapeutic radionuclides like ^{82}Sr and ^{32}P via radiochemical techniques enabled the validation and standardisation of their production methods. Detailed measurements were carried out on the excitation functions for the formation of $^{71,72,73,74}\text{As}$ and their production conditions could be optimised. Furthermore, new routes for production of ^{153}Sm and ^{169}Yb in no-carrier-added form were developed using 14 MeV d(Be) neutron and charged particle induced nuclear reactions. Finally, attempts were made to produce ^{73}Se via novel targetry.

7 Appendix

7.1 Standard sources for calibration

The following Tables 7-1 and 7-2 give the names and manufacturer of the radioactive standard sources used in this work for calibration of γ -ray and β^- -detectors.

Table 7-1 List of γ -ray standards used for the energy and efficiency calibration of detectors

Type of source	Reference No.	Manufacturer
^{22}Na	1X224	Amersham Buchler GmbH & Co.KG
^{137}Cs	7S256	Amersham Buchler GmbH & Co.KG
^{133}Ba	PTB – 458 – 78	Physikalisch Technische Bundesanstalt
^{152}Eu	PTB – 371 – 83	Physikalisch Technische Bundesanstalt
^{226}Ra	PTB – 404 – 84	Physikalisch Technische Bundesanstalt
	DW 539	Amersham Buchler GmbH & Co.KG
^{241}Am	7Q220	Amersham Buchler GmbH & Co.KG

Table 7-2 List of standard β^- -particle emitters used for detector calibration and absorption measurements

Type of source	Reference No.	Manufacturer
^{14}C	0.156 UC	New England Nuclear / NEN
^{36}Cl	0.0195 UC	New England Nuclear / NEN
^{90}Sr	0.0198 UC	New England Nuclear / NEN
^{99}Tc	0.035 UC	New England Nuclear / NEN
^{147}Pm	0.146 UC	New England Nuclear / NEN

7.2 Target materials and chemical compounds

In Table 7-3 a list of materials used in irradiation experiments is given. All metal foils used in this work for multiple foil activation as well as for beam current monitoring and backing of sediments were provided by *Goodfellow GmbH*.

Table 7-3 List of materials in irradiation experiments

Compound	Purity (%)	Manufacturer
S	99.98	Aldrich Chemical Company Inc.
AIAs	<i>technical</i>	Aldrich Chemical Company Inc.
GeO ₂	99.999	ChemPur Feinchemikalien und Forschungsbedarf GmbH
⁷² Ge*	96.42*	Chemotrade Chemiehandelsgesellschaft mbH
RbCl	98.5	Koch-Light Laboratories Ltd.
	99.99	Aldrich Chemical Company Inc.
ZrO ₂	99	Aldrich Chemical Company Inc.
Eu ₂ O ₃	99.9	Alfa Products, Ventron Corp.
Nd ₂ O ₃	99.999	Koch-Light Laboratories Ltd.
Tm ₂ O ₃	99.99	Koch-Light Laboratories Ltd.

* Enriched material, chemical purity > 99.99 %

All other chemical compounds, which were used during the radiochemical separations including solvents and chromatographic compounds, were obtained from *Merck KGaA*.

8 References

- Al-Abyad, M., Spahn, I., Sudár, S., Morsy, M., Comsan, M.N.H., Csikai, J., Qaim, S.M., Coenen, H.H., Nuclear data for production of the therapeutic radionuclides ^{32}P , ^{64}Cu , ^{67}Cu , ^{89}Sr , ^{90}Y and ^{153}Sm via the (n,p) reaction: Evaluation of excitation function and its validation via integral cross-section measurement using a 14 MeV d(Be) neutron source, *Appl. Rad. Isot.* **64**, 717 (2006).
- Amphlett, C.B., *Inorganic ion exchangers*, Elsevier, Amsterdam (1964).
- Basile, D., Birattari, C., Bonardi, M., Goetz, L., Sabbioni, E., Salomone, A., Excitation functions and production of arsenic radioisotopes for environmental toxicology and biomedical purposes, *Appl. Rad. Isot.* **32**, 403 (1981).
- Bauer, G.S., Physics and technology of spallation neutron sources, *Nucl. Instr. Meth. in Phys. Res.* **A463**, 505 (2001).
- Berger, M.J., Coursey, J.S., Zucker, M.A., Chang, J., *ESTAR, PSTAR, and ASTAR: Computer Programs for Calculating Stopping-Power and Range Tables for Electrons, Protons, and Helium Ions (version 1.2.3)*. Available: <http://physics.nist.gov/Star>. National Institute of Standards and Technology, Gaithersburg, MD., USA (2005).
- Bethe, H.A., Zur Theorie des Durchgangs schneller Korpuskularstrahlen durch Materie, *Ann. Phys.* **5**, 325 (1930).
- Bethe, H.A., A continuum theory of the compound nucleus, *Phys. Rev.* **57**, 1125 (1940).
- Birattari, C., Gadioli, E., Grassi, A.M., Strini, G., Tagliaferri, G., Pre-equilibrium processes in (p,n) reactions. *Nuclear Physics A* **201**, 579 (1973).
- Blann, M., Importance of the nuclear density distribution on pre-equilibrium decay, *Phys. Rev. Lett.* **28**, 757 (1972).
- Blann, M., Pre-equilibrium decay, *Ann. Rev. Nucl. Sci.* **25**, 123 (1975).
- Blessing, G., Weinreich, R., Qaim, S.M., Stöcklin, G., Production of ^{75}Br and ^{77}Br via the $^{75}\text{As}(^3\text{He},3n)^{75}\text{Br}$ and the $^{75}\text{As}(\alpha,2n)^{77}\text{Br}$ reactions using Cu_3As -alloy as a high-current target material, *Int. J. Appl. Radiat. Isot.* **33**, 333 (1982).
- Blessing, G., Qaim, S.M., An improved internal Cu_3As -alloy cyclotron target for the production of ^{75}Br and ^{77}Br and separation of the by-product ^{67}Ga from the matrix activity, *Appl. Radiat. Isot.* **35**, 927 (1984).

- Blessing, G., Lavi, N., Hashimoto, K., Qaim, S.M., Thermo chromatographic separation of radioselenium from irradiated Cu_3As -target: Production of no-carrier added ^{75}Se , *Radiochim. Acta* **65**, 93 (1994).
- Blessing, G., Bräutigam, W., Böge, H.G., Gad, N., Scholten, B., Qaim, S.M., Internal irradiation system for excitation function measurement via the stacked foil technique, *Appl. Radiat. Isot.* **46**, 955 (1995).
- Bloch, F., Zur Bremsung rasch bewegter Teilchen beim Durchgang durch Materie, *Ann. Phys.* **16**, 285 (1933).
- Blum, T., Development of no-carrier-added radioselenation methods for the preparation of radiopharmaceuticals, *Berichte des Forschungszentrums Jülich; 4044, Institut für Nuklearchemie Jül-4044, D 38 (Diss., Köln, Univ.)* 2003.
- Blum, T., Ermert, J., Coenen, H.H., Synthesis of assymetric [^{75}Se]selenoethers via carbodiimides, *J. Label. Compd. Radiopharm.* **44**, 587 (2001).
- Blum, T., Ermert, J., Wutz, W., Bier, D., Coenen, H.H., First no-carrier-added radioselenation of an adenosine- A_1 receptor ligand, *J. Label. Compd. Radiopharm.* **47**, 415 (2004).
- Bohr, N., Neutron capture and nuclear constitution, *Nature*, **137**, 344 (1936).
- Bremer, K.H., Anwendung von Radionukliden in der Medizin, in: *Ullmanns Enzyklopädie der technischen Chemie, Vol. 20, p. 59, VCH, Weinheim, Germany* (1981).
- Buthelezi, E.Z., Nortier, F.M., Schroeder, I.W., Excitation functions for the production of ^{82}Sr by proton bombardment of ^{nat}Rb at energies up to 100 MeV. *Appl. Radiat. Isot.* **64**, 915 (2006).
- Calamand, A., *Handbook of Nuclear Activation Cross-Sections*, International Atomic Energy Agency, Vienna, Austria (1974).
- Christiansen, J.-A., von Hevesy, G., and Lomholt, S., Recherches, par une méthode radiochimique, sur la circulation du bismuth dans l'organism. *C. r. Séan. Soc. Biol.* **178**, 1324 (1924).
- DeLand, F.H., James, A.E. Jr., Wagner, H.N. Jr., Hosain, F., 1971. Cisternography with ^{169}Yb -DTPA. *J. Nucl. Med.* **12**, 683.
- Dityuk, I., Konobeyev, A.Yu., Lunev, V.P., Shubin, Yu.N., New version of the computer code ALICE-IPPE. Report INDC (CCP)-410, International Atomic Energy Agency, Vienna, Austria (1998).

- Dmitriev, P.P., Molin, G.A., Radioactive nuclide yields for thick target at 22 MeV proton energy. *Vop. At.Nauki i Tekhn., Ser. Yadernye Konstanty*; **44**, Issue.5, 43 (1981).
- Evans, C.D., LaDow, K., Schumann, B.L., Savage Jr., R.E., Caruso, J., Vonderheide, A., Succop, P., Talaska, G., Effect of arsenic on benzo[α]pyrene DNA adduct levels in mouse skin and lung, *Carcinogenesis* **25** (4), 493 (2004).
- Experimental nuclear reaction data (EXFOR). Available: <http://www-nds.iaea.org/exfor/exfor00.htm>, IAEA-NDS (2003).
- Fan, P., Chiu-Tsao, S., Patel, N., Ravi, K., Sherman, W., Pisch, J., Harrison, L.B., Tsao, H.S., 2001. Yb-169: a promising new isotope for intravascular brachytherapy. *Cardiovascular Radiation Medicine* **2**, 52.
- Faßbender, M., Shubin, Yu.N., Lunev, V.P., Qaim, S.M., Experimental studies and nuclear model calculations on the formation of radioactive products in interactions of medium energy protons with copper, zinc and brass: Estimation of collimator activation in proton therapy facilities, *Appl. Radiat. Isot.* **48**, 1221 (1997).
- Faßbender, M., Shubin, Yu.N., Qaim, S.M., Formation of activation products in interactions of medium energy protons with Na, Si, P, Cl, Ca and Fe, *Radiochim. Acta* **84**, 59 (1999).
- Fernbach, S., Serber, R., Taylor, T.B., The scattering of high energy neutrons by nuclei, *Phys. Rev.* **75**, 1352 (1949).
- Firestone, R.B., Table of Isotopes, CDROM-Edition, Version Wiley-Interscience, New York, USA (1996).
- Fresca Fantoni, R., Gadioli, E., Guazzoni, P., Vergani, P., Zetta, L., Delleria, P.L., Tomasi, F., Diavola, G., Marchetta, C., RERAME: A facility for investigating heavy ion reactions with activation techniques, *Appl. Radiat. Isot.* **45**, 325 (1994).
- Gadioli, E., Hodgson, P.E., Pre-equilibrium nuclear reactions, Clarendon Press, Oxford, USA (1992).
- Griffin, J.J., Statistical model of intermediate structure, *Phys. Rev. Lett.* **17**, 478 (1966).
- Harman, J.B., Ledlie, E.M., Survival of polycythemia vera patients treated with radioactive phosphorus, *Br. Med. J.* **2**, 146 (1976).

- Haight, R.C., Paviotti-Corcuera, R., Summary report of the consultants' meeting on nuclear data for production of therapeutic radioisotopes, INDC(NDS)-432, International Atomic Energy Agency, Vienna (2002).
- Haxel, O., Jensen, J.H.D., Suess, H.E., Modellmäßige Deutung der ausgezeichneten Kernzahlen im Nukleonenbau, Z. Phys. **128**, 295 (1950).
- Heyding R.D., Despault, G.J.G., The copper/arsenic system and the copper arsenide minerals, Can. J. Chem. **38**, 2477 (1960).
- Herba, M.J., Illescas, F.F., Thirlwell, M.P., Boos, G.J., Rosenthal, L., Atri, M., Bret, P.M., Hepatic malignancies: improved treatment with intraarterial Y-90, Radiology **169**, 311 (1988).
- Hevesy, G., The absorption and translocation of lead by plants: A contribution to the application of the method of radioactive indicators in the investigation of the change of substance in plants, Biochem. J. **17**, 439 (1923).
- Hilaris, B., S., Henschke, U.K., General principles and techniques of interstitial brachytherapy, in: Handbook of interstitial brachytherapy (Hilaris, B.S. editor), p. 61, Publishing Science Group, Acton, USA (1975).
- Hilgers, K., Shubin, Yu.N., Coenen, H.H., Qaim, S.M., Experimental measurements and nuclear model calculations on the excitation functions of $^{nat}\text{Ce}(^3\text{He},xn)$ and $^{141}\text{Pr}(p,xn)$ reactions with special reference to production of the therapeutic radionuclide ^{140}Nd , Radiochim. Acta **93**, 553 (2005).
- Hoefnagel, C.A., Radionuclide therapy revised, Eur. J. Nucl. Med. **18**, 408 (1991).
- Hohn, A., Nortier, F.M., Scholten, B., van der Walt, T.N., Coenen, H.H., Qaim, S.M., Excitation functions of $^{125}\text{Te}(p,xn)$ -reactions from their respective thresholds up to 100MeV with special reference to the production of ^{124}I , Appl. Radiat. Isot. **55**, 149 (2001).
- Horiguchi, T., Kumahora H., Inoue H., Yoshizawa Y., Excitation functions of Ge(xnyp) reactions and production of ^{68}Ge , Int. J. Appl. Rad. Isot. **34**, 1531 (1983).
- IAEA-TECDOC-1114, Optimization of production and quality control of therapeutic radionuclides and radiopharmaceuticals, International Atomic Energy Agency, Vienna, Austria (1999).
- IAEA-TECDOC-1285, Reference neutron activation library, International Atomic Energy Agency, Vienna, Austria (2002).
- Ibn Majah, M., Chiadli, A., Sudár, S., Qaim, S.M., Cross sections of (n,p), (n, α) and (n,2n) reactions on some isotopes of zirconium in the neutron energy range of

- 10 – 12 MeV and integral tests of differential cross section data using a 14 MeV d(Be) neutron spectrum, *Appl. Rad. Isot.* **54**, 655 (2001).
- Ido, T., Hermanne, A., Detrói, F., Szűcs, Z., Mahunka, I., Tárkányi, F., Excitation functions of proton induced nuclear reactions on ^{nat}Rb from 30 to 70 MeV. Implication for the production of ^{82}Sr and other medically important Rb and Sr radioisotopes. *Nucl. Inst. Meth. B* **194**, 369 (2002).
- International Reactor Dosimetry File: IRDF-2002. Available: <http://www-nds.iaea.org/irdf2002>.
- Jennewein, M., Qaim, S.M., Hermanne, A., Jahn, M., Tsyganov, E., Slavine, N., Seliounine, S., Antich, P.A., Kulkarni, P.V., Thorpe, P.E., Mason, R.P., Rösch, F., A new method for radiochemical separation of arsenic from germanium oxide, *Int. J. Appl. Rad. Isot.* **63**, 343 (2005).
- Jennewein, M., Qaim, S.M., Kulkarni, P.V., Mason, R.P., Hermanne, A., Rösch, F., A no-carrier-added $^{72}\text{Se}/^{72}\text{As}$ radionuclide generator based on solid phase extraction, *Radiochim. Acta* **93**, 579 (2005).
- Kastleiner, S., Qaim, S.M., Nortier, F.M., Blessing, G., van der Walt, T.N., Coenen, H.H., 2002. Excitation functions of $^{85}\text{Rb}(p,xn)^{85m,g,83,82,81}\text{Sr}$ reactions up to 100 MeV: integral tests of cross section data, comparison of production routes of ^{83}Sr and thick target yield of ^{82}Sr . *Appl. Radiat. Isot.* **56**, 685 (2002).
- Kastleiner, S., Shubin, Yu.N., Nortier, F.M., van der Walt, T.N., Qaim, S.M., Experimental studies and nuclear model calculations on (p,xn) and (p,pxn) reactions on ^{85}Rb from their thresholds up to 100 MeV. *Radiochim. Acta* **92**, 449 (2004).
- Knoll, G.F., Radioisotope neutron sources, in: *Neutron Sources for Basic Physics and Applications* (Cierjacks, S., editor), p. 7, Pergamon Press, Oxford, Great Britain (1983).
- Kopecky, J., Atlas of neutron capture cross sections, Report INDC (NDS)-362, International Atomic Energy Agency, Vienna, Austria (1997).
- Környei, J., Ytterbium-169 ($^{169}\text{Yb}_{70}$), in *Manual for reactor produced radioisotopes*, IAEA-TECDOC-1340, p. 238, International Atomic Energy Agency, Vienna, Austria (2003).
- Kutzner, J., Grimm, W., Brod, K.H., Rösler, A., Die Yttrium-90-Therapie von Knochenmetastasen, *Dtsch. Med. Wochenschr.* **107**, 1360 (1982).

- Lieser, K. H., Einführung in die Nuklearchemie, Verlag Chemie, Weinheim, 3. Auflage (1991).
- Livingston, M.S., H.A., Nuclear dynamics, experimental, Rev. Mod. Phys. **9**, 245 (1937).
- Mason, D.L.D., Battista, J.J., Barnett, R.B., Porter, A.T., 1992. Ytterbium-169: Calculated physical properties of a new radiation source for brachytherapy. Med. Phys. **19**, 695.
- Mayer, M.G., On closed shells in Nuclei II, Phys. Rev. **75**, 1969 (1949).
- Mushtaq, A., Qaim, S.M., Stöcklin, G., Production of ^{73}Se via (p,3n) and (d,4n) reactions on arsenic, Appl. Radiat. Isot. **39**, 1085 (1988).
- Mushtaq, A. Qaim, S.M., Excitation functions of α - and ^3He -particle induced reactions on natural germanium: Evaluation of production routes for ^{73}Se , Radiochim. Acta **50**, 27 (1990).
- Musiol, G., Ranft, J., Reif, R., Seeliger, D., Kern- und Elementarteilchenphysik, VCH, Weinheim, 1988.
- Oláh, L., El-Megrab, A.M., Fenyvesi, A., Majdeddin, A.D., Dóczy, R., Semkova, V., Qaim, S.M., Csikai, J., Investigations of neutron fields produced in $^2\text{H}(d,n)^3\text{He}$ and $^9\text{Be}(d,n)^{10}\text{B}$ reactions, Nuclear Instruments and Methods in Physics Research **A404**, 373 (1998).
- Ortiz Escobar, M.E., Hue, N.V., Cutler, W.G., Recent developments on arsenic: contamination and remediation, in: Recent Research Developments in Bioenergetics **Vol. 4**, 1 (Pandalai, S.G. editor), Transworld Research Network, Trivandrum, India (2006), *in press*.
- Plenevaux, A., Guillaume, M., Brihaye, C., Lemaire, C., Cantinau, R., Chemical processing for production of no-carrier-added selenium-73 from germanium and arsenic targets and synthesis of L-2-amino-4-([^{73}Se]methylseleno) Butyric Acid (L-[^{73}Se]Selenomethionine), Appl. Rad. Isot. **41**, 829 (1990).
- Qaim, S.M., Nuclear data relevant to cyclotron produced short-lived medical radioisotopes, Radiochim. Acta **30**, 147 (1982).
- Qaim, S.M., Wölfle, R., Rahman, M.M., Ollig, H., Measurement of (n,p) and (n, α) reaction cross sections on some isotopes of Nickel in the energy region of 5 to 10 MeV using a deuterium gas target at a compact cyclotron, Nucl. Sci. Eng. **88**, 143 (1984).

- Qaim, S.M., d(Be) neutron fields and their applications in nuclear reaction cross-section studies in: Properties of Neutron Sources, IAEA-TECDOC-410, p. 90, International Atomic Energy Agency, Vienna (1987).
- Qaim, S.M., Target development for medical radioisotope production at a cyclotron, Nucl. Instr. and Meth. **A282**, 289 (1989).
- Qaim, S.M., Nuclear data for medical applications: an overview, Radiochim. Acta **89**, 189 (2001). (a)
- Qaim, S.M., Therapeutic radionuclides and nuclear data, Radiochim. Acta **89**, 297 (2001). (b)
- Qaim, S.M., Nuclear data relevant to the production and application of diagnostic radionuclides, Radiochim. Acta **89**, 223 (2001). (c)
- Qaim, S.M., Tárkányi, F., Takács, S., Hermanne, A., Nortier, F.M., Obložinský, P., Scholten, B., Shubin, Yu.N., Zhuang Youxiang, Positron emitters, in Charged particle cross-section database for medical radioisotope production: diagnostic radioisotopes and monitor reactions. IAEA-TECDOC-1211, pp. 234 (2001).
- Qaim, S.M., Cyclotron production of medical radionuclides, in Handbook of nuclear chemistry (Vértes, A., Nagy, S., Klencsár, Z., editors), Vol. 4, p. 47, Kluwer Academic Publishers, Dordrecht, The Netherlands (2003).
- Qaim, S.M., Coenen, H.H., Produktion pharmazeutisch relevanter Radionuklide, Pharm. Unserer Zeit **34** No.6, 460 (2005).
- Qaim, S.M., Steyn, G.F., Spahn, I., Spellerberg, S., van der Walt, T.N., Coenen, H.H., Yield and purity of ^{82}Sr via the $^{\text{nat}}\text{Rb}(p,xn)^{82}\text{Sr}$ process, Appl. Radiat. Isot. **65**, 247 (2007).
- Rösch, F., Qaim, S.M., Stöcklin, G., Nuclear data relevant to the production of the positron emitting radioisotope ^{86}Y via the $^{86}\text{Sr}(p,n)$ and $^{\text{nat}}\text{Rb}(^3\text{He},xn)$ -processes. Radiochim. Acta **61**, 1 (1993).
- Sakamoto, K., Dohniva, M., Okada, K. Excitation functions for (p,xn) and (p,pxn) reactions on natural $^{79+81}\text{Br}$, $^{85+87}\text{Rb}$, ^{127}I and ^{133}Cs upto $E_p = 52$ MeV. Int. J. Appl. Radiat. Isot. **36**, 481 (1984).
- Schicha, H., Schober, O., Nuklearmedizin (Compact Lehrbuch), 3rd Edition, Schattauer Verlag, Stuttgart, Germany (1997).
- Shapiro B., Andrews, J., Fig, L., Carey, J., Walker-Andrews, S., Smith, J., Ensminger, W., Therapeutic intra-arterial administration of yttrium-90 glass microspheres for hepatic tumours, in: Nuclear Medicine – quantitative analysis in imaging and

- function, 589 (Schmidt, H.A.E, Chambron, J., editors), Schattauer, Stuttgart, Germany (1989).
- Shubin, Yu.N., Lunev, V.P., Konobeyev, A.Yu., Dityuk, A.I., Proton reaction data library for nuclear activation, MENDL-2P (Medium Energy Nuclear Data Library). IAEA-NDS-204, International Atomic Energy Agency, Vienna, Austria (1998).
- Spahn, I., Coenen, H.H., Qaim, S.M., Enhanced production possibility of the therapeutic radionuclides ^{64}Cu , ^{67}Cu and ^{89}Sr via (n,p) reactions induced by fast spectral neutrons, *Rapid Communication*, *Radiochim. Acta* **92**, 183 (2004).
- Stöcklin, G., Qaim, S.M., Rösch, F., The impact of radioactivity on medicine, *Radiochim. Acta* **70/71**, 249 (1995).
- Stoll, T., Kastleiner, S., Shubin, Yu.N., Coenen, H.H., Qaim, S.M., Excitation functions on proton induced reactions on ^{68}Zn from threshold up to 71 MeV, with specific reference to the production of ^{67}Cu , *Radiochim. Acta* **90**, 309 (200).
- Sublet, J.-Ch., Capote Noy, R., Summary report of the second research coordination meeting on nuclear data for production of therapeutic radionuclides, Report INDC(NDC)-465, International Atomic Energy Agency, Vienna, Austria (2004).
- Sudár, S., A solution for the neutron spectrum unfolding problem without using input spectrum, IAEA-INDC (HUN)-026/L, International Atomic Energy Agency, Vienna, Austria (1989).
- Szelecsényi, F., Steyn, G.F., Kovacs, Z., Vermeulen, C., van der Meulen, N.P., Dolley, S.G., van der Walt, N.T., Suzuki, K., Mukai, K., Investigation of the $^{66}\text{Zn}(p,2n)^{64}\text{Cu}$ and the $^{68}\text{Zn}(p,x)^{64}\text{Cu}$ nuclear processes up to 100 MeV: production of ^{64}Cu , *Nucl. Instr. and Meth. in Phys. Res. B* **240**, 625 (2005).
- Taasan, V., Shapiro, B., Taren, J.A., Beierwaltes, W.H., McKeever, P., Wahl, R., Carey, J.E., Petry, N., Malette, S., Phosphorus-32 therapy of cystic grade IV astrocytomas: technique and preliminary application, *J. Nucl. Med.* **26**, 296 (1985).
- Tárkányi, F.T., Takács, S., Gul, K., Hermanne, A. Mustafa, M.G., Nortier, M., Obložinský, P., Qaim, S.M., Scholten, B., Shubin, Yu.N., Zhuang, Y., Monitor reactions, in Charged particle cross section database for medical radioisotope production. IAEA-TECDOC-1211, p. 49, International Atomic Energy Agency, Vienna (2001).
- Tárkányi, F.T., Hermanne, A., Takács, S., Ditroi, F., Spahn, I., Kovalev, S.F., Ignatyuk, A., Qaim, S.M., Activation cross sections of the $^{169}\text{Tm}(d,2n)$ reaction

- for production of the therapeutic radionuclide ^{169}Yb , *Appl. Radiat. Isot.*, *to be published*.
- Uttley, C.A., Sources of monoenergetic neutrons, in: *Neutron Sources for Basic Physics and Applications* (Cierjacks, S., editor), p. 19, Pergamon Press, Oxford, Great Britain (1983).
- Wang, Z-Y., Arsenic compounds as anticancer agents, *Cancer Chemother. Pharmacol.* **48**, 72 (2001).
- Weinreich, R., Schult, O., Stöcklin, G., Production of ^{123}I via the $^{127}\text{I}(\text{d},6\text{n})^{123}\text{Xe}(\beta^+, \text{EC})^{123}\text{I}$ process, *Int. J. Appl. Radiat. Isot.* **25**, 535 (1974).
- Weisskopf, V.F., Ewing, D.H., On the yield of nuclear reactions with heavy elements, *Phys. Rev.* **57**, 472 (1940).
- Weizsäcker, C.F., Zur Theorie der Kernmassen, *Z. Phys* **96**, 431 (1935).
- Wiberg, N., *Lehrbuch der anorganischen Chemie*, 101. Auflage, de Gruyter, Berlin (1995).
- Williamson, C.F., Boujot, J.P., Picard, J., Tables of range and stopping power of chemical elements for charge particles of energy 0.5 to 500 MeV, *Rapport CAE-R 3042* (1966).

Acknowledgement

First of all, I thank Prof. Dr. Dr. h.c. S. M. Qaim for suggesting the interesting topic of this thesis and for his continuous guidance and support in all regards during my work in Jülich, Debrecen and Somerset West.

I thank Prof. Dr. H. H. Coenen for his interest in the project, for encouragement and for providing excellent working conditions.

For their steady help and assistance in experimental aspects I thank Mr. S. Spellerberg and Dr. B. Scholten.

Mr. M. Al-Abyad I thank for the co-operation in the measurement of integral cross sections and the validation of excitation functions.

I am grateful to Prof. Dr. Dr. h.c. J. Csikai for giving me the possibility to do part of my work in cooperation with the University of Debrecen and the Institute of Nuclear Research (ATOMKI) in Hungary as a DAAD stipend holder, and for his encouragement. I thank Dr. F. Tárkányi for his support at the ATOMKI and for his interest in my work. My thanks are also due to Dr. R. Doczi and Prof. Dr. S. Sudár for their cooperation and guidance in some experimental work and neutron spectrum characterisation via the code SULSA.

Dr. N. T. van der Walt and Dr. G. F. Steyn I would like to thank for giving me the possibility to work at iThemba LABS in South Africa and for their hospitality under the Scientific Exchange Programme.

Many thanks to the then trainees Mr. P. Kaufholz and Mr. D. Zeitz for their assistance in the laboratory.

Furthermore, I thank the operators of the four cyclotrons (Jülich, Debrecen, Somerset West) for carrying out the numerous irradiations, which were the basis of my experimental work and the Deutscher Akademischer Austauschdienst (DAAD) e.V. for granting me a five months' scholarship in Hungary.

Last but not least, I would like to thank all my colleagues and friends for their support, for the many interesting and pleasant discussions and for making me enjoy my daily work.

Ich versichere, dass ich die von mir vorgelegte Dissertation selbständig angefertigt, die benutzten Quellen und Hilfsmittel vollständig angegeben und die Stellen der Arbeit – einschließlich Tabellen, Karten und Abbildungen –, die anderen Werken im Wortlaut oder dem Sinn nach entnommen sind, in jedem Einzelfall als Entlehnung kenntlich gemacht habe; dass diese Dissertation noch keiner anderen Fakultät oder Universität zur Prüfung vorgelegen hat; dass sie – abgesehen von unten angegebenen Teilpublikationen – noch nicht veröffentlicht worden ist sowie, dass ich eine solche Veröffentlichung vor Abschluss des Promotionsverfahrens nicht vornehmen werde. Die Bestimmungen der Promotionsordnung sind mir bekannt. Die von mir vorgelegte Dissertation ist von Prof. Dr. Dr. h.c. Syed M. Qaim betreut worden.

Jülich, im Dezember 2006

Teilveröffentlichungen

- Spahn, I., Takács, S., Shubin, Yu. N., Tárkányi, F., Coenen, H. H., Qaim, S. M., Cross-section measurement of the $^{169}\text{Tm}(p,n)$ reaction for the production of the therapeutic radionuclide ^{169}Yb and comparison with its reactor-based generation. *Applied Radiation and Isotopes* **63**, 235 (2005).
- Al-Abyad, M., Spahn, I., Sudár, S., Morsy, M., Comsan, M.N.H., Csikai, J., Qaim, S.M., Coenen, H.H., Nuclear data for production of the therapeutic radionuclides ^{32}P , ^{64}Cu , ^{67}Cu , ^{89}Sr , ^{90}Y and ^{153}Sm via the (n,p) reaction: Evaluation of excitation function and its validation via integral cross-section measurement using a 14 MeV $d(\text{Be})$ neutron source, *Appl. Rad. Isot.* **64**, 717 (2006).
- Qaim, S.M., Steyn, G.F., Spahn, I., Spellerberg, S., van der Walt, T.N., Coenen, H.H., Yield and purity of ^{82}Sr via the $^{\text{nat}}\text{Rb}(p,xn)^{82}\text{Sr}$ process, *Appl. Radiat. Isot.* **65**, 247 (2007).
- Spahn, I., Al-Abyad, M., Hilgers, K., Sudár, S., Tárkányi, F., Qaim, S.M., Coenen, H.H., Nuclear reaction data for new production routes of the therapeutic radionuclides ^{32}P , ^{89}Sr , ^{153}Sm , ^{169}Yb and ^{192}Ir , Technetium, Rhenium and Other Metals in Chemistry and Nuclear Medicine 7 (Mazzi, U., editor), p. 577 (2006).